Plasmas of Arbitrary Neutrality

Xabier Sarasola Martin

SUBMITTED IN PARTIAL FULFILLMENT OF THE

REQUIREMENTS FOR THE DEGREE

OF DOCTOR OF PHILOSOPHY

IN THE GRADUATE SCHOOL OF ARTS AND SCIENCES

Columbia University

2011

Abstract

Plasmas of Arbitrary Neutrality

Xabier Sarasola Martin

The physics of partially neutralized plasmas is largely unexplored, partly because of the difficulty of confining such plasmas. Plasmas are confined in a stellarator without the need for a plasma current, and regardless of the degree of neutralization. The Columbia Non-neutral Torus (CNT) is a stellarator dedicated to the study of non-neutral, and partially neutralized plasmas. This thesis describes the first systematic studies of plasmas of arbitrary neutrality. The degree of neutralization of the plasma can be parameterized through the quantity $\eta \equiv |n_e - Zn_i|/|n_e + Zn_i|$. In CNT, η can be varied continuously from pure electron ($\eta = 1$) to quasi-neutral ($\eta \approx 0$) by adjusting the neutral pressure in the chamber, which controls the volumetric ionization rate. Pure electron plasmas are in macroscopically stable equilibria, and have strong self electric potentials dictated by the emitter filament bias voltage on the magnetic axis. As η decreases, the plasma potential decouples from the emitter, and spontaneous fluctuations begin to appear. Partially neutralized plasmas ($10^{-3} < \eta < 10^{-1}$) generally exhibit multi-mode oscillations in CNT. However, when magnetized ions are present, the electron-rich plasma oscillates at a single dominant mode (20 - 100 kHz). As the plasma approaches quasi-neutrality ($\eta < 10^{-5}$), it also reverts to single mode behavior (1 - 20 kHz).

A parametric characterization of the single mode fluctuations detected in plasmas of arbitrary neutrality is presented in this thesis along with measurements of the spatial structure of the oscillations. The single mode fluctuations observed for $\eta \approx 0.01 - 0.8$ are identified as an ion resonant instability propagating close to the $\mathbf{E} \times \mathbf{B}$ velocity of the plasma. The experiments also show that these oscillations present a poloidal mode number m = 1, and a toroidal number n = 0, which is identical to the spatial structure of the diocotron instability in pure-toroidal traps [75], and implies that the ion-driven instability breaks parallel force balance and the conservation of poloidal flux in CNT.

The low frequency oscillations detected in the quasi-neutral regime are a global instability convected by the $\mathbf{E} \times \mathbf{B}$ flow of the plasma. In this case, the mode aligns almost perfectly with the field lines, and presents a resonant m = 3 poloidal structure.

Contents

Acknowledgments **ix**

1 Introduction **1**

2 The CNT Experiment **6**

2.1 Technical parameters 7

2.2 Creation of plasmas 9

2.3 Confinement 10

2.4 Equilibrium 11

2.5 Diagnostics 12

2.5.1 Equilibrium measurements 12

2.5.2 Spatial structure of the oscillations 14

2.5.3 Data acquisition 17

2.6 Relevant frequencies of CNT's plasmas 18

3 Plasmas of Arbitrary Neutrality **21**

3.1 Presence of ions in CNT 22

3.2 Degree of non-neutralization (η) 24

3.3 Plasma potential 27

3.3.1 Methods for the measurement of ϕ_p 29

3.3.2 Parameter dependence 29

3.4 Ion gyro-radius and electron temperature. 35

3.5 Perpendicular dielectric constant 37

3.6 Oscillations in plasmas of arbitrary neutrality. Basic observations 38

3.7 Summary 41

4 Oscillations in electron-rich non-neutral plasmas 45

4.1 Previous results 46
4.2 Parameter dependence of the oscillations 46
4.2.1 Effect of the conducting boundary at the plasma edge 47
4.2.2 Dependence on η, ϕ_{plasma} and B field strength 49
4.2.3 Effect of different ion species 51
4.2.4 Effect of the magnetic configuration 53
4.2.5 Local phase shift between density and potential fluctuations 56
4.3 Spatial Structure 60
4.3.1 Theoretical considerations 60
4.3.2 Experimental results 62
4.4 Multi-mode oscillations in partially neutralized plasmas. 64
4.4.1 Multi-mode oscillations 65
4.4.2 Jumps between equilibrium states 67
4.5 Summary and discussion 68

5 Oscillations in CNT's quasi-neutral plasmas 72

5.1 Equilibrium measurements in quasi-neutral plasmas 73
5.2 Parameter dependence of the oscillations 75
5.2.1 Theoretical considerations 75
5.2.2 Dependence on η, ϕ_{plasma}, B field strength, and different ion species . 76
5.2.3 Effect of the magnetic configuration 77
5.2.4 Frequency profiles across the plasma 79
5.2.5 Local phase shift between density and potential fluctuations 82
5.3 Spatial Structure 85
5.3.1 Fast camera. Experimental considerations 85
5.3.2 Fast camera. Experimental results 91
5.3.3 Capacitive probes 101
5.3.4 Discussion 102

5.4 Summary and Discussion 104

6 Conclusions **108**

7 Possible Future Studies **112**

A Simulation of the mode number **123**

B Symbols and variables **127**

List of Figures

2.1 CAD drawing of the Columbia Non-Neutral Torus 8
2.2 Layout of the capacitive probe arrays 15
2.3 View ports of the chamber used by the High Speed camera 17
2.4 Relevant frequencies in CNT's plasmas 20

3.1 Ion content in CNT as a function of p_n and ϕ_e 23
3.2 Degree of non-neutralization as a function of p_n and ϕ_e 25
3.3 Comparison of the measured electron density with the estimation of n_e assuming a cylindrical geometry 27
3.4 Different terms of Eq. 3.4 as a function of p_n 28
3.5 Plasma potential at $\psi \approx 0.1$ as a function of the degree of non-neutralization 28
3.6 ϕ_p/ϕ_e as function of p_n for different emitter bias voltages 30
3.7 ϕ_p/ϕ_e as function of n_i 31
3.8 Emission current limit vs. emitter bias for different filament temperatures . . 32
3.9 ϕ_p/ϕ_e as function of p_n evaluating the effect of different filament temperatures and the presence of an additional ceramic rod 33
3.10 ϕ_p/ϕ_e for different B field strengths 34
3.11 ϕ_p/ϕ_e for different ion species 35
3.12 ϕ_p/ϕ_e as a function of p_n for different magnetic configurations 36
3.13 Comparison of ϕ_p as a function of B for different magnetic configurations . . 36
3.14 Electron temperature and normalized ion gyro-radius as a function of the degree of non-neutralization 38
3.15 Perpendicular dielectric constant at low B field strengths 39
3.16 Perpendicular dielectric constant vs. η 39

3.17 Charge loss rate and RMS on a floating emissive probe as a function of the degree of non-neutralization 41
3.18 Power spectrum of the signal on a floating probe vs. degree of non-neutralization. B = 0.02 T 42
3.19 Oscillations in $|e\phi_{plasma}|$ normalized to T_e as a function of the degree of non-neutralization 43

4.1 Oscillations in partially neutralized plasmas. Effect of the conducting boundary at the plasma edge 48
4.2 Power spectrum of the signal on a floating probe vs. degree of non-neutralization. Partially neutralized plasmas. B = 0.02 T vs. B = 0.08 T 49
4.3 Frequency of the mode in partially neutralized plasmas vs. p_n for different B field strengths 50
4.4 Frequency of the mode in partially neutralized plasmas vs. ϕ_{plasma} 51
4.5 E/B scaling of the dominant mode in partially neutralized plasmas 52
4.6 Frequency of the dominant mode in partially neutralized plasmas vs. E/B. Figs. 4.1 and 4.5-right overlaid. 52
4.7 $He^+ - e^-$ plasma. Frequency of the mode vs. ϕ_{plasma} and B field strength . . 53
4.8 Measured frequency vs. E/B for different ion species. Partially neutralized plasmas 54
4.9 Power spectrum of the signal on a floating probe vs. degree of non-neutralization. 78° configuration. B = 0.08 T. 55
4.10 Frequency of the mode in partially neutralized plasmas vs ϕ_p/B in the 78° configuration 56
4.11 Phase shift introduced by the electronic circuits 57
4.12 Determination of the phase difference between the signals measured in nw4 ♯2 and ♯3 58
4.13 Dominant frequency of the cross correlations $\widetilde{\phi}$ - $\widetilde{\phi}$ and $\widetilde{n}$ - $\widetilde{\phi}$ 59
4.14 $\widetilde{n}$ - $\widetilde{\phi}$ phase difference in partially neutralized plasmas 60
4.15 Measured phase shift of the ion-driven mode detected on the poloidal capacitive probes 63

4.16 Measured phase shift of the ion-driven mode detected on the toroidal capacitive probes 65
4.17 Phase difference between two capacitive probes separated 180° toroidally from each other 66
4.18 Partially neutralized plasma switching between two equilibrium states 69

5.1 Measured T_e at $\psi \approx 0.15$ vs. B field strength in quasi-neutral plasmas 74
5.2 Density profiles at different B field strengths. Quasi-neutral plasmas 74
5.3 Power spectrum of the signal on a floating probe vs. p_n. Quasi-neutral plasmas. B = 0.08 T 77
5.4 Frequency and amplitude of the oscillations in quasi-neutral plasmas vs. B field strength 78
5.5 Frequency of the mode in quasi-neutral plasmas vs. ϕ_{plasma} 78
5.6 Measured frequency vs. ϕ_{plasma}/B for different ion species. Quasi-neutral plasmas 79
5.7 Measured frequency of the mode in quasi-neutral plasmas vs. ϕ_{plasma} and ϕ_{plasma}/B. 78° configuration 80
5.8 Frequency profile of the quasi-neutral mode. B = 0.03 T 81
5.9 Frequency profile of the quasi-neutral mode. B = 0.06 T 82
5.10 $\widetilde{n}$ - $\widetilde{\phi}$ phase difference in quasi-neutral plasmas 83
5.11 Langmuir I-V characteristics. Quasi-neutral regime 84
5.12 Oscillations in n. Influence of the sheath thickness and the variation of T_e . . 86
5.13 Measured frequency vs. B field strength emitting with 50 W and 10 W filaments 88
5.14 Alignment of the mode with the magnetic field lines. Visualization of the luminescent traces of the field lines from the top window 89
5.15 Alignment of the mode with the magnetic field lines. Set of movies properly aligned 90
5.16 Alignment of the mode with the magnetic field lines. Set of misaligned movies 90
5.17 Contour plot of the dominant frequency in each pixel. Side view 92
5.18 Histogram of the number of pixels oscillating at a particular frequency . . . 92

5.19 Contour plot of the phase at the dominant frequency of the cross-correlation power spectrum. 64° tilt angle. Top view port 94
5.20 Contour plot of the phase at the dominant frequency of the cross-correlation power spectrum. B = 0.02 T. 64° tilt angle. Side view port 95
5.21 Contour plot of the phase at the dominant frequency of the cross-correlation power spectrum. B = 0.05 T. 64° tilt angle. Side view port 95
5.22 Contour plot of the phase at the dominant frequency of the cross-correlation power spectrum. 78° tilt angle. Side view port 96
5.23 Contour plot of the phase at the dominant frequency of the cross-correlation power spectrum. 78° tilt angle. Top view port 97
5.24 Simulation of the propagation of m = 1, 2, 3 and 4 modes. Phase plots . . . 98
5.25 Two synchronized views with one camera 100
5.26 Movies from the top window at usual and reversed polarity 102
5.27 Measured phase shift of the quasi-neutral oscillations on the poloidal capacitive probes 103

A.1 Interpolated light intensity of a m = 2 mode 124
A.2 Frames of the simulated integral light intensity from the top window of the chamber 126

List of Tables

2.1 Location of the capacitive probes 16

3.1 Estimation of η for other representative plasmas 25

5.1 Drift waves vs. Rayleigh-Taylor instability. Comparison of experimental results and theoretical predictions 106

B.1 Table of symbols and variables 127

Acknowledgments

I would like to thank my advisor, Professor Thomas Pedersen, for his guidance and encouragement during my thesis. I also greatly appreciate the opportunity Professor Pedersen gave me as a student recently graduated from college to participate in the assembly and initial operation of CNT in 2004. The enthusiasm and dynamism I found in the CNT group were fundamental to raise in me a strong interest in Plasma Physics and Experimental Science. That was clearly a life changing experience.

Many thanks to my colleagues in CNT, especially Paul Brenner, Benoit Durand de Gevigney, Mike Hahn, and Peter Traverso. The collaborative environment of the group has made CNT an excellent experiment to complete my thesis. Additional thanks to Professor Michael Mauel for his helpful comments, and for letting me use CTX's High Speed Camera, which has become an essential diagnostic for my thesis.

I would also like to thank my father, mother, and sisters for their love and support. Special thanks to my father for his tireless love of life, and for always encouraging curiosity and critical thinking in me.

Chapter 1

Introduction

Stellarators [7] have been used to confine quasi-neutral plasmas for half a century [46], and have been recently employed for the study of non-neutral plasmas [59]. Non-neutral plasmas are characterized by intense self electric fields, $|e\phi_p|/T_e \gg 1$, which constitutes a regime not accessible for quasi-neutral plasmas. Traditionally, the research on non-neutral plasmas has been conducted on Penning-Malmberg traps [18,47,56] and pure toroidal traps [1, 57, 74, 81]. In Penning traps a solenoid creates a straight magnetic field which provides radial confinement, while the axial confinement relies on electrostatic potentials from biased grids at each end. Since a potential well is used for axial confinement, Penning traps can only confine particles of a single sign of charge having temperatures less than the well depth. Pure toroidal traps use the space charge generated $\mathbf{E} \times \mathbf{B}$ flow as an effective rotational transform [76], otherwise curvature and ∇B drifts will cause particles to rapidly drift out the confining region.

The physics of non-neutral plasmas on magnetic surfaces are essentially different from plasmas in Penning and pure toroidal traps. The Columbia Non-neutral Torus (CNT) is the first stellarator designed specifically to the study of pure electron and other non-neutral plasmas [62]. CNT has demonstrated that stable, small Debye length pure electron plasmas can be created in a magnetic surface configuration [43]. Confinement times over 100 ms [10] have been measured, confirming the existence of macroscopically stable equilibria, and the presence of well confined particle orbits despite the fact that the magnetic configuration is not optimized to prevent magnetically trapped particle losses.

Stellarators present fundamental advantages for the study of non-neutral plasmas. A stellarator does not require internal currents for confinement (in contrast to tokamaks), can confine plasma even in the absence of significant space charge (unlike pure toroidal traps), and can confine both signs of charge simultaneously (since no externally applied electric fields are required, in contrast to Penning traps). Therefore, stellarators can confine plasmas of arbitrary degree of neutralization (from pure electron to quasineutral plasmas). Q.R. Marksteiner describes in [50] the first observations of an ion-driven instability in CNT's electron-rich plasmas. However, partially neutralized plasmas have not been studied theoretically or experimentally in detail in the past, and there are few predictions as to how the plasma will evolve from single-component to quasi-neutrality [60]. This thesis discusses the first systematic characterization of plasmas of arbitrary neutrality, addressing many questions of interest to basic plasma physics:

- How is the plasma equilibrium affected when the degree of neutralization is varied continuously between two radical extremes: pure electron to quasi-neutral? Chapter 3 shows that, among other relevant changes, the plasma potential profiles decouple from the emitter bias voltage, and the plasma develops spontaneous unstable fluctuations as the degree of neutrality is varied from pure electron to quasi-neutral.

- To what degree is confinement degraded as the plasma evolves from a regime characterized by strong negative electric fields (pure electron) to much more modest electric fields (quasi-neutral)? The radial electric field has been observed to be very beneficial for confinement in pure electron plasmas (the strong $\mathbf{E} \times \mathbf{B}$ drift closes trapped particle orbits and reduces the neoclassical transport) and also in quasi-neutral plasmas [22]. As discussed in Chapters 3 and 4, transport across the plasma grows as electron-rich non-neutral plasmas evolve to quasi-neutrality, and is enhanced by the presence of an ion-resonant instability.

- How does the presence of a conducting boundary at the plasma edge affect the ion-driven instability characterized by Marksteiner in [50]? A conducting boundary was installed conforming to the shape of the plasma to impose the electrostatic ground at the edge of the plasma, and thus improve the match between equipotential and

magnetic surfaces [58]. The experiments with the conducting boundary installed (described in Section 4.2) show that single mode ion-driven oscillations are only detected when the ions are magnetized and travel close to the $E \times B$ rotation of the plasma. Otherwise, multi-mode oscillations are observed. The frequency scaling of the single mode ion-driven oscillations is very similar with and without the conducting boundary.

- How does the magnetic shear of the stellarator affect the detected oscillations? CNT can operate at three different tilt angles between its two interlocking coils. The three tilt angles represent three rather different shapes of the plasma and explore three generic shear configurations. Although the magnetic shear is predicted to have a stabilizing effect, Chapters 4 and 5 show that the single mode oscillations detected in electron-rich and quasi-neutral plasmas present almost identical behavior in the 64° (reversed shear) and 78° (essentially shear-less) configurations.

- How does the spatial structure of the detected modes evolve with the degree of neutralization? The spatial structure of the modes detected in the electron-rich and quasi-neutral plasmas is studied in Sections 4.3 and 5.3 respectively.

- How do the fluctuations align with the magnetic field lines? The ion-resonant instability detected in CNT's standard configuration (64° tilt angle) presents a poloidal[1] mode number m = 1 [50], which is the same as that of ion-driven instabilities in Penning and pure-toroidal traps [17, 24, 76, 79], but is the first time an instability non-resonant with a rational surface is observed in a stellarator. Section 4.3 of this thesis studies the spatial structure of the ion-driven mode in the 78° configuration, showing that the mode does not align with the magnetic field lines even in the presence of low order rational surfaces. The spatial structure of the quasi-neutral oscillations is described in Section 5.3. CNT's quasi-neutral mode is almost perfectly aligned with the magnetic field lines.

- What is the toroidal[2] mode number of the ion-driven oscillations? Although the toroidal structure of this mode is predicted to be n > 0 to conserve the poloidal

[1]The poloidal direction is around the minor circumference of the torus.
[2]The toroidal direction is around the major circumference of the torus.

flux in the stellarator (even in the absence of parallel force balance), Section 4.3 shows that the measured toroidal mode of these oscillations is n = 0, which is identical to what is observed in pure toroidal traps [75].

- What is the underlying mechanism driving CNT's quasi-neutral oscillations? Chapter 5 presents a detailed characterization of the spontaneous oscillations emerging in CNT's quasi-neutral plasmas, and compares the characteristics of this mode with instabilities typically observed in other low-β plasmas confined in toroidal magnetic configurations.

- The characterization of plasmas of arbitrary neutrality presented in this thesis also provides a valuable background for future research on positron-electron plasmas in PET (Positron-Electron Torus). PET is a superconducting stellarator based on CNT design that will be dedicated to the study of the first positron-electron plasmas.

This thesis is organized as follows:

Chapter 2 gives an introduction on CNT, summarizing the relevant parameters of the experiment and previously published results.

Chapter 3 analyzes the presence of ions in CNT, defines the degree of non-neutralization η (essential parameter for the characterization of plasmas of arbitrary neutrality), and studies how the properties of the plasma change as we vary continuously η from pure electron to quasi-neutral.

One of the most characteristic changes observed in partially neutralized and quasi-neutral plasmas in CNT is the spontaneous appearance of fluctuations. Chapter 4 shows how the frequency and magnitude of the ion-driven mode detected in partially neutralized plasmas are affected by the magnetic field strength, emitter bias voltage, degree of non-neutralization, different ion species, and magnetic configuration of the stellarator. The spatial structure of this mode is investigated using a set of external capacitive probes. This Chapter also discusses the presence of broadband fluctuations, and jumps between equilibrium states observed in partially neutralized plasmas.

In Chapter 5, the parameter characterization and spatial structure of the mode observed in CNT's quasi-neutral plasmas are presented. Since these plasmas emit sufficient light in the visible spectrum, a high speed camera was used to observe the spatial structure of this

mode.

The results are summarized and discussed in Chapter 6.

This thesis constitutes the first systematic characterization of plasmas of arbitrary neutrality, and there are still many interesting questions to answer in order to fully understand this largely unexplored regime of plasma physics. Some ideas for future research in partially neutralized plasmas are presented in Chapter 7.

Chapter 2

The CNT Experiment

Tokamaks and stellarators are the two most successful magnetic configurations for confining plasmas. Confinement in both of these systems relies on the use of magnetic surfaces [9]. Magnetic surfaces are limited to the shape of the torus [7] and require field lines to wind toroidally and poloidally in the toroid. The rotational transform (ι) describes the poloidal twist of the field lines around the torus [7]. The difference between tokamaks and stellarators lies in the way the poloidal flux is created: in tokamaks the poloidal flux is created by a toroidal current in the plasma, while stellarators use helical shaping of the torus to produce at least part of the poloidal field component [9].

Stellarators do not require driven plasma currents for confinement, which can be essential for the design steady-state disruption-free burning plasma experiments. But stellarators can also be used for basic plasma physics research. In non-neutral plasmas, confinement by an axial magnetic field in a cylinder is limited by the Brillouin density [13]:

$$n_B \equiv \frac{\varepsilon_0 B^2}{2m_e} \tag{2.1}$$

which sets a rather low density limit in pure electron plasmas compared to relevant quasi-neutral plasmas (see Table 3.1). When non-neutral plasmas are confined by magnetic surfaces, the density limit can be much lower than the Brillouin limit [8]. Therefore, the creation of strong toroidal currents in non-neutral plasmas is impossible from a practical point of view, and prevents the use of tokamaks as confinement devices for non-neutral plasma research.

Penning-Malmberg traps [18, 47, 56] and pure toroidal traps [1, 57, 74, 81] have been tra-

ditionally used to study non-neutral plasmas. However, these two concepts cannot confine quasi-neutral plasmas. Penning traps rely on the presence of external electric fields, and cannot confine both signs of charge simultaneously. The strong self-electric field in a non-neutral plasma makes possible the use of a pure toroidal field for confinement (in a pure toroidal trap the fast $\mathbf{E}\times\mathbf{B}$ rotation of the plasma acts as an effective rotational transform). Otherwise, the charged particles will rapidly ∇B drift out in a purely toroidal configuration.

Therefore, stellarators are excellent candidates for the study of plasmas of arbitrary neutrality (ranging from pure electron to quasineutral plasmas), and the Columbia Non-Neutral Torus (CNT) is the first stellarator dedicated to the study of pure electron plasmas, and plasmas of arbitrary degree of neutralization. Magnetic dipoles have been used to confine pure electron [70, 71], and also quasi-neutral plasmas [25, 51], but to the best of my knowledge no one has made a systematic study of plasmas of arbitrary neutrality in magnetic dipoles, even though such a study appears to be possible. Thus, this thesis represents the first detailed experimental characterization of this previously unexplored regime of plasma physics.

2.1 Technical parameters

CNT is a university-scale, two period, classical stellarator. Magnetic surfaces are created by two pairs of circular planar copper coils: one pair of interlocked (IL) coils inside the vacuum vessel, and another pair (PF coils) is placed outside the vacuum chamber forming a Helmholtz pair (Fig. 2.1). A 200 kW steady-state DC power supply drives the IL and the PF coils, which are connected in series. Two additional 4.5 kW DC supplies power two pancakes on each PF coil to fine-tune the optimum current ratio between the IL and the PF coils, which can range between $I_{IL}/I_{PF} = 3.0$ and 4.25, depending on the magnetic configuration. CNT can achieve nominal magnetic field strengths[1] up to 0.3 T, and its maximum pulse length ($>$ 15 s at full current and $>$ 60 s at half the design current) is determined by the allowable temperature rise of its four water cooled copper coils. At B $\leq$ 0.055 T equilibrium is reached between the power provided to the coils and removed by the cooling system,

[1]The nominal magnetic field strength in CNT corresponds to the B field on the magnetic axis in the thin cross-section of the torus ($\varphi = 0°$)

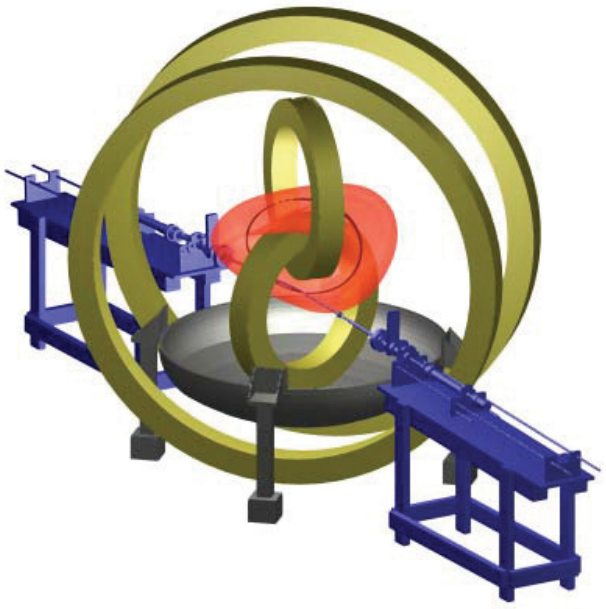

Figure 2.1: A CAD drawing of CNT showing the set of coils (in yellow), the last closed magnetic surface (in red), and the ceramic rods inserted in the plasma with their corresponding stands (in blue) [43].

and the coils can be run indefinitely [62]. All the experiments described in this thesis were performed at nominal B field strengths between 0.01 and 0.1 T.

The tilt angle between the two IL coils can be adjusted in three positions: 64°, 78° and 88°. These tilt angles were chosen such that each has a large volume of good magnetic surfaces and relative resilience against field errors, represent three rather different shapes of the plasma and explore three generic shear configurations: the 64° configuration presents reversed shear (ι increasing from the axis to the edge), the 78° tilt angle is essentially shear free, and the 88° configuration has normal shear [61]. The topology of the magnetic surfaces is mainly determined by the tilt angle between the IL coils, but also the current ratio I_{IL}/I_{PF} has an important effect on the shape and the ι profile of the surfaces. During the course of this thesis, CNT switched from the 64° tilt angle to the 78° configuration. Results will be presented comparing how the magnetic configuration affects the behavior of quasi-neutral, and electron-rich non-neutral plasmas.

The degree of neutralization of the plasma in CNT is controlled by adjusting the neutral

pressure in the chamber, which determines the volumetric ionization rate (more details in Chapter 3). At base neutral pressures (in the 10^{-9} Torr range) the ion and neutral content are negligible, and CNT operates in the pure electron regime[2]. CNT is mainly designed to confine pure electron plasmas, and the ultra-high vacuum level required for pure electron plasma operation is not easily achieved in a $\sim 6\,\mathrm{m}^3$ vacuum chamber. The CNT vacuum chamber is made of 316L stainless steel and can be baked to 200°C. The interlocked coils are encased in vacuum tight 316L stainless steel cases, and all seals in the chamber are hard copper seals [62]. The base neutral pressure is attained using two cryogenic pumps operating respectively at $620\,l/s$ and $710\,l/s$ effective pumping speeds (factoring in the conductance of the ports between the pumps and the chamber). In order to adjust the degree of neutralization of the plasma from pure electron to quasi-neutral, the neutral pressure for the experiments described in this thesis was varied from 10^{-9} to $5 \cdot 10^{-5}$ Torr.

2.2 Creation of plasmas

In CNT, steady state plasmas are created by thermionic emission, injecting electrons from a negatively biased 10 W tungsten filament held on the magnetic axis. Parallel transport fills the magnetic axis with electrons in a few μs, and electrons diffuse outward from the axis filling the remaining magnetic surfaces in a much slower timescale. Since steady-state is reached between electron emission and loss, the confinement time of the plasma (τ_e) can be measured from the emission current, $I_e = eN_e/\tau_e$, once the total number of electrons in the plasma (N_e) is known. The electron density can be determined directly from the interpretation of Langmuir I-V characteristics [42, 43], or from numerical 3D reconstructions of the density profiles obtained using the experimental potential profiles as inputs [45].

So far, research in CNT has been mainly focused on the study of pure electron plasma. A typical $\phi_{plasma} = -200\,\mathrm{V}$ pure electron plasma is characterized by a flat temperature profile with T_e between 2 and 7 eV and a density profile peaked off-axis with $n_e \approx 3 \cdot 10^{12}\,\mathrm{m}^{-3}$. These measurements imply that the Debye length in CNT is $\lambda_D \approx 1$ cm. The average minor radius of the plasma is $\langle a \rangle = 15\,\mathrm{cm}$, and thus the plasma criterion $\lambda_D/\langle a \rangle \ll 1$ is satisfied

[2] At $\mathrm{p_n} = 2 \cdot 10^{-8}$ Torr, the ion fraction ($f_i = n_i/n_e$) is $f_i < 1\%$ [2]

in CNT [43]. This is an accomplishment for a non-neutral plasma.

Pure electron plasmas have also been created in CNT using an electron gun [29]. However, these plasmas were characterized by long Debye lengths. Higher electron temperatures and lower densities were measured compared to the plasmas created by using a heated biased filament.

2.3 Confinement

Stellarators cannot be toroidally symmetric, and the toroidal variation of the magnetic field strength creates a significant fraction of locally trapped particles in classical stellarators, which reduces confinement [9]. This was thought unacceptable for the future use of stellarators as fusion reactors, but quasi-symmetric and link mirror concepts use complicated coil sets to reduce trapped particle losses [7].

CNT is a "classical" stellarator (non-optimized to prevent trapped particle losses) with large variations of $|B|$ along the field lines ($|B|_{max} \approx 1.8|B|_{min}$ on axis, on outer surfaces is even bigger), and a sizeable fraction of trapped particles ($> 50\%$, [21]). However, excellent confinement times were predicted in CNT's non-neutral plasmas as a result of the strong self-electric fields ($|e\phi_p|/T_e \gg 1$) [3,59]. Confinement times over 100 ms [10] have been measured experimentally, confirming that the fast $E \times B$ drift is able to close trapped particle orbits in a non-optimized stellarator.

Ceramic rods are used to hold the emitter filament and the diagnostic probes into the plasma. There are 3 filament arrays in CNT: the "nw4" and "se8" probe arrays (which consist of 4 and 8 equally spaced filaments respectively, and are located in the thin cross-section of the plasma, $\varphi = 0°$), and the "rotating" probe array (with 8 filaments held in the thick cross-section of the torus, $\varphi = 90°$). The innermost filament of each probe array is usually aligned with the magnetic axis when they are inserted in the plasma, but the probe arrays can be also completely extracted away from the plasma. The "nw4" and "se8" probe arrays can be seen in Fig. 2.1 along with their corresponding stands.

The ceramic rods present in the plasma are the dominant source of transport in CNT at base neutral pressure ($p_n < 2 \cdot 10^{-8}$ Torr) [3]. Due to the finite T_e the ceramic rods charge up negatively with respect to the plasma, an electric field develops around the rods, and the

resulting $E \times B$ drift allows the electrons to leave the confining region.

A retractable emitter has been installed in CNT to study the confinement of plasmas in the absence of ceramic rods [4]. The system is designed to extract the emitter from the plasma faster than the confinement time. However, the measured confinement times after retraction are shorter than in steady-state plasmas. P.W. Brenner's thesis [11] describes the efforts conducted to create and diagnose plasmas without internal ceramic rods, which will be essential for the future operation of positron-electron plasmas in a stellarator.

The other major source of transport in pure electron plasmas is neutral-driven transport, which is presumably caused by electron-neutral collisions, but is much higher than expected [3]. In order to understand this apparent inconsistency, the particle orbits in CNT's complicated 3D geometry were numerically simulated by B. Durand de Gevigney [21], showing that the variation of the electric potential on magnetic surfaces leads to the existence of open orbits for a large fraction of the electrons.

A conducting boundary was installed in CNT's 64° tilt angle configuration in order to set the electrostatic boundary condition at the plasma edge, thereby improving the match between equipotential and magnetic surfaces. This was predicted to improve confinement by making the electrons $E \times B$ drift within a magnetic surface ($\mathbf{v}_{E\times B} = (\mathbf{B} \times \nabla\psi)/B^2\, \partial\phi/\partial\psi$), thus reducing the cross-surface transport [21,45]. Although this did lead to improved confinement, the improvement in neutral-driven transport with the conducting boundary installed was less than expected, presumably because the boundary was significantly misaligned to the magnetic surfaces [10].

Progress in the understanding and improvement of confinement in CNT is presented in detail in P.W. Brenner's thesis [11].

2.4 Equilibrium

Force balance and the fast temperature equilibration along the magnetic field lines determine that the electrons are in a Boltzmann distribution function on each magnetic surface, $n_e = N(\psi) \exp\left(e\phi/T_e(\psi)\right)$ [59]. ψ is the magnetic flux enclosed by a magnetic surface, and is commonly used as the magnetic surface coordinate [9] (on the magnetic axis of the surfaces, $\psi = 0$; while $\psi = 1$ corresponds to the last closed magnetic surface).

Equilibrium also has to satisfy Poisson's equation. Therefore, the fundamental equation describing the equilibrium of a pure electron plasma confined on magnetic surfaces is [59]:

$$\nabla^2\phi = \frac{e}{\varepsilon_0} N(\psi) \exp\left(\frac{e\phi}{T_e(\psi)}\right) \tag{2.2}$$

This non-linear equation has been solved numerically [20,45,58], showing some interesting features of CNT's equilibrium. Publications by T.S. Pedersen [58] and R.G. LeFrancois [45] investigate the benefits of having a conducting boundary conforming to the edge of the plasma, and the effects of varying the number of Debye lengths in the plasma. The electrostatic potential tends to be constant on surfaces where many Debye lengths are present ($\langle a \rangle / \lambda_D > 10$), but the potential varies significantly on magnetic surfaces for plasmas with few Debye lengths ($\langle a \rangle / \lambda_D \lesssim 1$).

Another intrinsic characteristic of the equilibrium in CNT is the existence of large density variations along the magnetic field lines. A similar effect has been observed in Penning traps [23], but the density variation in CNT is enhanced due to the large toroidal variation of the shape of the magnetic surfaces [44]. This large density variation was predicted numerically by R.G. Lefrancois [44], and confirmed experimentally by M.S. Hahn [28].

2.5 Diagnostics

2.5.1 Equilibrium measurements

Basic equilibrium experiments involve measuring the plasma potential, temperature, and density. Measurements of the radial profiles of these parameters are also done with simple 10 W tungsten filaments, working as emissive (hot) probes or Langmuir (cold) probes. The probes are mounted on the same ceramic rods used to hold the emitter filament. The emitter is usually aligned close to the magnetic axis to create the plasma, and the other filaments are used to diagnose the plasma at different radial locations between the axis and the plasma edge.

Electron temperature and density

T_e and n_e are determined through the interpretation of Langmuir I-V characteristics [42], which requires the simultaneous measurement of the current and voltage of a biased filament probe. The potential is measured using a voltage divider, and the current from the voltage drop across a resistor in series with the bias power supply and the probe.

In a pure electron plasma n_e cannot be obtained from the ion saturation current, as it is usually done in quasi-neutral plasmas [34]. However, n_e and T_e can still be determined from the Langmuir I-V characteristics. If the electrons are in a Maxwellian distribution, the I-V characteristics will present an exponential region, which becomes linear in a semi-logarithmic plot $\log(I_{probe})$ vs $V_{probe} - \phi_{plasma}$. This linear region has a slope proportional to $1/T_e$, and a y-intercept given by $\ln\left(\frac{1}{4} e n_e \bar{v}_e A\right)$ [42], where $\bar{v}_e$ is the average thermal speed of the electrons, and A is the area of the probe. Hence, T_e is obtained from the slope of a fit in the linear region, and n_e from the y-intercept. This method exponentially amplifies uncertainties in the y-intercept of the fit, which results in error bars in n_e of one order of magnitude in some cases. This measurement procedure was first developed by J.P. Kremer [42], then further refined by J.W. Berkery and M.S. Hahn, and is also extended in my thesis.

Plasma potential

The plasma potential was measured in this thesis using two different methods: the *deviation potential* [42] and the *emissive probe floating potential* [29]. The *deviation potential* method studies the hot (emissive) and cold (non-emissive) I-V characteristics of the same filament probe and determines the plasma potential as the potential at which the hot characteristic deviates from the cold curve (i.e., the hot probe becomes slightly more negative than the local plasma potential and begins to emit electrons). The *emissive probe floating potential* method measures the voltage required to float a hot emissive filament inserted in the plasma. The *deviation potential* method is generally more precise, but requires voltage sweeps over long time scales, and only steady-state values of the potential can be measured. A more detailed description of both procedures can be found in [29, 42] and also in Section 3.3.1 of this thesis.

The fluctuations in the plasma potential described in Chapters 4 and 5 were detected by

measuring the oscillating current in an internal emissive filament floated by having a capacitor to ground. The amplitude of the oscillations is given by the fluctuations of the potential in the plasma (converted from measurements of the current by using the I-V characteristic of the emissive filament). The floating emissive probe was attached electrically to a simple op-amp current to voltage converter circuit.

2.5.2 Spatial structure of the oscillations

Capacitive probes

A new set of capacitive probes[3] was designed and constructed for this thesis to study the toroidal and poloidal structure of the oscillations observed in the 78° tilt angle configuration. This method requires the use of a limiter to effectively measure the oscillations of the image charge in the probes. The limiter was installed at the thick poloidal cross-section of the torus scraping off the plasma at $\psi > 0.8$, and thus ensuring that the electrons leaving the plasma are not collected by the capacitive probes. Nevertheless, capacitive probes were successfully used in CNT's 64° configuration without a limiter installed in order to measure the poloidal structure of the ion-driven instability [50]. In that case, the capacitive probe misaligned furthest acted like a limiter collecting all of the electrons in the intersected magnetic surface.

Each capacitive probe was made of a copper disc of 5 cm in diameter, and was installed facing the plasma $\sim$ 2 cm away from the outermost magnetic surface. The probes were arranged in two different arrays perpendicular to each other. One array was made up of 5 probes placed around the thick poloidal cross-section of the stellarator. The second array consisted of 6 probes located along the toroidal angle. Fig. 2.2 shows the location of both probe arrays in a toroidal and a poloidal cross-section of the torus. The copper discs and the limiter were held by aluminium rods (0.45 cm in diameter), and ceramic washers were used to ensure that the probes were electrically isolated from the grounded aluminum structure. The assembly of the image charge probes and the limiter was installed in the spot normally used for the rotating probe. Although the two arrays consist of a discrete number of probes, they provide enough spatial resolution to determine the poloidal and toroidal mode numbers,

[3] I designed the set of capacitive probes and supervised its construction by the undergraduate students Derek Hernandez, Ignacio García-Cruzado, and Daniel Cosson.

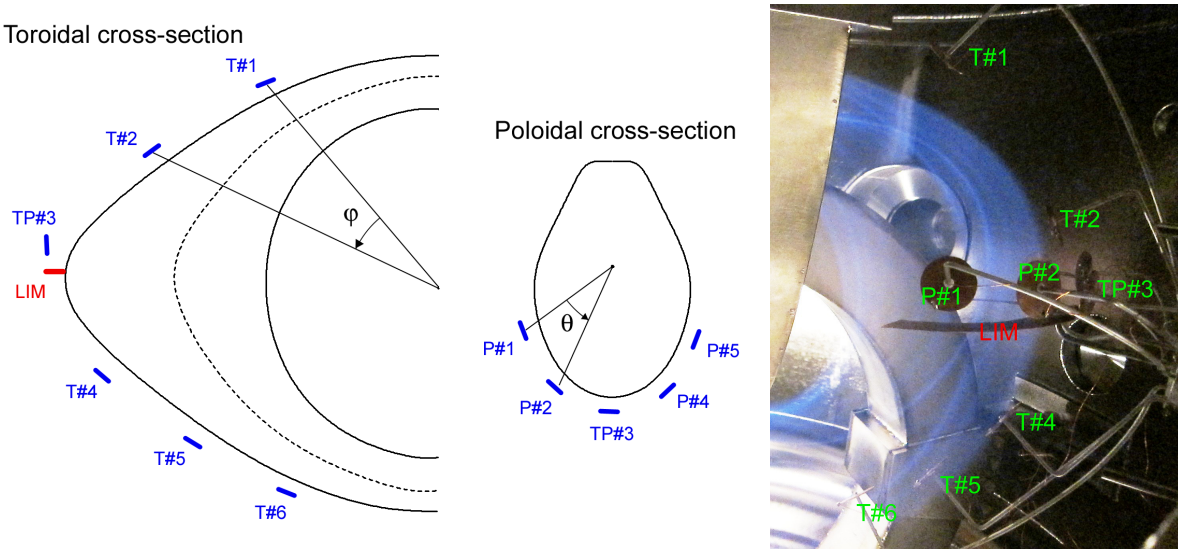

Figure 2.2: *Left and center:* Layout of the capacitive probe arrays in a toroidal cross-section, and around the thick poloidal cross-section of the torus (the dashed line is a projection of the magnetic axis). *Rigth:* The capacitive probes installed in the stellarator. $\psi = 0.8$ surface glowing in order to align the limiter and the probes.

and the direction of propagation of the mode by measuring the phase delay of the oscillations detected in the different probes.

Conducting boundary

The conducting boundary installed in CNT's 64° configuration consisted of 13 copper meshes electrically isolated from each other, so the different sectors could be also used as capacitive probes to characterize the structure of the modes. The conducting boundary was significantly misaligned (the meshes cut off $\psi > 0.63$ surfaces), and a limiter probe (initially installed to use the copper meshes as capacitive probes) was removed for the experiments conducted during this thesis, because it reduced the plasma volume even further.

The layout of the copper sectors was designed to provide some spatial resolution to measure the toroidal and poloidal structure of the modes. However, the spatial resolution of conducting boundary was quite limited (e.g., there were only 4 meshes covering the toroidal angle) and this resulted in significant spatial aliasing. For this reason, the measurements of

Table 2.1: Location of the capacitive probes. See layout of the probes in Fig. 2.2

Toroidal array	
Probe	φ angle wrt probe T♯1
T♯2	31°
TP♯3	44°
T♯4	63°
T♯5	83°
T♯6	105°

Poloidal array	
Probe	θ angle wrt probe P♯1
P♯2	26°
TP♯3	60°
P♯4	103°
P♯5	124°

the mode structure obtained with the conducting boundary were not conclusive by themselves. The spatial structure of the modes described in this thesis was studied by using the set of capacitive probes described in the previous subsection and a high speed camera.

Fast camera

Since CNT's plasmas emit sufficient light in the visible range for $p_n > 10^{-5}$ Torr [12], the characteristic low frequency oscillations of our quasi-neutral plasmas (Chapter 5) have been successfully observed for the first time in this thesis with a *Vision Research Phantom v7.1* camera [4]. This is a high speed SR-CMOS 8-bit monochrome camera. Movies at full resolution (800×600 pixels) can be taken at 4,800 fps (frames per seconds), but the camera can also record at sampling frequencies up to 160,000 fps at reduced resolution (limited by the maximum amount of data that the camera can handle per second). For this thesis, movies were typically captured at sampling frequencies between 40,000 and 75,000 fps, providing enough spatial and temporal resolution for the characterization of the mode. Higher frame rates yield unacceptable signal-to-noise ratios in CNT (less light is captured per frame as the sampling frequency is increased).

The plasma was recorded from two different observation ports in the vacuum chamber (Fig. 2.3): the "nw" side window (which looks radially into the plasma), and the top view window (looking perpendicularly at the thick poloidal cross section of the plasma). The fast

[4]The High Speed Camera was borrowed from the CTX experiment.

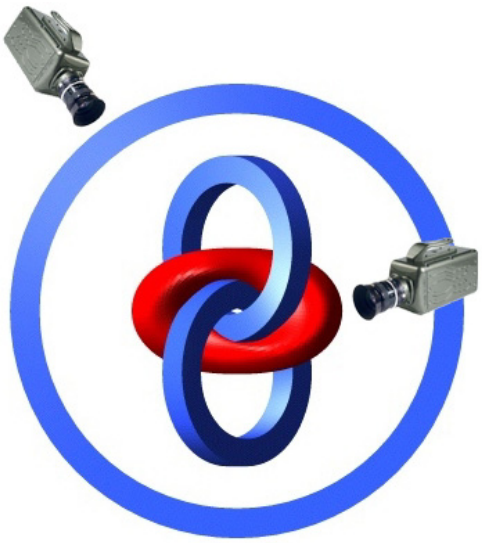

Figure 2.3: Representation of the view ports of the chamber used to record the plasma with the High Speed Camera: "nw" side port, and the top view port.

imaging experiments also made use of a floating emissive filament in order to correlate the density oscillations observed in the camera with the fluctuations of the plasma potential, and also use the signal in the electrostatic probe as the time reference to compare movies taken from different view ports.

2.5.3 Data acquisition

The different electronic circuits used to measure ϕ_{plasma}, T_e, n_e, the emission current, or the oscillations in the image charge provide an analog output between -10 and +10 V proportional to the plasma parameter of interest. These signals are collected by a 12 bit digitizer [5] operated at a maximum sampling frequency of $1.25/n$ MHz per channel (where n is the number of channels used in each card). In my experiments one card was usually sampling at low frequencies (typically 1-10 kHz per channel) to measure steady state parameters of the plasma (e.g., emitter bias voltage or emission current), while the other cards measured the oscillations in the plasma potential and higher sampling frequencies were required (sometimes only one channel had to be used per card to provide the maximum Nyquist frequency

[5] *National Instruments* PXI-6071E cards

available, 625 kHz). Signals recorded at high sampling frequencies were always filtered at the Nyquist frequency to avoid artifacts.

2.6 Relevant frequencies of CNT's plasmas

Most of my research concerns the characterization of oscillations in plasmas of arbitrary neutrality. In order to identify the physics involved in these oscillations it is essential to estimate the relevant frequencies in CNT and study its dependence on experimentally adjustable parameters (such as the magnetic field strength). Some important frequencies and timescales of our plasmas are briefly described below and summarized in Fig. 2.4:

1. **Electron parallel equilibration timescale**. The parallel equilibration timescale of electrons in magnetic surfaces ($\tau_{\|}$) can be estimated as the time a thermal electron needs to travel toroidally and poloidally around a magnetic surface.

$$\tau_{\|} \approx \frac{2\pi R}{\iota v_{th}} \tag{2.3}$$

   where R is the major radius of the plasma, ι is the rotational transform, and v_{th} is the electron thermal velocity ($v_{th} = \sqrt{2T_e/m_e}$). For a typical 4 eV plasma, $\tau_{\|} \approx 6\mu s$. Therefore, a plasma in equilibrium is expected to damp all frequencies below 150 kHz through parallel force balance.

2. **$\mathbf{E}\times\mathbf{B}$ rotation frequency**. Non-neutral plasmas present fast $\mathbf{E}\times\mathbf{B}$ drifts, due to their strong self $\mathbf{E}$ fields. In order to have an equilibrium, the plasma has to equilibrate on a magnetic surface through parallel dynamics faster than the $\mathbf{E}\times\mathbf{B}$ drift. Otherwise, a diocotron type instability [39] is likely to occur. The $\mathbf{E}\times\mathbf{B}$ rotation frequency is:

$$f_{E\times B} = \frac{E/B}{2\pi\langle a\rangle} \tag{2.4}$$

   where $\langle a\rangle$ is the minor radius of the plasma. CNT usually operates at magnetic field strengths between 0.02 and 0.1 T and the potential drop across the plasma is 50 V (when the 0 V boundary condition is set at the coils and the chamber) to 200 V (with a conducting boundary installed at the edge of the plasma). Thus, $f_{E\times B}$ typically ranges between 5 and 70 kHz.

3. **Ion bounce frequency**. Heavy ions (such as N_2^+) are largely unmagnetized in CNT (Fig. 3.14) and they follow complicated trajectories in the plasma. As heavy ions are drawn into the electron rich plasma, a large fraction of the potential drop in the plasma is transferred to their parallel velocity, and they bounce from one side of the electron plasma to another. In Penning traps the ion motion is analytically solvable [19], but in CNT ions do not present a simple well defined poloidal rotation frequency. Marksteiner's thesis [49] studied the distribution of the ion bounce frequencies in CNT, showing that essentially all N_2^+ ions at 0.02 T bounce between 14 and 83 kHz, with 25 kHz being the dominant bounce frequency.

4. **Cyclotron frequency**. A charged particle moving perpendicularly to the direction of a uniform magnetic field performs a circular motion at the cyclotron frequency. The cyclotron frequency is defined as:

$$f_c = \frac{qB}{2\pi m} \tag{2.5}$$

   Fig. 2.4 includes the electron cyclotron frequency and the cyclotron frequencies of the most commonly used ions in CNT.

5. **Plasma frequency**. The plasma (or Langmuir) frequency is defined as:

$$f_p = \frac{1}{2\pi}\sqrt{\frac{e^2 n_e}{\varepsilon_0 m_e}} \tag{2.6}$$

   The use of electrostatic Langmuir waves has been proposed to measure the electron density in CNT [29,41], but so far attempts to use this method have been unsuccessful, probably because of the poor RF coupling between the function generator and the antenna.

   For a pure electron -200 V plasma, $n_e \approx 10^{12}$ m^{-3}, while the density of CNT's quasineutral plasmas is $n_e \approx 10^{15}$ m^{-3}. Therefore, f_p ranges from 9 to 290 MHz.

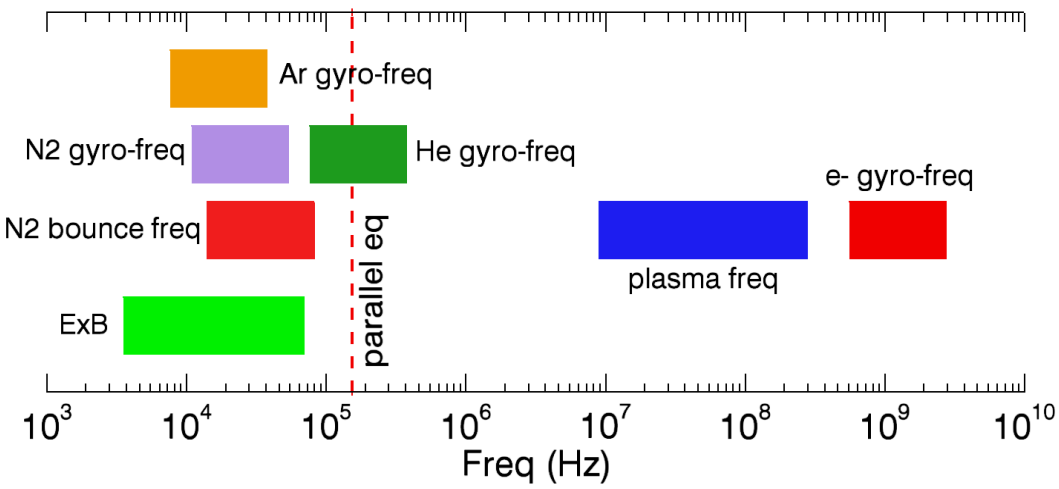

Figure 2.4: Relevant frequencies in typical CNT plasmas ($\phi_e = -200$ V, $0.02 \leq B \leq 0.1$ T).

Chapter 3

Plasmas of Arbitrary Neutrality

Even at CNT's base pressure ($p_n \leq 2 \cdot 10^{-8}$ Torr), neutrals are ionized in the vacuum chamber (preferentially at locations of high T_e, near the outer magnetic surfaces) and ions are drawn into the electron rich plasma, which would cause the neutralization of the plasma in ~ 0.5 s in the absence of an ion loss mechanism [2]. However, the ceramic rods inserted in the plasma act as steady state sinks for ions. The rods are charged up negatively with respect to the plasma (due to the finite T_e) and ions become neutralized when they collide with the rods. The ion content in our plasmas can be controlled by adjusting the neutral pressure in the chamber, thus varying the steady state balance between the ionization of neutrals and the recombination at the rods. At $p_n = 2 \cdot 10^{-8}$ Torr, the ion fraction ($f_i = n_i/n_e$) is calculated to be $f_i < 1\%$ [2]. CNT's pure electron plasmas are macroscopically stable [43], but the accumulation of ions affects the equilibrium and changes the properties of the plasma radically. This section describes how the plasma potential, ion gyro-radius, electron temperature, and dielectric constant evolve with the degree of neutralization of the plasma. An overview on the spontaneous oscillations detected in plasmas of arbitrary neutrality is given in Section 3.6. Chapters 4 and 5 describe in detail the oscillations observed in partially neutralized ($10^{-4} < \eta < 1$) and quasi-neutral plasmas ($\eta < 10^{-4}$) respectively.

Unless otherwise specifically stated, the experimental results shown in this Chapter refer to the 64° tilt angle configuration with the conducting boundary installed.

3.1 Presence of ions in CNT

A 7.4 cm^2 copper plate was inserted at $\psi \approx 0.4$ in the $\varphi = 90^\circ$ cross section of the torus in order to measure the ion density, and explore the role of the magnetic field strength, emitter bias, and neutral pressure. The ion density was determined through the interpretation of Langmuir I-V characteristics. Since the probe sheath expands as the probe is biased more negatively [34], the collected ion current increases with the probe potential, and I_{sat} was determined as the current at which $\phi_{\mathrm{probe}} - \phi_{\mathrm{plasma}} = -100\,\mathrm{V}$ from a linear fit of the ion saturation region. Ions in CNT are only weakly magnetized and are predicted to have kinetic energies that are a large fraction of the potential drop across the plasma, so the ion saturation current scales like Eq. 3.1:

$$I_{\mathrm{sat}} \approx eA_{\mathrm{probe}} n_i \sqrt{\frac{e\phi_p + 3T_e}{8m_i}} \tag{3.1}$$

This estimate was used to compute the ion content (n_i), instead of the Bohm sheath criterion. For electron-rich non-neutral plasmas ($|e\phi_p| \gg T_e$), Eq. 3.1 gives the ions a higher arrival rate than the Bohm criterion, while for CNT's quasineutral plasmas ($|e\phi_p| \ll T_e$) the ion velocity is essentially determined by the electron temperature, which is consistent with the Bohm criterion.

Both neutral pressure and emitter bias voltage are predicted to increase the ion content of the plasma since the ionization frequency scales linearly with the neutral number density, and the electron density and temperature increase with the emitter bias, causing the rate of ionization of neutrals to grow. Experimental results confirm the linear dependence of the ion density on neutral pressure and show a rapid increase of the ion fraction with the emitter bias (Fig. 3.1).

Although the magnetic field strength may reduce the transport rate, it does not affect the equilibrium in CNT directly and no clear relationship was found experimentally between n_e and B [41]. Numerical simulations [49] predict that the ion fraction can be 3.7 times higher at B = 0.1 T than at 0.02 T for plasmas with a non-negligible fraction of H_2^+. However, the effects of the magnetic field strength on the ion content are not totally understood based on the experimental results. The measured ion saturation current usually decreases slightly with the magnetic field strength, but this can be caused by an indirect effect of the measuring procedure. At higher B fields, ions become somewhat magnetized and their orbits may be

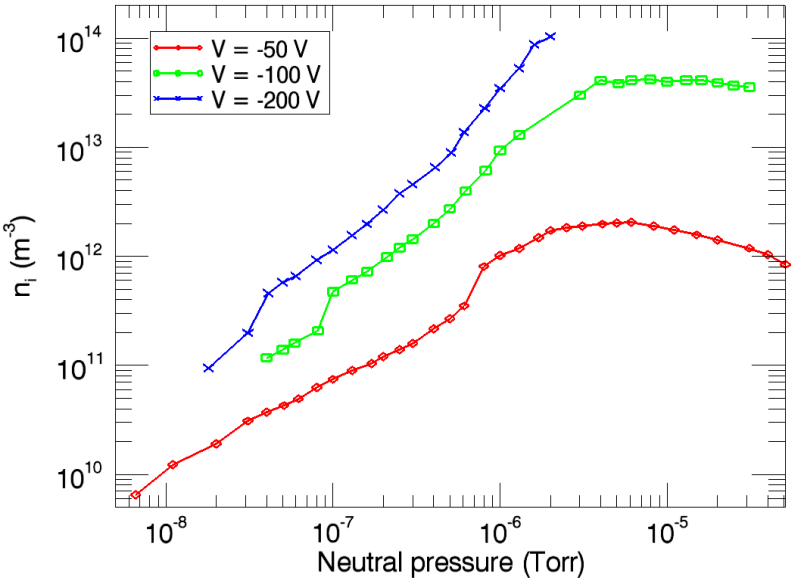

Figure 3.1: Ion content in CNT as a function of the neutral pressure for three different emitter biases ($N_2^+ - e^-$ plasmas at B = 0.08 T).

sufficiently affected that the probe cannot collect ions from all directions, thus reducing the ion saturation current.

For $B \geq 0.06\,\mathrm{T}$ and $\phi_e \geq -100\,\mathrm{V}$, the ion content saturates for neutral pressures above $4 \cdot 10^{-6}$ Torr (Fig. 3.1). This observation may be a further proof that our plasmas become quasi-neutral at high neutral pressures. The saturation of the ion content at high neutral pressures is also expected for the most negative emitter bias (-200 V). However, the power supplies used for these experiments cannot handle ion saturation currents above $100\,\mu A$ (which corresponds to $n_i \approx 1.5 \cdot 10^{14}\,\mathrm{m}^{-3}$), and also when values of the measured current approach this technical limit, it becomes harder to interpret the Langmuir I-V characteristics (no linear slope associated to the ion saturation current is observed in the I-V curves). This is the reason why the ion content at $\phi_e = -200\,\mathrm{V}$ could not be measured above $2 \cdot 10^{-6}$ Torr in Fig. 3.1. At the highest neutral pressures ($p_n \geq 10^{-5}$ Torr) the emission current is a strong function of the temperature of the emitter filament, and the slight drop of the ion density at the lower bias voltages is believed to be related with a small fall in the power supplied by the batteries used to heat the emitter filament.

Ion probes of the same dimensions and characteristics were aligned parallel and perpendicularly to the magnetic field lines (minimizing for each orientation the fraction of magnetic surfaces intersected by the probe). It was observed that the measured ion saturation current is not dependent on the orientation of the probe relative to the field lines, which is typical for plasmas where the ions are weakly magnetized.

3.2 Degree of non-neutralization (η)

In order to obtain more meaningful interpretations of the behavior of the relevant parameters under study in partially neutralized plasmas, it is convenient to define the degree of non-neutralization of the plasma (η) as the difference between the electron and the ion density divided by the total density of charged particles in the plasma (Eq. 3.2):

$$\eta \equiv \left| \frac{n_e - Z n_i}{n_e + Z n_i} \right| \tag{3.2}$$

Fig. 3.2 shows how CNT can vary continuously η from 1 (pure electron plasmas, essentially reached at base pressures) to $\ll 1$ (quasi-neutral plasmas) by adjusting the neutral pressure in the chamber, thus varying the steady state balance between the ionization of neutrals and the recombination at the rods. CNT is not only able to vary continuously η, but also to operate steadily at any given value of η shown in Fig. 3.2. Penning-Malmberg traps and pure toroidal cannot confine partly neutralized or quasi-neutral plasmas, and operate close to $\eta = 1$. Table 3.1 provides an estimation of η for other representative plasmas, showing that CNT can operate in a range of η values that expand 5 orders of magnitude, while other quasi-neutral experiments present very limited flexibility to vary η significantly, but typically operate at degrees of non-neutralization 3 orders of magnitude lower. The estimates of η for quasi-neutral experiments in Table 3.1 assumed $|e\phi| \approx T_e$, which is generally true in quasi-neutral plasmas to satisfy ambipolarity.

η cannot be accurately determined using the experimentally measured values of n_e and n_i only. The measurements of n_e in CNT are affected by large uncertainties (almost one order of magnitude in some cases); the I-V characteristics used to determine n_e are rather noisy in partially neutralized plasmas [42], and the probe bias power supplies cannot handle the currents involved in measurements above 10^{-6} Torr ($n_e \gtrsim 10^{14}$ m^{-3}).

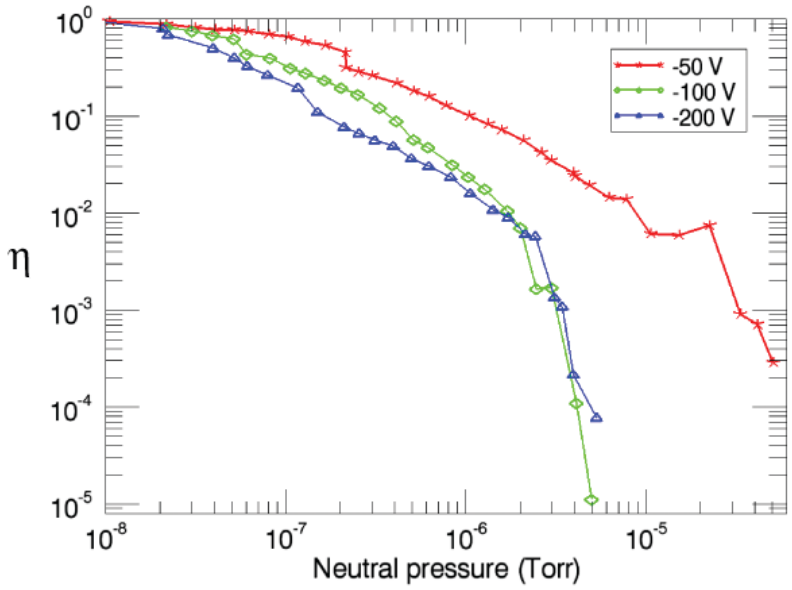

Figure 3.2: Degree of non-neutralization (η) as a function of the neutral pressure in the chamber for different emitter bias voltages ($N_2^+ - e^-$ plasmas at 0.02 T).

Table 3.1: Estimation of η for other representative plasmas

	n_e (m^{-3})	T_e (eV)	minor radius (m)	η
Penning-Malmberg trap [48]	10^{12} - 10^{13}	1	0.015	1
LNT-II pure toroidal trap [76]	$5 \cdot 10^{12}$	1 - 100	0.05	1
CNT	10^{12} - 10^{16}	4 - 60	0.15	$10^{-5} - 1$
JT60 [36]	$3 \cdot 10^{19}$	10^4	0.89	$5 \cdot 10^{-8}$
HBT-EP [52, 72]	10^{19}	70	0.15	$3 \cdot 10^{-8}$
DIII-D [68]	10^{20}	$5 \cdot 10^3$	0.7	10^{-8}
ITER [31, 73]	10^{20}	$5.3 \cdot 10^3$	2	$1.5 \cdot 10^{-9}$

In this thesis η is determined with good accuracy using Poisson's equation, and assuming CNT plasma has a cylindrical geometry of radius $r = 0.15$ m. From Poisson's equation in a cylinder:

$$\frac{1}{r}\frac{\partial}{\partial r}\left(r\frac{\partial \varphi}{\partial r}\right) = -\frac{\sigma}{\varepsilon_0}$$
$$\varphi(r) = -\frac{\sigma}{4\varepsilon_0}r^2 + \varphi(0) \tag{3.3}$$

where, $\sigma = q_i n_i - e n_e$, the electron and ion density profiles are assumed to be flat, n_i is measured from the ion saturation current in a copper probe (affected by smaller error bars than n_e), the plasma is grounded at the edge ($\varphi(r = 0.15) = 0\,\mathrm{V}$), and $\varphi(0)$ is taken from the measurements of the plasma potential very close to the magnetic axis ($\psi \approx 0.1$, see Section 3.3), which is typically known within ± 1 V.

Therefore, the electron density can be calculated as:

$$n_e = n_i - \frac{4\varepsilon_0}{er^2}\varphi(0) \tag{3.4}$$

And the determination of η is trivial using Eq. 3.2:

$$\eta = \left|\frac{-\frac{4\varepsilon_0}{er^2}\varphi(0)}{2n_i - \frac{4\varepsilon_0}{er^2}\varphi(0)}\right| \tag{3.5}$$

In order to check the validity of the method, the electron density was calculated using Eq. 3.4 and compared with the experimental measurements of n_e obtained interpreting the I-V characteristic of a cold filament [42]. Fig. 3.3 shows that the estimated values of n_e in the cylindrical plasma are in good agreement with the experimental measurements. For pressures below $2 \cdot 10^{-7}$ Torr, the estimation of n_e in a cylinder is within the error bars of the experimental results, and for higher pressures, the value obtained from Eq. 3.4 seems to be a reasonably good estimate. At base neutral pressures ($\mathrm{p_n} \leq 2 \cdot 10^{-8}$ Torr), the estimate obtained from Poisson's equation can also be compared with numerical reconstructions of the equilibrium in CNT [20], finding also good agreement between the approximate expression of Eq. 3.4 in a cylinder, and the numerical reconstructions in CNT's complicated 3D geometry.

There are two factors that account for the rapid drop of η when the neutral pressure is increased (Fig. 3.2). Most importantly, as n_i increases, the number of electrons grows accordingly trying to maintain the voltage drop across the plasma, and the term $\frac{4\varepsilon_0}{er^2}\varphi(0)$

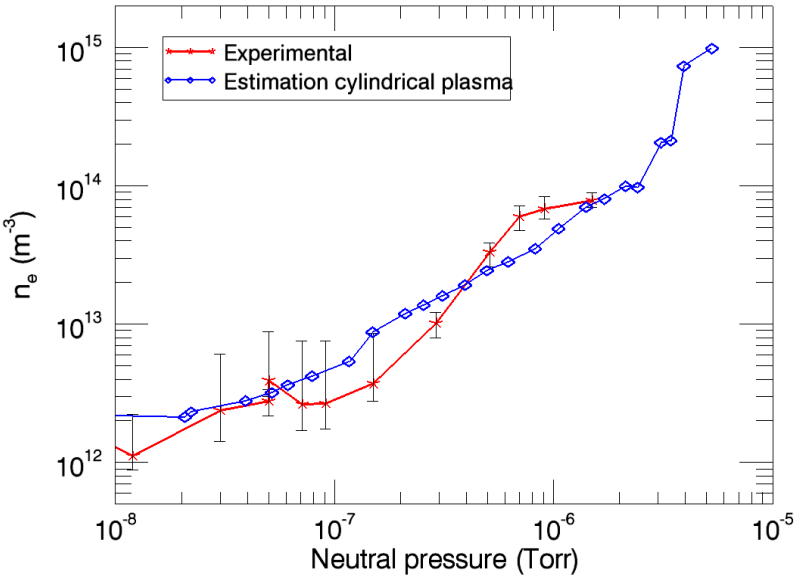

Figure 3.3: Comparison of the measured electron density with the estimation of n_e assuming a cylindrical geometry (Eq. 3.4). $N_2^+ - e^-$ plasmas, B = 0.02 T, ϕ_e = -200 V.

matters less. But also when the plasma decouples from the emitter bias (see Section 3.3), the term $\frac{4\varepsilon_0}{er^2}\varphi(0)$ becomes smaller, specially for $p_n > 2 \cdot 10^{-6}$ Torr (see Fig. 3.4).

3.3 Plasma potential

One of the clearest consequences of the accumulation of ions in CNT is the decoupling of the potential profiles from the emitter bias voltage. In pure electron plasmas the emitter bias voltage dictates the plasma potential. Even when the degree of non-neutralization decreases from $\eta \approx 1$ to 0.1, the ion content grows, but the electron density increases accordingly to maintain the voltage drop across the plasma (Fig. 3.5). However, for $\eta < 0.1$ the plasma potential (ϕ_p) begins to decouple from the emitter bias (ϕ_e). Pure electron plasmas in CNT are characterized by strong negative electric fields imposed by the emitter bias, but as our plasmas approach quasineutrality the electrostatic potential is much more modest, since it comes close to that which would be set by ambipolarity as the injection of electrons matters less for the radial fluxes of charge.

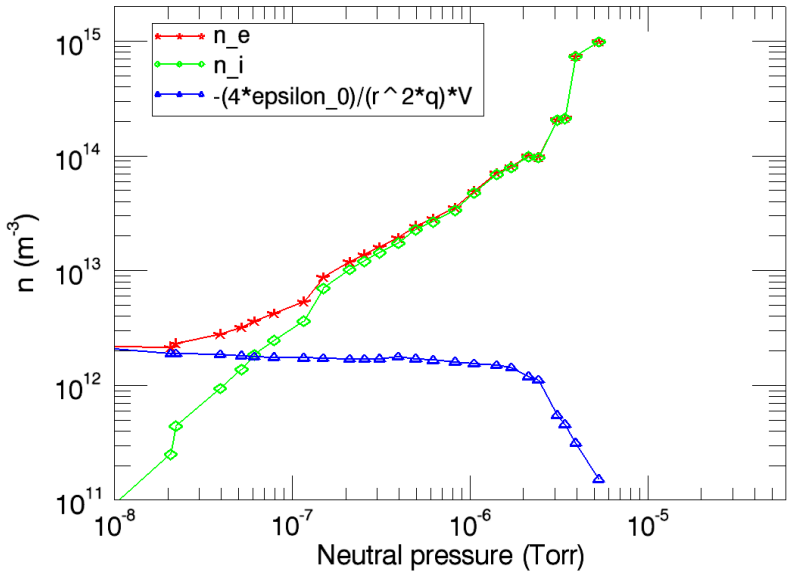

Figure 3.4: Evolution of the different terms in Eq. 3.4 as a function of neutral pressure ($N_2^+ - e^-$ plasmas, B = 0.02 T, ϕ_e = -200 V).

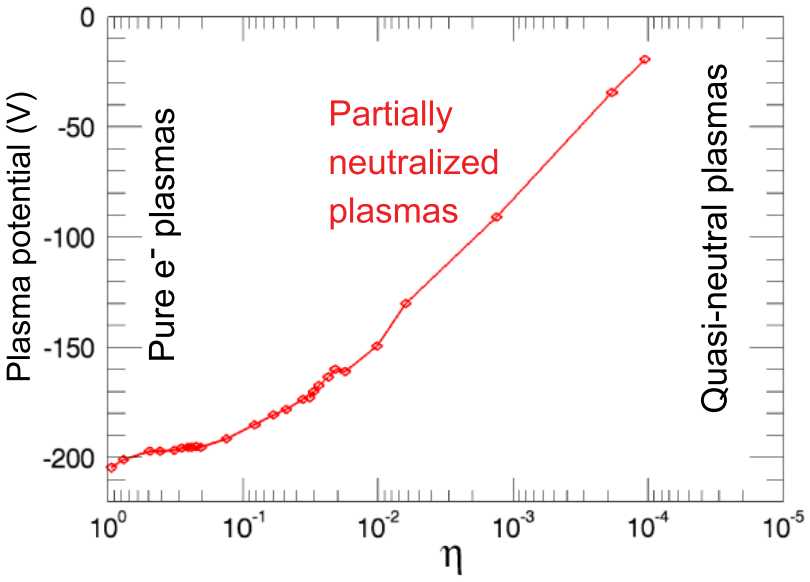

Figure 3.5: Evolution of the plasma potential at $\psi \approx 0.1$ while emitting electrons on the magnetic axis at -200 V ($N_2^+ - e^-$ plasmas, B = 0.02 T).

3.3.1 Methods for the measurement of ϕ_p

Two methods have been used in order to determine the plasma potential: the *deviation potential* [42] and the *emissive probe floating potential* [29]. The *deviation potential* method compares the hot (emissive) and cold (non-emissive) I-V characteristics of the same probe. The probe used is a halogen filament, which can only collect charged particles when cold, but can emit electrons by thermionic emission when the filament is heated. The plasma potential is determined as the potential at which the hot probe is slightly more negative than the plasma potential, and starts to emit electrons (the hot I-V characteristic deviates from the cold curve). The *emissive probe floating potential* method measures the voltage required to float a hot emissive filament. For this purpose, a current source is used to bias the heated filament at the voltage where the current is set to emit a few nA, thus the hot filament is reasonably close to floating. Having a source emitting a few nA only affects marginally our plasmas at base neutral pressures, where the emission currents are of the order of a few μA.

For $\eta > 0.1$, the *deviation potential* method is more accurate, but as the ion content increases, the plasma becomes hotter, and the characteristic of the hot filament becomes less sharp resulting in less accurate measurements. Also, the *deviation potential* requires voltage sweeps over a long time and the power supplies used to bias the probes cannot handle the currents involved in the measurements where $\eta < 0.01$. The *emissive probe floating potential* method introduces a systematic error in the measurements ($\phi_{float} = \phi_p - \alpha T_e/e$, where $\alpha \leq 1$ [80]), but the method is robust in the entire range of pressures explored experimentally and measurements are in good agreement with the *deviation potential* results where it is possible to use both methods.

3.3.2 Parameter dependence

A series of experiments were conducted to study systematically the dependence of the plasma potential on the degree of non-neutralization, emitter bias voltage, magnetic field strength, ion species, and magnetic configuration. For the experiments described in this Section, the potential was measured using a heated emissive filament placed at $\psi \approx 0.15$ (spot ♯2 of the nw4 probe array) and floated by using the current source circuit.

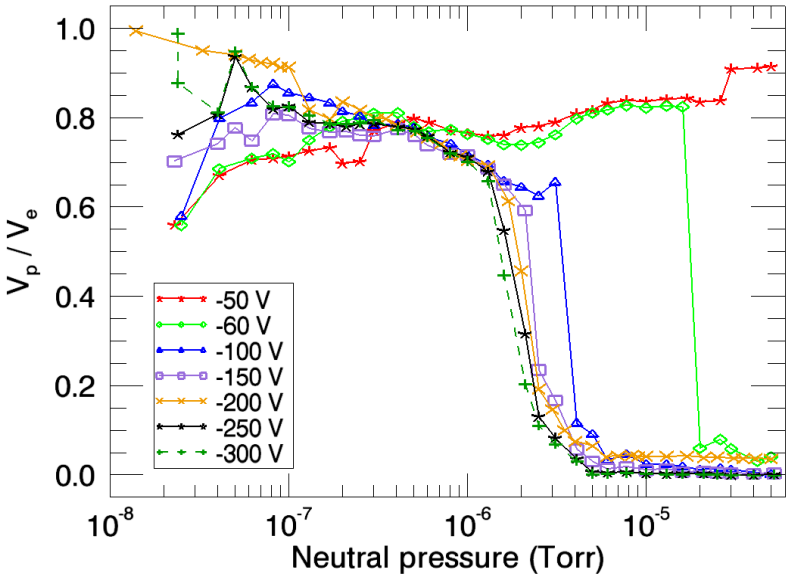

Figure 3.6: ϕ_p/ϕ_e at $\psi \approx 0.15$ as the neutral pressure is increased for different emitter bias voltages ($N_2^+ - e^-$ plasmas at 0.06 T).

Effect of the emitter bias and the ion content

Basic observations show that the plasma potential decouples rather abruptly from the emitter bias at a certain neutral pressure threshold. This threshold is a function of the emitter bias, at lower emitter biases the plasma decouples from the emitter at higher pressures (Fig. 3.6). Even the potential profiles do not detach from the emitter in a $\phi_e = -50$ V plasma at $B \geq 0.04$ T for the range of pressures explored in the experiments ($p_n \leq 5 \cdot 10^{-5}$ Torr). This suggests that the ion content may be responsible of the separation of the plasma potential profiles from the emitter (more negative emitter bias voltages are associated with higher electron densities, and thus higher ionization rates).

Analyzing the plasma potential as a function of the ion content in our plasma, it can be seen that the potential of the floating emissive probe drops below 50% of the emitter bias when the ion content exceeds a threshold between $5 \cdot 10^{13}$ and 10^{14} m^{-3} (Fig. 3.7). In the experiments performed with -50 V plasmas, the ion content only reaches $5 \cdot 10^{13}$ m^{-3} at the lowest B field explored (B = 0.02 T) and therefore the potential in the floating emissive probe always remains close to the emitter bias ($0.7 < \phi_p/\phi_e < 1$) for $B \geq 0.04$ T.

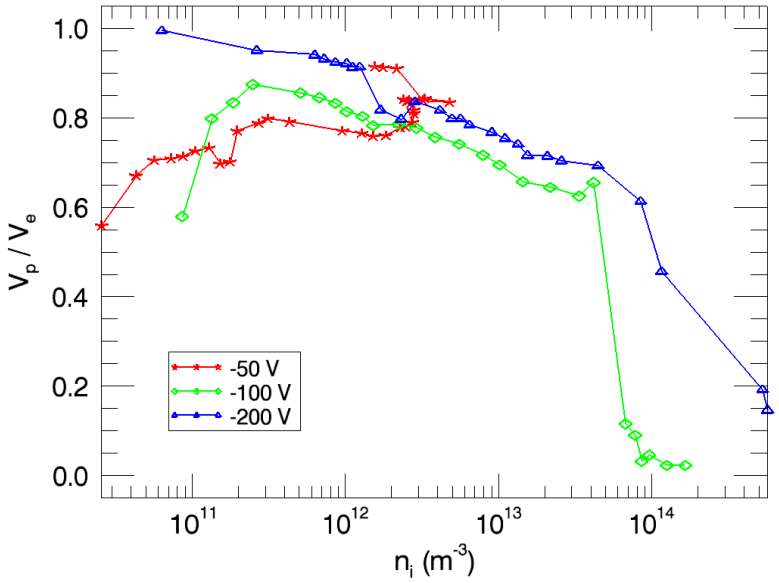

Figure 3.7: ϕ_p/ϕ_e at $\psi \approx 0.15$ as a function of the ion content in the plasma ($N_2^+ - e^-$ plasmas at 0.06 T).

However, the abrupt decoupling of the plasma potential from the emitter bias voltage coincides with the onset of the saturation of the emission current (see Fig. 3.17), suggesting that the decoupling might be related to the emission limit of the filament used to create the plasma. The emitter filaments used in CNT are rated for 6 V, but 4 V batteries produce enough heating to emit electrons and are normally used to produce our plasmas. The emission limit depends on the temperature of the emitter filament, which in turn, is a function of the current supplied by the heating battery. Fig. 3.8 shows the emission current limit of CNT's filaments when a 4 V and a 6 V battery are used for heating. In order to eliminate the effect of the plasma in the investigation of the emission limit, no B field was generated by the coils during these experiments, which prevented the formation of plasma. For $\phi_e = -200$ V (which is a usual operating point in our experiments), a filament heated by a 6 V battery can emit 4 times more current than when a 4 V battery is used.

Therefore, in order to clarify whether the separation of the plasma potential from the emitter is caused by an emission limit or occurs when a threshold ion content is exceeded, a set of experiments was conducted to study how the decoupling threshold depends on the emitter

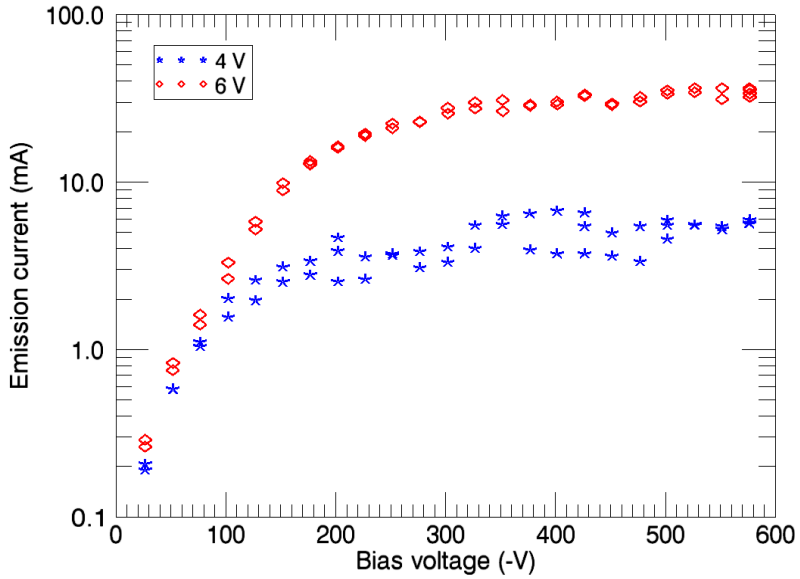

Figure 3.8: Emission current limit of the filament used to create the plasma as function of the filament bias voltage and for two different heating batteries (4 and 6 V). The filament did not create a plasma during these experiments.

filament temperature and the presence of an additional ceramic rod in the plasma. Although the emitter filament is able to emit significantly higher currents when a 6 V battery is used for heating, Fig. 3.9 shows that the decoupling of the plasma potential occurs essentially at the same neutral pressure when either a 4 V or a 6 V battery is used, implying that the mechanism of the plasma potential detachment is not related to the emission limit. When an additional rod is inserted in the thin cross section of the plasma, the ion density at a given neutral pressure is halved everywhere [49]. The neutral pressure scan performed with a second ceramic rod inserted in the plasma shows that the pressure threshold where the plasma potential drops below 50% of the emitter bias occurs at approximately two times higher pressure (Fig. 3.9), which essentially corresponds to the same ion content threshold as when a single rod is present. This provides strong evidence to conclude that the ion content is responsible of the decoupling of the plasma potential from the emitter bias.

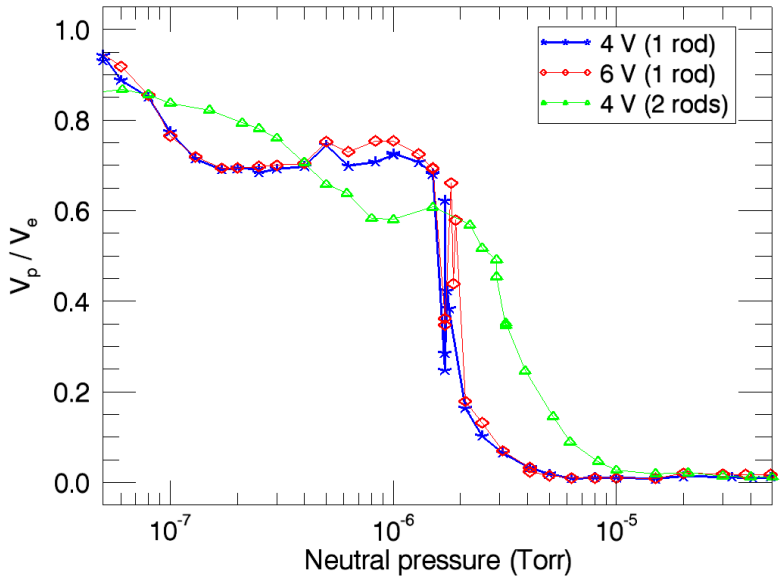

Figure 3.9: ϕ_p/ϕ_e as function of p_n, evaluating the effect of different filament temperatures (4 and 6 V heating batteries) and the presence of an additional ceramic rod in the plasma ($N_2^+ - e^-$ plasmas at 0.04 T).

Effect of the magnetic field strength

The role of the magnetic field strength on the threshold required for the plasma potential to decouple remains unclear. For low emitter bias voltages ($|\phi_e| \leq 100$ V), plasmas with more magnetized ions detach from the emitter bias at higher neutral pressures (Fig. 3.10). However, for $|\phi_e| \geq 150$ V the pressure threshold of the potential decoupling is independent of the magnetic field strength.

When the plasma is completely decoupled from the emitter ($0 < \phi_p/\phi_e < 0.1$), $|\phi_p|$ increases with the magnetic field strength (charge is confined better at higher B field strengths), and typically higher $|\phi_e|$ are associated to slightly lower measured values of $|\phi_p|$ (because plasmas created by more negative emitter bias voltages present higher ion contents). When the plasma potential is dictated by the emitter ($0.8 < \phi_p/\phi_e < 1$), $|\phi_p|$ is somewhat smaller for higher magnetic field strengths.

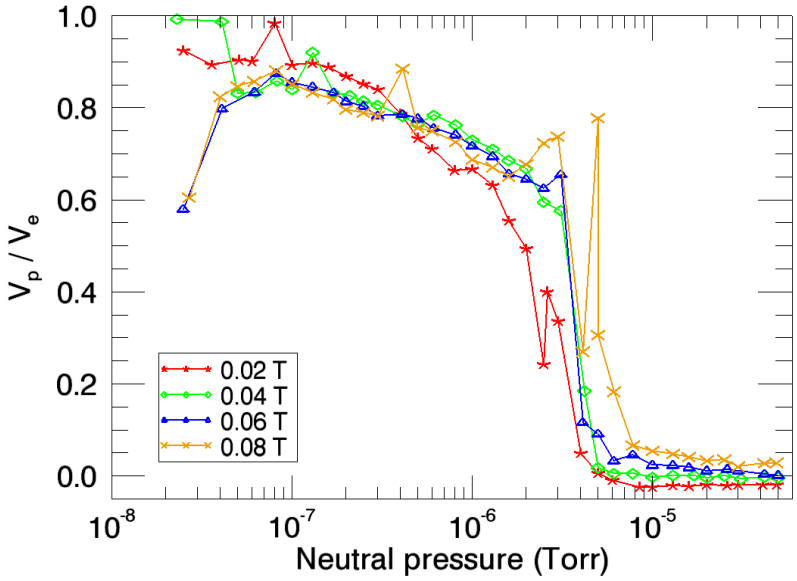

Figure 3.10: Evolution of ϕ_p/ϕ_e at $\psi \approx 0.15$ while emitting electrons on axis at -100 V (background pressure of N_2).

Effect of different ions species

The behavior of the potential in a floating emissive probe inserted in plasmas with different ion masses ($Ar^+ - e^-$ and $He^+ - e^-$ plasmas) is very similar to the results described so far for $N_2^+ - e^-$ plasmas (Figs. 3.6 to 3.10). The ionization energies for Ar and N_2 are very similar (15.76 eV for Ar, and 14.53 eV for N) and Fig. 3.11 shows that the plasma potential detaches from the emitter at essentially the same pressure (slightly lower for the case of Ar). He has a much higher ionization energy (24.59 eV) and the plasma potential decouples from the emitter bias at one order of magnitude higher pressures ($\sim 10^{-5}$ Torr).

Effect of the magnetic configuration

The behavior of the plasma potential is almost identical in the 78° and the 64° configurations. However, at high magnetic fields strengths ($B \geq 0.06$ T) and degrees of neutralization close to quasi-neutrality ($4 \cdot 10^{-6} < p_n < 2 \cdot 10^{-5}$ Torr), the measured floating emissive potential is more negative for the 78° tilt angle (Fig. 3.12).

The dependence of the floating emissive potential on the emitter bias voltage and the

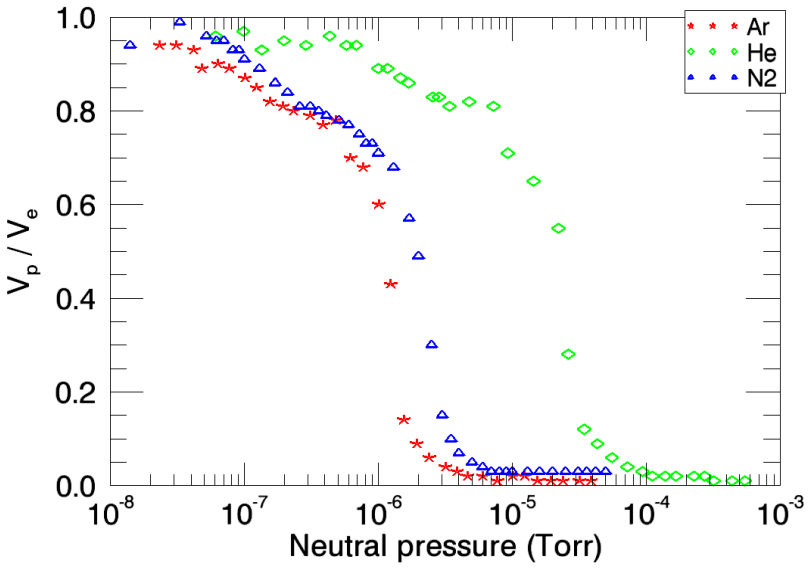

Figure 3.11: ϕ_p/ϕ_e vs. neutral pressure for $Ar^+ - e^-$, $He^+ - e^-$ and $N_2^+ - e^-$ plasmas ($\phi_e = -200$ V, B = 0.04 T).

magnetic field strength is very similar for both tilt angles. Partially neutralized plasmas ($p_n < 10^{-6}$ Torr) present potentials very close to the emitter bias for both configurations and all the magnetic field strengths and emitter voltages explored ($0.02 \leq B \leq 0.1$ T, and $-400 \leq \phi_e \leq -100$ V). Partially neutralized plasmas in the 78° configuration exhibit potentials somewhat closer to the emitter bias ($\phi_p/\phi_e > 0.80$ for the 78° configuration, while $\phi_p/\phi_e > 0.73$ for the 64° configuration). Quasineutral plasmas present plasma potentials slightly more negative in the 78° tilt angle. The behavior of the plasma potential in quasineutral plasmas is essentially the same in both configurations: $|\phi_p|$ increases with the magnetic field strength (Fig. 3.13), and more negative emitter biases are associated to higher ion content, and thus the ratio ϕ_p/ϕ_e gets closer to ~ 0.

3.4 Ion gyro-radius and electron temperature.

As the plasma potential (ϕ_p) decouples from the emitter bias (ϕ_e), the emitted electrons are accelerated ($\triangle\phi = \phi_e - \phi_p$) and, since CNT is essentially a collisionless plasma, the electrons

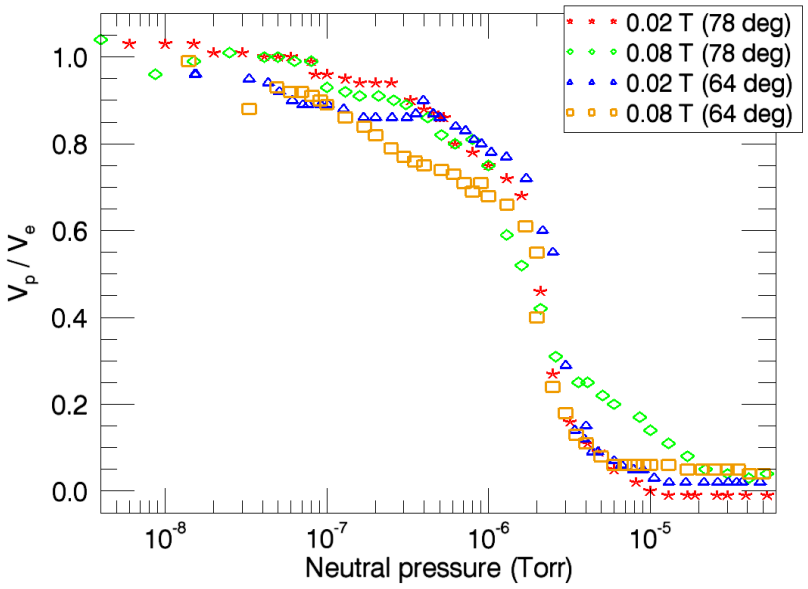

Figure 3.12: ϕ_p/ϕ_e vs. neutral pressure for the two stellarator configurations studied so far: 64° and 78° tilt angle (electron-rich N_2^+ plasmas, $\phi_e = -200$ V, 0.02 and 0.08 T).

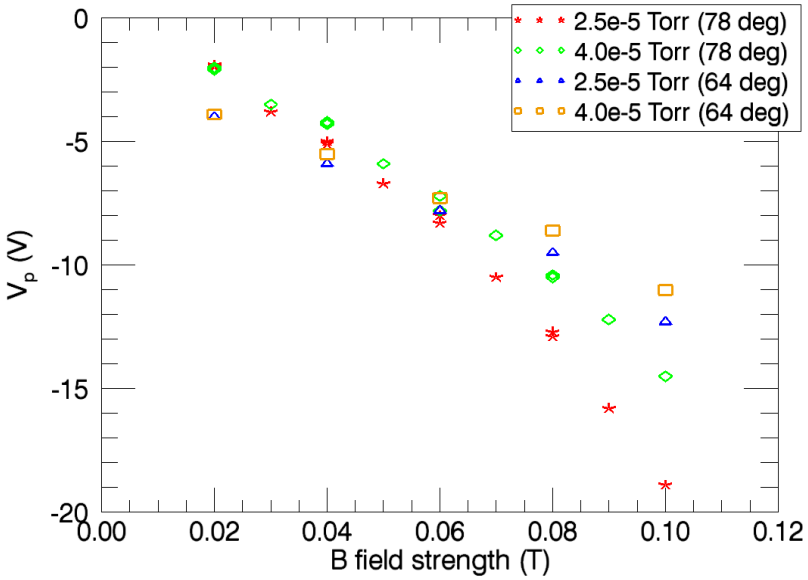

Figure 3.13: Comparison of the dependence of the plasma potential on the magnetic field strength for the 64° and the 78° tilt angle ($N_2^+ - e^-$ quasineutral plasmas, $2.5 \cdot 10^{-5}$ and $4.0 \cdot 10^{-5}$ Torr, $\phi_e = -200$ V).

become hotter (Fig. 3.14). The limitations with the power supplies described earlier in this chapter prevented us from measuring T_e for $\eta < 10^{-2}$ in this set of experiments.

Ions, however, exhibit the opposite behavior. Part of the potential drop across the plasma is transferred to the ions' kinetic energy as they are drawn into the electron-rich plasma. The ion motion is analytically solvable in a simple cylindrical plasma confined by an axial magnetic field. The ion fluid rotates as a rigid body at a frequency ω_i given by [18]:

$$\omega_i = -\frac{1}{2}\omega_{ci}\left[1 - \left(1 + \frac{4\omega_{E\times B}}{\omega_{ci}}\right)^{1/2}\right] \tag{3.6}$$

where ω_{ci} is the ion cyclotron frequency, $\omega_{ci} = qB/m_i$, and $\omega_{E\times B}$ is the equilibrium $E \times B$ rotation frequency of the plasma. In the presence of strong magnetic fields and for light ion species, ω_i approaches $\omega_{E\times B}$, thus as the plasma detaches from the emitter bias (the potential drop across the plasma becomes smaller), the ions get colder. Fig. 3.14 assumes the average perpendicular velocity of the ions in CNT is the $E \times B$ velocity, and shows how the ion gyro-radius ($r_{Li} = m_i v_{E\times B}/qB$) normalized wrt the average minor radius of the torus ($\langle a \rangle = 0.15$ m) evolves with η for a typical operating point of our experiments (B = 0.02 T). When $\eta \approx 1$ the ion gyro-radius is substantially bigger than the minor radius of the plasma, $r_{Li} \gg \langle a \rangle$ (ions are highly unmagnetized), but quasi-neutral plasmas ($\eta \approx 0$) present ion gyro-radii of a few centimeters ($r_{Li} < \langle a \rangle$).

3.5 Perpendicular dielectric constant

In CNT's partially neutralized plasmas the measured frequency of the electric field oscillations (ω) is comparable to the ion gyro-frequency (ω_{ci}), therefore the perpendicular dielectric constant ($\varepsilon_\perp$) has to be evaluated as [27]:

$$\varepsilon_\perp = 1 + \frac{q^2 n_i}{\varepsilon_0 m_i(\omega_{ci}^2 - \omega^2)} \tag{3.7}$$

At low B field strengths ($B \leq 0.04$) partially neutralized plasmas present oscillations such that $\omega > \omega_{ci}$ (see Fig. 2.4 and Chapter 4), hence $\varepsilon_\perp$ is negative, and incident waves will not penetrate deep into these plasmas. Fig. 3.15 evaluates $\varepsilon_\perp$ for B $\leq$ 0.04 T taking ω as the measured frequency of the ion resonant mode characterized in Section 4.2. For B $\geq$ 0.06 T

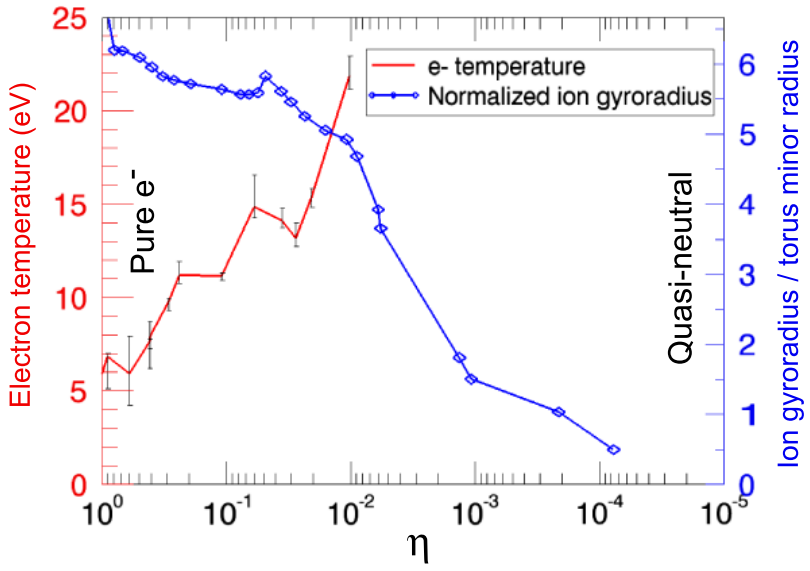

Figure 3.14: Measured electron temperature compared to the normalized ion gyro-radius as a function of the degree of non-neutralization ($N_2^+ - e^-$ plasmas at $\phi_e = -200$ V and B = 0.02 T).

$\varepsilon_\perp$ is always positive and grows more that 3 orders of magnitude as the plasma evolves from pure electron ($\varepsilon_\perp \approx 1$) to quasineutral ($\varepsilon_\perp \approx 2 \cdot 10^3$, Fig. 3.16). In Fig. 3.16 (B = 0.06 T) we can also see that the electric field oscillations hit the resonance $\omega \approx \omega_{ci}$ at $\eta \approx 0.1$. Since ω_{ci} grows with the B field strength and the measured frequency of the E field oscillations decreases slightly with B, this resonance is not observed at higher magnetic field strengths.

3.6 Oscillations in plasmas of arbitrary neutrality. Basic observations

One of the most relevant changes observed in partially neutralized plasmas in CNT is the spontaneous appearance of unstable fluctuations when a certain ion content is exceeded. Figs. 3.17 and 3.18 summarize the characteristics of the oscillations observed in partially neutralized plasmas. Pure electron plasmas exhibit stable behavior: the charge loss rate (emission current) scales linearly with the neutral pressure, and only oscillations with a very

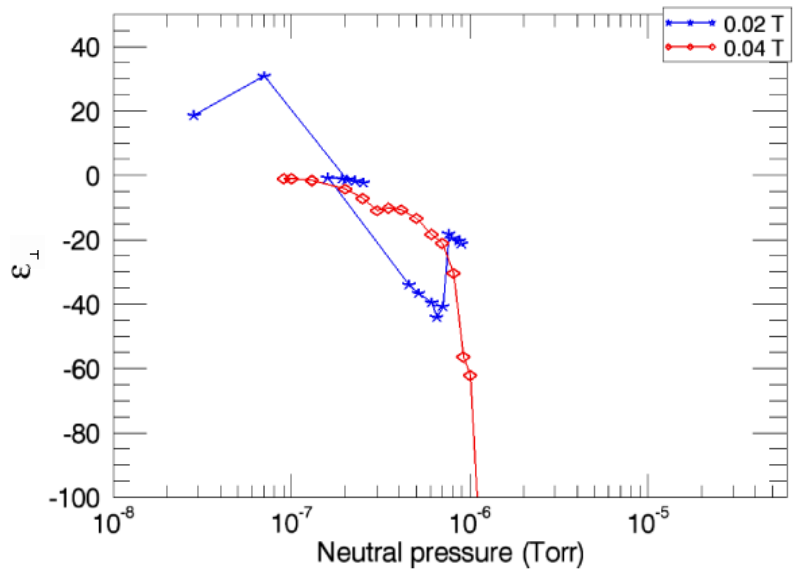

Figure 3.15: The perpendicular dielectric constant ($\varepsilon_\perp$) presents negative values for $B \leq 0.04$ T ($N_2^+ - e^-$ plasmas at $\phi_e = -200$ V). The frequency of the electric field oscillations (ω) is taken from the characterization of the ion-driven mode presented in Section 4.2.

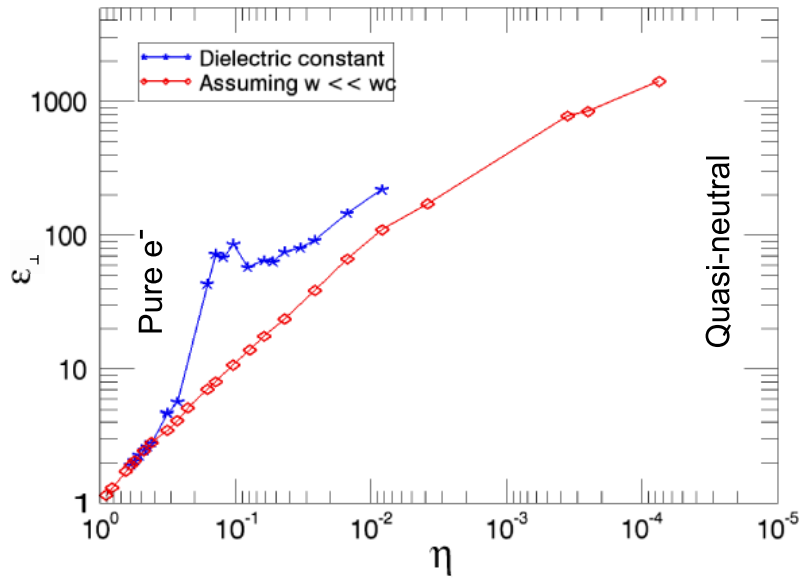

Figure 3.16: Perpendicular dielectric constant ($\varepsilon_\perp$) as a function of the degree of non-neutrality of our plasma ($N_2^+ - e^-$ plasmas at $\phi_e = -200$ V and B = 0.06 T).

small signal-to-noise ratio are detected in a floating emissive probe inserted in the plasma. The amplitude of the plasma oscillations starts increasing for $\eta \lesssim 0.1$, and simultaneously the loss rate of confined particles is enhanced, implying than the unstable fluctuations degrade confinement. This was first reported by Q.R. Marksteiner [50], and was also observed in this thesis (Fig. 3.17). A typical Fourier Spectrum of the detected oscillations is shown in Fig. 3.18. When partially neutralized plasmas become robustly unstable, multimode fluctuations are observed. The power spectrum broadens for $\eta < 4 \cdot 10^{-2}$ and is eventually dominated by a ~ 200 kHz mode. As the plasma accumulates more ions, the amplitude of the oscillations grows steadily until a maximum is reached at $\eta \approx 3 \cdot 10^{-3}$, coinciding with the onset of the saturation of the charge loss rate. Partially neutralized plasmas with more magnetized ions (either by raising the B field above 0.04 T or introducing light ions species, such as He^+) exhibit a single dominant mode (20 - 100 kHz) for degrees of non-neutralization between $\eta = 0.01$ and 0.1. When the plasma approaches quasi-neutrality ($\eta < 10^{-4}$) the amplitude of the oscillations decreases, the spectrum narrows down, and finally the plasma reverts to single mode behavior (1 - 20 kHz), even for weakly magnetized ions.

The electrostatic fluctuations in the plasma potential ($\widetilde{\phi}$) are detected by measuring the oscillating current in an internal emissive filament which floats by virtue of having a capacitor to ground. The amplitude of the detected oscillations is given by the fluctuations of the potential in the plasma. The amplitude of the plasma potential oscillations is estimated using the I-V characteristic of an emissive filament close to floating and the measured value of the oscillating current shown in Fig. 3.17. The standard deviation of $|e\widetilde{\phi}|$ normalized to the measured T_e is presented in Fig. 3.19, showing that the plasma is always subjected to small oscillatory perturbations ($|e\widetilde{\phi}|/T_e < 1$).

Since the current collected in an ion saturation probe (electrostatic probe strongly negatively biased with respect to the plasma) is a reasonably good estimator of the plasma density [34], a $9\,\mathrm{cm}^2$ ion probe was used to measure the oscillations in the plasma density ($\widetilde{n}$). The ion probe was biased 100 V more negatively than the local plasma potential, and the current collected was measured through the voltage drop across 1 to 100 kΩ resistors using a circuit identical to the one used to measure the emission current in our experiments [42].

Chapter 4 is devoted to the detailed characterization of the spontaneous oscillations observed in electron-rich non-neutral plasmas ($10^{-4} < \eta < 1$). Chapter 5 describes the

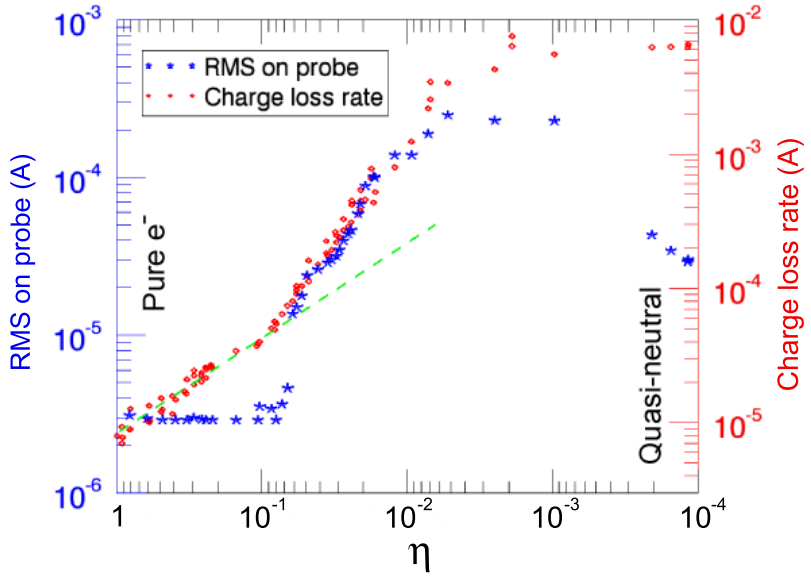

Figure 3.17: Evolution of the charge loss rate and the RMS of the oscillations in a floating emissive probe as a function of the degree of non-neutralization ($N_2^+ - e^-$ plasmas, $B = 0.02$ T, $\phi_e = -200$ V, 64° configuration).

parameter dependence and spatial structure of the mode detected in CNT's quasi-neutral plasmas ($\eta < 10^{-4}$).

3.7 Summary

CNT can vary continuously the degree of neutralization of the plasma (η) from $\eta = 1$ (pure electron plasmas) to $\eta \ll 1$ (quasi-neutral plasmas) by adjusting the neutral pressure in the chamber, which controls the volumetric ionization rate. CNT can also operate steadily at any given value of η between 10^{-5} and 1, while other devices traditionally used for the investigation of non-neutral and quasi-neutral plasmas present very limited flexibility to change η significantly (Table 3.1).

As η evolves from pure electron to quasi-neutral, spontaneous fluctuations appear, and the plasma potential decouples from the emitter. The insertion of an additional ceramic rod in the plasma halves the total ion population at a given neutral pressure. It has been observed that the neutral pressure threshold for both the development of fluctuations [49],

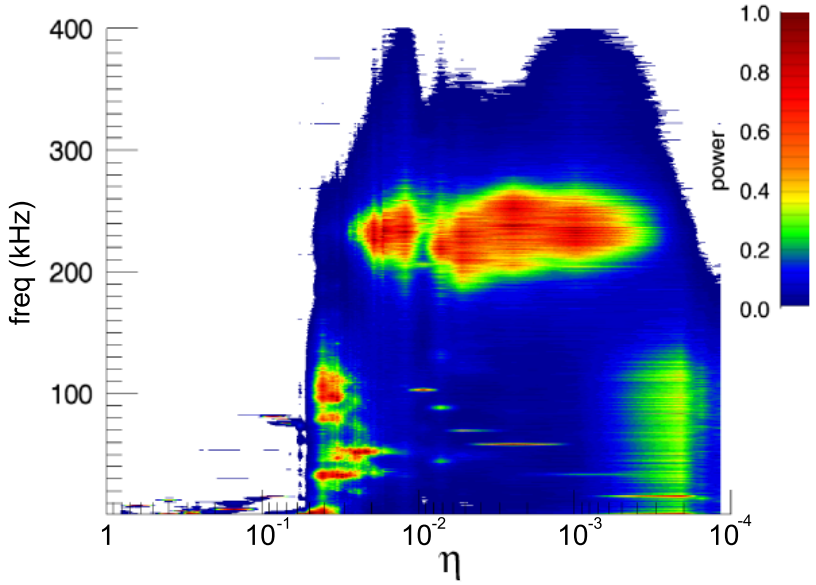

Figure 3.18: Power spectrum of the signal on a floating emissive probe vs. degree of non-neutralization. When partially neutralized plasmas become robustly unstable ($\eta < 0.1$), multi-mode fluctuations are observed. ($N_2^+ - e^-$ plasmas, $B = 0.02$ T, $\phi_e = -200$ V, 64° configuration).

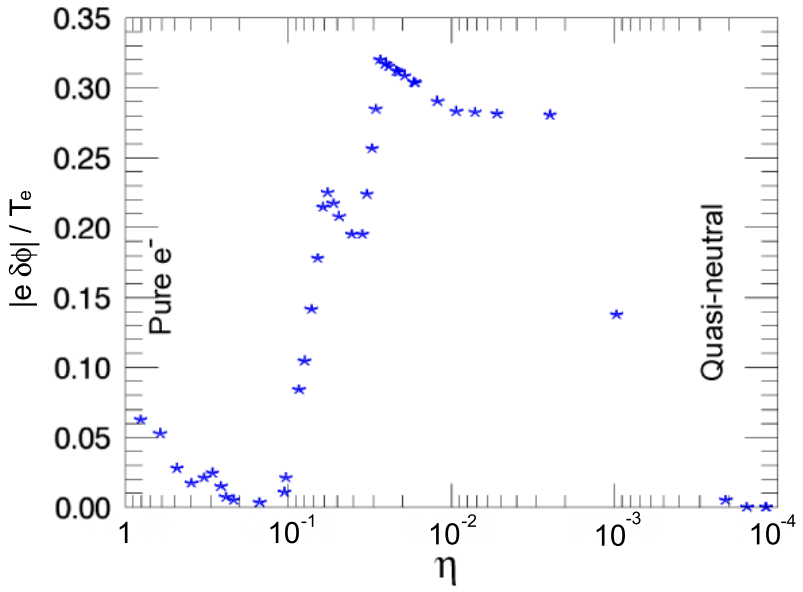

Figure 3.19: Standard deviation of $|e\widetilde{\phi}|$ normalized to T_e as a function of the degree of non-neutralization ($N_2^+ - e^-$ plasmas, $B = 0.02$ T, $\phi_e = -200$ V, 64° configuration).

and for the separation of the plasma potential (Section 3.3.2) is approximately doubled when a second ceramic rod is present in the plasma, providing strong evidence that these changes occur when a threshold ion content is exceeded.

In order to confirm that the decoupling of the plasma potential is not caused by an emission limit of the filament creating the plasma, a set of experiments was also conducted to study how the decoupling threshold was affected by the emitter filament temperature. When 6 V batteries are used to heat the emitter, the filament can emit significantly higher currents than with 4 V batteries. However, the separation of the plasma potential occurs essentially at the same neutral pressure when either a 4 V or a 6 V battery is used (Fig. 3.9).

This chapter also evaluates how electron temperature, ion gyro-radius, and perpendicular dielectric constant of the plasma change as η is varied 5 orders of magnitude. As a result of the separation of ϕ_p from the emitter bias, the emitted electrons are accelerated, and become hotter (Fig. 3.14). Ions, however, get colder as the plasma detaches from the emitter bias. Since the average perpendicular velocity of the ions can be approximated as the $E \times B$ velocity at high magnetic fields and for light ion species (Section 3.4), the ion gyro-radius

becomes smaller when the plasma decouples from the emitter bias (Fig. 3.14). In CNT, N_2^+ ions are essentially unmagnetized for $\eta \approx 1$, but r_{Li} is smaller than the minor radius of the plasma for quasi-neutral plasmas.

Chapters 4 and 5 describe in detail the spontaneous oscillations observed in partially neutralized ($10^{-4} < \eta < 1$) and quasi-neutral plasmas ($\eta < 10^{-4}$) respectively.

Chapter 4

Oscillations in electron-rich non-neutral plasmas

As the ion content increases in an electron-rich non-neutral plasma ($1 > \eta > 10^{-4}$), the plasma becomes unstable, and fluctuations are detected in electrostatic emissive probes inserted in the plasma. This Chapter presents a description of the oscillations observed in this regime, analyzing the dependence of the fluctuations on experimentally adjustable parameters (magnetic field strength, plasma potential, degree of non-neutralization, different ion species, and magnetic configuration), and the spatial structure of the detected modes.

Ions in CNT are typically largely unmagnetized ($r_{Li} \gg \langle a \rangle$ [1]), and exhibit a clear bouncing motion as they are drawn into the electron-rich plasma [49]. Partially neutralized plasmas with weakly magnetized ions develop multimode oscillations. However, more magnetized ions travel closer to the $\mathbf{E} \times \mathbf{B}$ velocity and single mode oscillations are detected when ions with $r_{Li} < \langle a \rangle$ are present in the plasma. The first observations of this type of mode were described by Q.R. Marksteiner et al. in [50] and are briefly summarized in Section 4.1.

Most of the results described in this Chapter concern the single mode oscillations observed in electron-rich non-neutral plasmas. The presence of broadband fluctuations and other relevant characteristics of partially neutralized plasmas (such as the jumps between equilibrium states) are described in Section 4.4.

In the experiments described in this Chapter, a floating emissive probe was used to

[1] $\langle a \rangle$ is the average minor radius of the torus, $\langle a \rangle = 0.15$ m

measure the oscillations of the plasma potential. The probe was located at $\psi \approx 0.15$ in the thin cross section of the plasma (unless otherwise stated), while steady state plasmas were created emitting electrons on the magnetic axis. The oscillating current in the probe was measured with an op-amp current-to-voltage converter circuit. The oscillations in the plasma density were measured with a cold Langmuir probe strongly negatively biased with respect to the plasma. Section 4.2.5 show that density fluctuations are well correlated with the oscillations of the plasma potential, and study the local phase shift between $\widetilde{\phi}$ and $\widetilde{n}$. The results of the experiments conducted to investigate the spatial structure of the single mode oscillations in partially neutralized plasmas are discussed in Section 4.3.

4.1 Previous results

The first observations of an ion-driven instability in electron-rich plasmas confined on magnetic surfaces were reported by Marksteiner in [50] for CNT's 64° tilt angle configuration prior to the installation of a conducting boundary conforming to the shape of the plasma. The instability occurred when the ion fraction exceeded 10% ($\eta \approx 0.8$), and was characterized by the development of 20 - 80 kHz oscillations and the degradation of confinement in the plasma. The measured frequency of the unstable mode scales linearly with the emitter bias voltage and decreases with the magnetic field strength, suggesting a link to the $\mathbf{E} \times \mathbf{B}$ flow of the plasma. However, the frequency does not scale exactly as $1/B$, and depends on the ion species present in the plasma. Measurements on the spatial structure of the instability indicate that the mode travels in the $\mathbf{E} \times \mathbf{B}$ direction of the electron plasma and that the instability has a poloidal mode number m = 1, which does not correspond to a rational surface and implies that the parallel force balance is broken.

4.2 Parameter dependence of the oscillations

Since Marksteiner conducted his research on the ion driven instability [49, 50], CNT has experienced significant modifications. Most importantly, a conducting boundary at the edge of the plasma was installed in CNT's 64° tilt angle configuration (Section 2.5.2), and later CNT switched to the 78° tilt angle. The conducting boundary was removed for the experiments

in the 78° configuration (the shape of the plasma is rather different in the three magnetic configurations in which CNT can operate, and the 64° conducting boundary could not be reused for the 78° tilt angle).

The parameter dependence of the detected oscillations in electron-rich non-neutral plasmas is explored in this Section, focusing on the effects of the conducting boundary and the magnetic configuration.

4.2.1 Effect of the conducting boundary at the plasma edge

The installation of a conducting boundary sets the 0 V electrostatic condition at the edge of the plasma (otherwise, the 0 V condition is set at the surface of the vacuum chamber and the IL coils). Hence, the conducting boundary results in an increased potential drop across the plasma for a given emitter bias, which in turn leads to three times denser electron plasmas. Results with the conducting boundary installed confirm the presence of an instability in partially neutralized plasmas. However, as described in Section 3.6, the behavior of the oscillations is significantly different compared to previous results without the conducting boundary (Section 4.1).

In order to evaluate the effect of the conducting boundary on the oscillations observed in partially neutralized plasmas, the fluctuations of the plasma were measured for a set of pressure and B field scans where the emitter bias voltage was held at -60 V. This emitter bias was chosen to reproduce the voltage drop across the plasma when emitting electrons at -200 V before the installation of the conducting boundary [43]. Higher ion contents are required to destabilize the plasma with the boundary at the plasma edge (the threshold for instability with the boundary installed is $n_i \approx 10^{12}\,\mathrm{m}^{-3}$, which corresponds to $\eta \approx 0.2$). The parameter dependence of the oscillations is very similar for both electrostatic boundary conditions. When the conducting boundary is installed, the frequency of the dominant mode also scales linearly with the plasma potential (ϕ_p) and decreases with the magnetic field strength. Fig. 4.1 shows that the measured frequency of the fluctuations scales close to linear with ϕ_p/B, indicating that the physics behind these oscillations may be identical to the situation without the conducting boundary. However, an offset frequency of a few kHz is observed at $\phi_p/B = 0$, which does not agree with a purely $\mathbf{E} \times \mathbf{B}$ rotation of plasma.

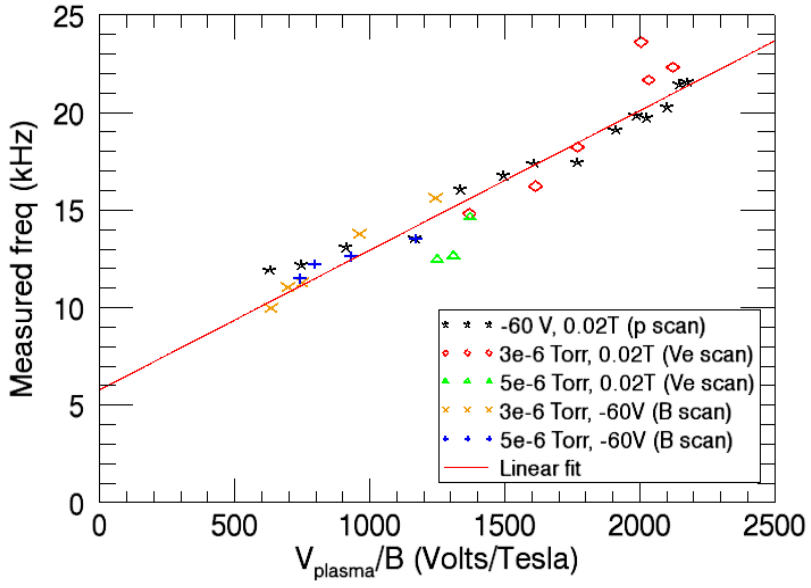

Figure 4.1: Frequency of the dominant modes vs ϕ_p/B while emitting electrons at low bias voltages (ϕ_e between -40 and -100 V) with the conducting boundary installed. Neutral pressure of N_2 between $8 \cdot 10^{-7}$ and $8 \cdot 10^{-6}$ Torr and B field strengths ranging from 0.02 to 0.07 T.

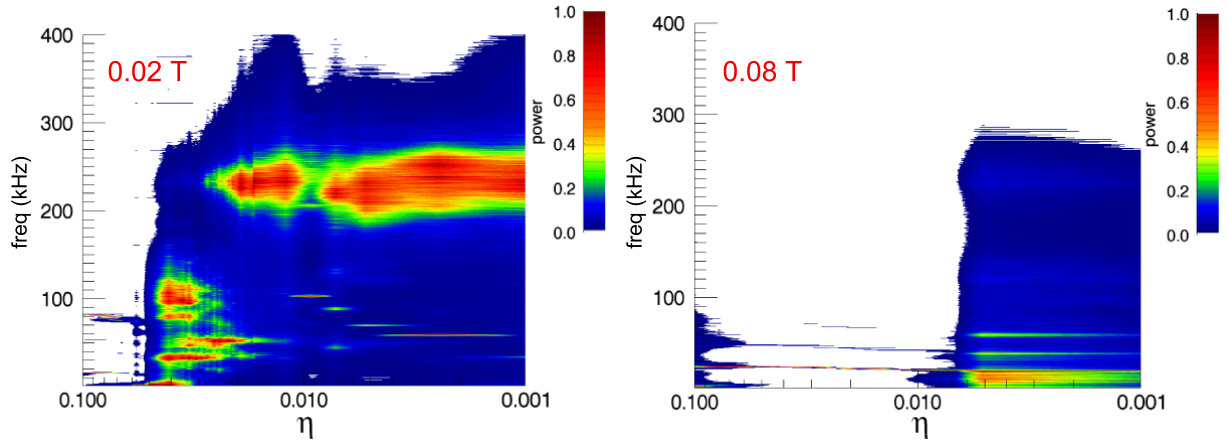

Figure 4.2: Power spectrum of the signal on a floating emissive probe vs. degree of non-neutralization. $N_2^+ - e^-$ plasmas, $\phi_e = -200$ V, 64° configuration. *Left:* B = 0.02 T. *Right:* B = 0.08 T

4.2.2 Dependence on η, ϕ_{plasma} and B field strength

The behavior of partially neutralized plasmas is rather different when operating at emitter bias voltages more negative than −100 V with the 0 V boundary condition at the plasma edge. The power spectrum of the oscillations in a floating emissive probe shows multiple peaks and broad band behavior (Figs. 3.18 and 4.2-left). However, for magnetic field strengths above 0.04 T and degrees of non-neutralization between $\sim$ 0.001 and 0.1 partially neutralized plasmas exhibit oscillations with a dominant mode between 20 and 100 kHz (Fig. 4.2-right). Although the amplitude of the oscillations increases significantly when η decreases down to 10^{-3} for all the emitter bias voltages and magnetic field strengths explored (as seen in Fig. 3.17), the frequency of the dominant mode does not present a strong dependency on η (Fig. 4.2-right). A slight decrease of the frequency is observed as the ion content increases, due to the decoupling of the plasma potential from the emitter bias voltage in this range of degrees of neutralization (Fig. 4.3). This is observed for the whole range of B field strengths where this mode appears, and clearly the frequency of the mode does not scale like $\sqrt{n_i}$, which eliminates the possibility of having a sheath instability related to the ions [55].

Fig. 4.3 also shows that the measured frequency of the oscillations decreases with the B field strength, but not as fast as $1/B$. The frequency of the mode grows with $|\phi_p|$ but a clear

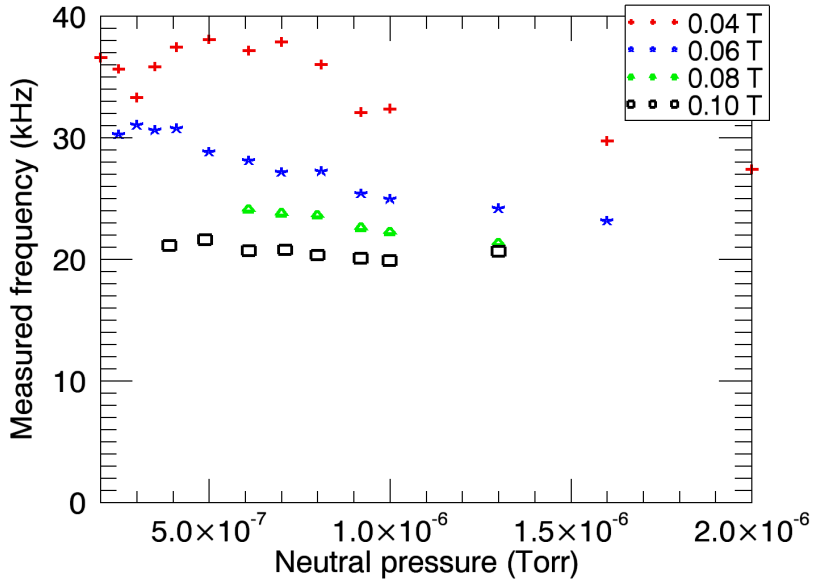

Figure 4.3: Measured frequency of the dominant mode vs. p_n. $N_2^+ - e^-$ plasmas, $\phi_e = -200$ V, 64° configuration.

linear scaling is not observed for all the B fields explored (Fig. 4.4). However, experiments conducted at constant ϕ_e/B ratio indicate that this mode may scale linearly with E/B (Fig. 4.5-left). This hypothesis is confirmed in Fig. 4.5-right, implying that the single mode oscillations observed in partially neutralized plasmas can be related to the $\mathbf{E} \times \mathbf{B}$ rotation. Nevertheless, a $\sim$ 10 kHz offset can be also seen in Fig. 4.5-right for $\phi_p/B = 0$, implying that the detected mode it is not simply caused by the $\mathbf{E} \times \mathbf{B}$ flow. The linear dependency of the mode frequency on ϕ_p/B breaks down at high emitter bias voltages and low magnetic field strengths, or even no clear dominant mode is observed because the plasma presents multimode or broadband behavior.

Results shown in Fig. 4.1 and 4.5-right are overlaid in Fig. 4.6. The measured frequency of the dominant mode has the same linear scaling with E/B both in Fig. 4.1 and 4.5-right, suggesting that the single mode detected in partially neutralized plasmas with the conducting boundary installed might be identical to the ion-driven instability reported by Marksteiner [50].

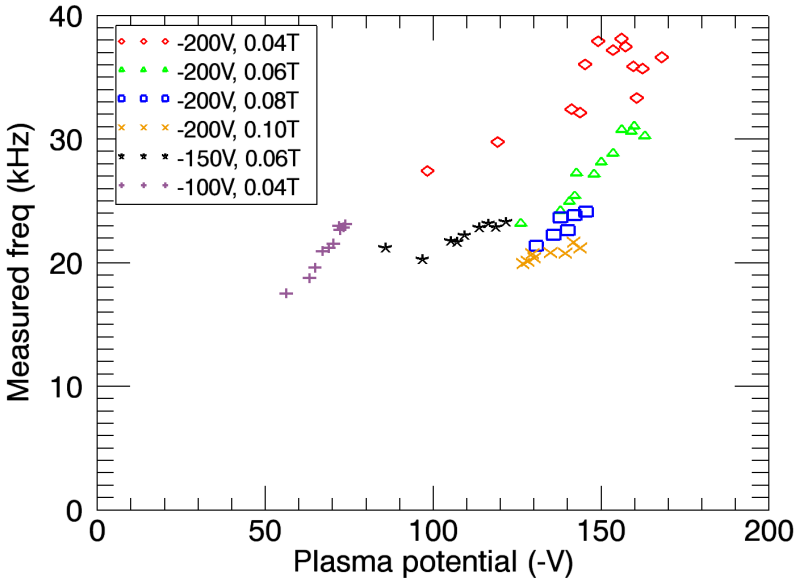

Figure 4.4: Frequency of the detected mode as a function of the measured plasma potential. $N_2^+ - e^-$ plasmas, $4 \cdot 10^{-7} < p_n < 2 \cdot 10^{-6}$ Torr, 64° configuration.

4.2.3 Effect of different ion species

The behavior of the oscillations in partially neutralized $N_2^+ - e^-$ plasmas has been described in Section 4.2.2, but it remained to be studied how the introduction of ions with different masses affects the oscillations. Experiments were conducted for partially neutralized $Ar^+ - e^-$, $He^+ - e^-$ plasmas in the 64° tilt angle configuration with the conducting boundary installed, exploring the dependence of the mode on the degree of neutralization, electric, and magnetic field strength.

As the ion content increases in the plasma, an unstable mode also develops in $Ar^+ - e^-$ and $He^+ - e^-$ plasmas [1]. The oscillations in both Ar^+, He^+ plasmas present an almost identical behavior compared to N_2^+ plasmas. The frequency of these fluctuations has negligible dependence on η, scales close to linear with ϕ_p, and decreases with the magnetic field strength. This is particularly evident in the case of He^+ (Fig. 4.7). Fig. 4.8 summarizes how the frequency of this mode depends on E/B for Ar^+, He^+ and N_2^+. When lighter ion

[1] In Ar^+ plasmas the mode is clearly observed for neutral pressures between 10^{-7} and $6 \cdot 10^{-7}$ Torr, and $-250 < \phi_e < -50$ V. In He^+ plasmas, for neutral pressures between $3 \cdot 10^{-6}$ and $2 \cdot 10^{-5}$ Torr.

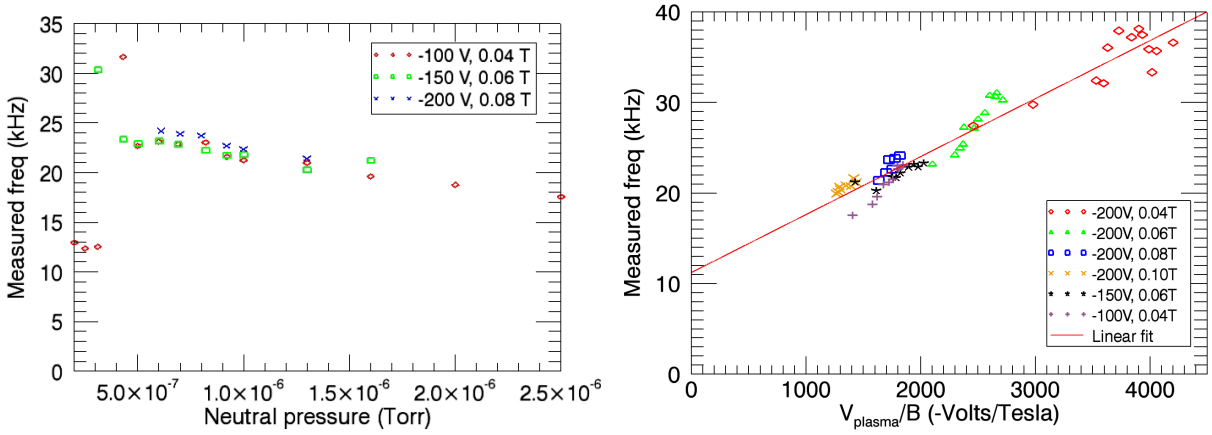

freq vs. p_n (constant ϕ_e/B) freq vs. ϕ_p/B

Figure 4.5: E/B scaling of the dominant mode in partially neutralized plasmas. $N_2^+ - e^-$ plasmas, 64° configuration. *Left:* Measured frequency as a function of p_n at constant ϕ_e/B ratio. The measured frequency decreases slightly as ϕ_p starts decoupling from ϕ_e (Section 3.3). *Right:* Measured frequency vs. ϕ_p/B. The frequency of the mode scales linearly with ϕ_p/B. However, a $\sim$ 10 kHz offset is observed at $\phi_p/B = 0$, which does not agree with a purely $\mathbf{E} \times \mathbf{B}$ rotation.

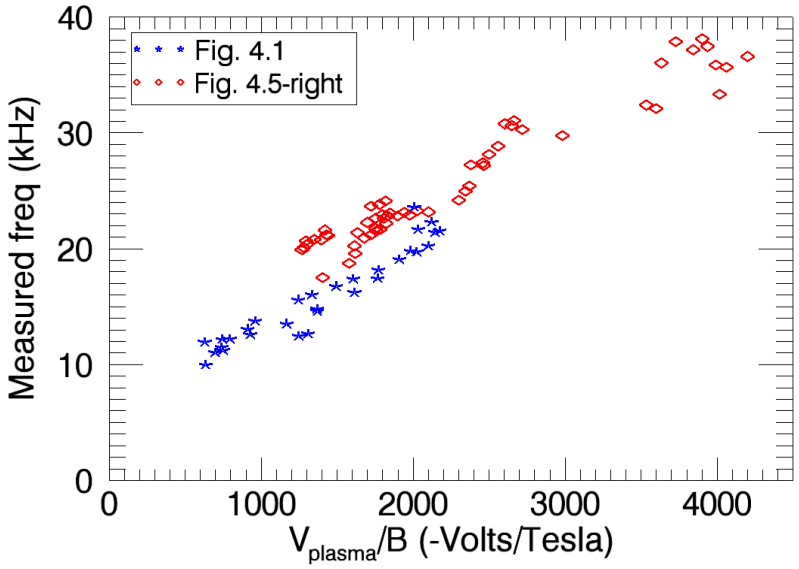

Figure 4.6: Frequency of the dominant mode in partially neutralized plasmas vs. E/B with the conducting boundary installed in the 64° configuration. Figs. 4.1 and 4.5-right overlaid.

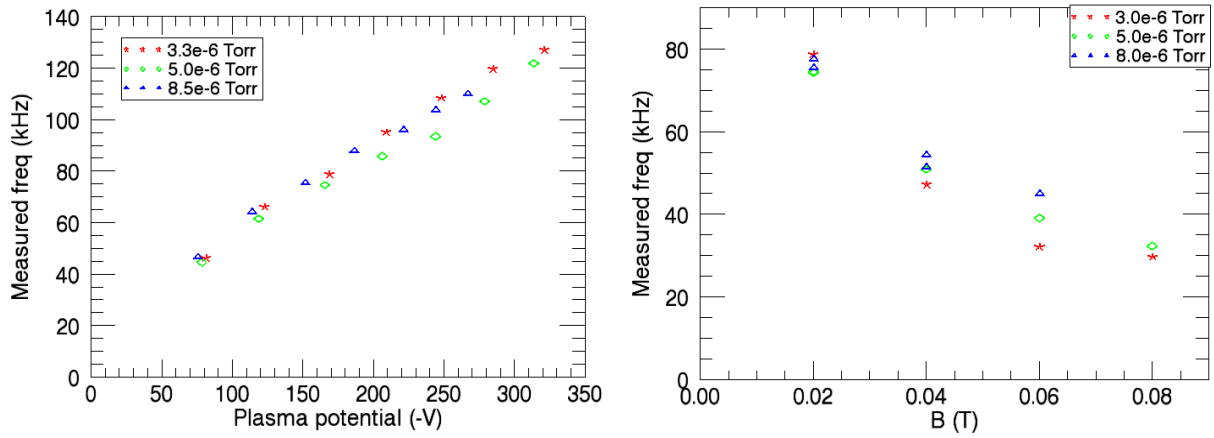

freq vs. ϕ_p (B = 0.02 T) freq vs. B field ($\phi_e = -200$ V)

Figure 4.7: Dependence of the measured frequency of the mode on the plasma potential (left) and the magnetic field strength (right). $He^+ - e^-$ plasmas in the 64° configuration.

species (He^+) are introduced in the plasma, slightly higher frequencies are measured, but in all cases the measured frequency scales close to linear with E/B.

When an additional rod is inserted in the thin cross section of the plasma, the shape of the ion density profile is not affected, but the ion density at a given neutral pressure is halved everywhere in the plasma [49]. The set of experiments described in Section 3.1.3 of [49] were reproduced here to study how the presence of an additional ceramic rod in the plasma affects the threshold for instability when the conducting boundary was installed. The results of the experiments with two ceramic rods are identical for both electrostatic boundary conditions at the edge of the plasma: the pressure threshold for instability occurs at approximately two times higher pressure when a second rod is present, which approximately corresponds to the same ion content threshold as when a single rod is present. This confirms that the presence of ions is responsible of the appearance of spontaneous oscillations in electron-rich non-neutral plasmas.

4.2.4 Effect of the magnetic configuration

The three tilt angles of operation in CNT represent three rather different shapes of the plasma and explore three generic shear configurations. The results described so far in this

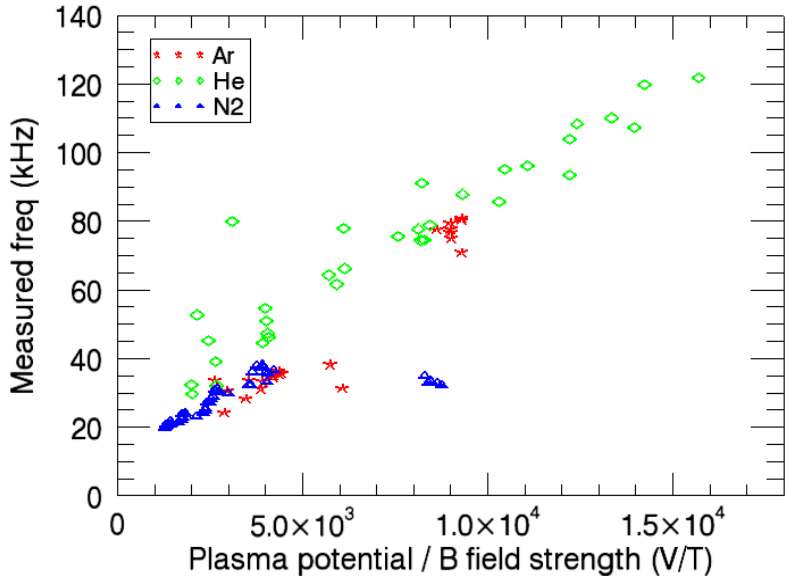

Figure 4.8: Measured frequency vs. E/B for $Ar^+ - e^-$, $He^+ - e^-$ and $N_2^+ - e^-$ plasmas in partially neutralized plasmas. 64° configuration.

Section refer to the 64° configuration, but CNT's tilt angle was switched to 78° in the course of this thesis. The 64° configuration presents reversed shear, while the 78° tilt angle is essentially shear free.

Unstable fluctuations were also detected in the 78° configuration when the ion content exceeds a certain threshold and the plasma starts decoupling from the emitter bias. These oscillations present a dominant peak between 20 and 70 kHz for $10^{-7} \leq p_n \leq 10^{-6}$ Torr (Fig. 4.9). The amplitude and frequency of the oscillations observed in partially neutralized plasmas are lower in the 78° configuration, probably due to the smaller potential drop across the plasma when the 0 V boundary condition is set by the chamber and the coils. The frequency of these fluctuations scales linearly with ϕ_p, but does not have a clear $1/B$ dependence. Fig. 4.10 shows that the measured frequency of the mode scales reasonably well with E/B. It seems also that the dominant mode switches to a higher frequency harmonic for high ϕ_p/B ratios. Hence, these experiments confirm that partially neutralized plasmas behave quite similarly in both stellarator configurations studied so far, despite having completely different shape and magnetic shear.

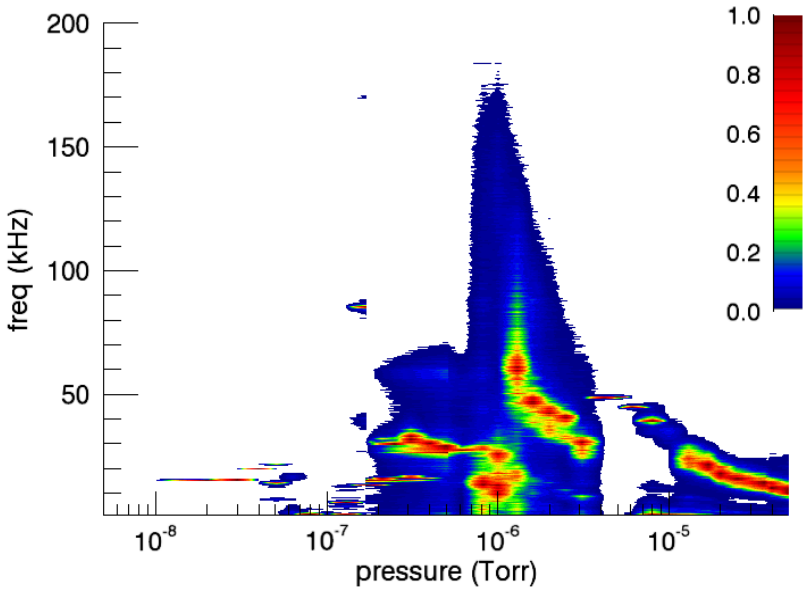

Figure 4.9: Power spectrum of the signal on a floating emissive probe vs. neutral pressure. $N_2^+ - e^-$ plasmas, $B = 0.08$ T, $\phi_e = -200$ V, 78° configuration.

Nevertheless, notable differences were appreciated in the 78° configuration. For instance, when the plasma abruptly decouples from the emitter bias ($0.2 < \phi_p/\phi_e < 0.8$, corresponding to $10^{-6} < \mathrm{p_n} < 5{\cdot}10^{-6}$ Torr), the power spectrum also broadens considerably, but a dominant peak can always be observed in this regime at high magnetic field strengths (B $\geq$ 0.06 T) for the 78° tilt angle (Fig. 4.9). The frequency of this oscillation decreases as the degree of non-neutralization gets closer to quasi-neutrality (in this regime the plasma potential is very sensitive to the degree of neutrality). And the dominant mode seems to jump to a higher frequency when a certain degree of neutrality is exceeded, probably indicating a higher spatial mode number of the oscillations (see Fig. 4.9 between 10^{-6} and 10^{-5} Torr). This hypothesis will be confirmed in the Sections exploring the spatial structure of the modes (Section 4.3 for partially neutralized, and Section 5.3 for quasi-neutral plasmas), showing that the ion-driven oscillations observed in electron-rich non-neutral plasmas present a poloidal mode number m = 1, while the quasi-neutral oscillations align with the field lines and exhibit a m = 3 poloidal structure.

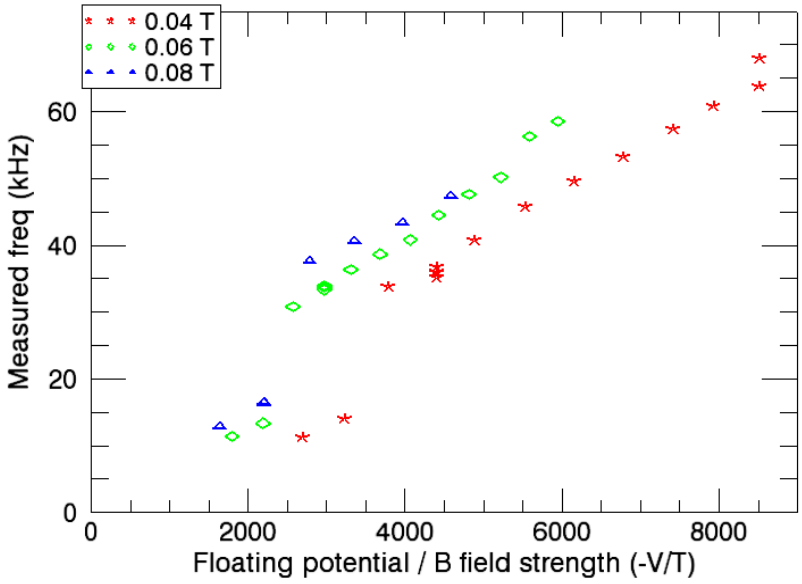

Figure 4.10: Measured frequency of the oscillations in partially neutralized plasmas vs ϕ_p/B in the 78° configuration (electron-rich N_2^+ plasmas, $p_n = 3.1 \cdot 10^{-7}$ Torr, $-400 \leq \phi_e \leq -100$ V).

4.2.5 Local phase shift between density and potential fluctuations

Experiments were also conducted to measure the local phase difference between density and potential oscillations in CNT, since this phase shift between $\widetilde{n}$ and $\widetilde{\phi}$ usually determines the nature of the oscillation in quasi-neutral plasmas [38]. These experiments were only performed in the 78° configuration.

Method

A relatively simple method to determine the local phase shift between $\widetilde{n}$ and $\widetilde{\phi}$ involves the use of two probes in two different sets of experiments. A series of experiments measured the oscillations of the potential by floating an emissive filament at location ♯2 of the nw4 probe array (which corresponds to $\psi \approx 0.15$ in the thin cross section of the plasma), and another set of experiments reproduced the same experimental conditions but now replacing the floating emissive filament by an ion probe to measure the density oscillations at the same location. A different floating emissive filament was also used in both sets of experiments to

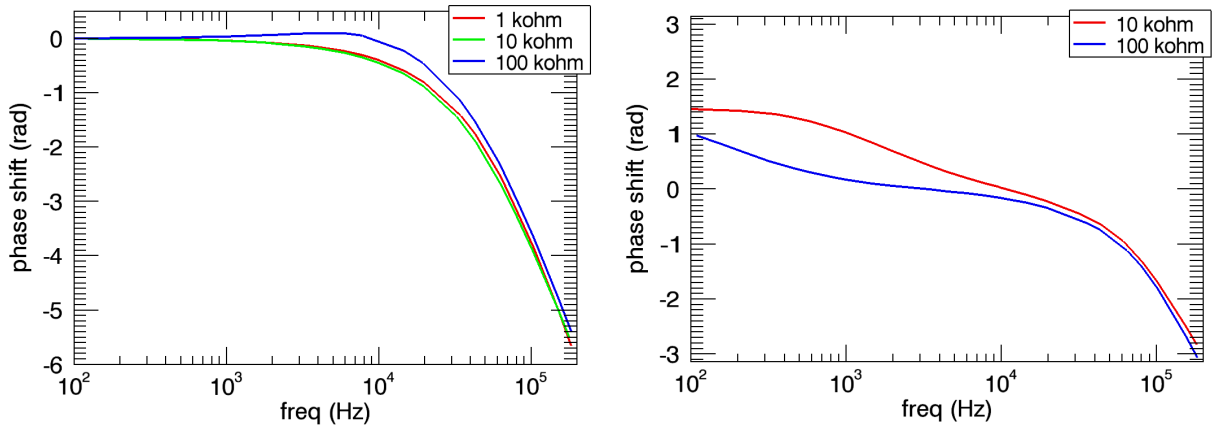

Emitter circuit I-V converter

Figure 4.11: Phase shift introduced by the electronic circuits used to measure the fluctuations in the plasma.

measure the potential oscillations at location ♯3 of the nw4 probe array ($\psi \approx 0.45$), and use the signal in this probe as the reference to correlate the density and potential fluctuations in nw4 ♯2.

The circuits used in these experiments were calibrated to determine the phase shift introduced by the electronics and correct the measurements accordingly. The emitter circuit used to measure the current fluctuations in the ion probe does not introduce any phase shift for frequencies below 10 kHz, but delays more than π rad signals above 100 kHz (Fig. 4.11-left). The phase response of the I-V converter that measured the plasma potential oscillations in the emissive probes is shown in Fig. 4.11-right.

The real phase shift between the signals measured in nw4 ♯2 and ♯3 (α) can be determined from the measured phase difference (α') and the phase delays introduced by the electronics (δ_1 and δ_2), as shown in Fig. 4.12:

$$\alpha = \alpha' - \delta_1 + \delta_2 \tag{4.1}$$

The Fourier power spectrums of the fluctuations detected in nw4 ♯2 and ♯3 are comparable, and clear sinusoidal oscillations proportional to the plasma density and potential are detected in partially neutralized and quasineutral plasmas. The cross-correlation between $\widetilde{n}$ and $\widetilde{\phi}$ also confirms that density fluctuations are well correlated with the oscillations of the

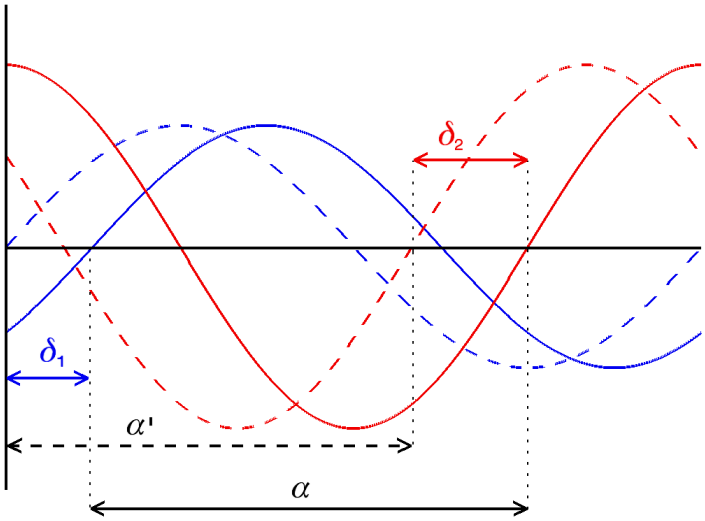

Figure 4.12: Determination of the phase difference between the signals measured in nw4 ♯2 and ♯3. The dashed lines represent the measured signals, and solid lines are the real signals. α is the real phase difference between the oscillations, α' is the measured phase shift, and δ_1 and δ_2 are determined through the calibration of the electronics (Fig. 4.11)

plasma potential.

The dominant frequency of the cross-correlation between the density (measured in nw4 ♯2) and the potential (nw4 ♯3) oscillations are shown in Fig. 4.13-right for a pressure and a B field scan. In Fig. 4.13-right two regions can be identified with the usual scalings: 1) partially neutralized plasmas present oscillations between 25 and 35 kHz whose frequency decreases slightly with the magnetic field strength, and 2) quasineutral plasmas exhibit lower frequency oscillations (1 - 8 kHz) and its frequency increases with the magnetic field strength. An identical behavior is observed in the dominant frequency of the cross-correlation between the potential fluctuations measured in nw4 ♯2 and nw4 ♯3 as the degree of neutralization and the magnetic field strength are varied (Fig. 4.13-left).

The phase difference between the signal in two probes was extracted using the cross-correlation function [37]. Since the phase of the cross-correlation is a function of the frequency, the value of phase shift shown in this Section corresponds to the dominant frequency of the cross-power spectrum.

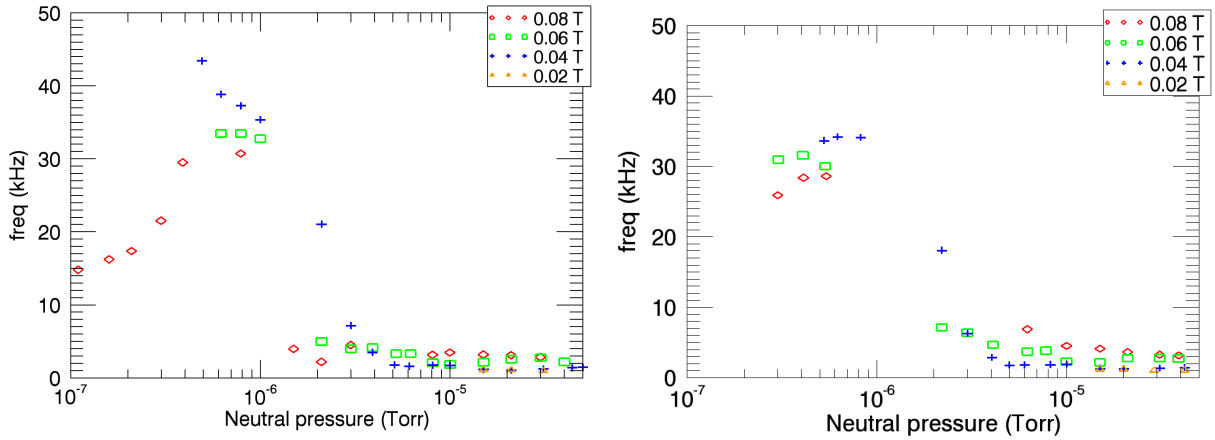

Dominant freq cross-correlation $\widetilde{\phi}_2$ - $\widetilde{\phi}_3$ Dominant freq cross-correlation $\widetilde{n}_2$ - $\widetilde{\phi}_3$

Figure 4.13: *Left:* Dominant frequency of the cross correlation between the potential fluctuations measured in nw4 ♯2 and nw4 ♯3 as the degree of neutralization and the B field are varied. *Right:* Dominant frequency of the cross correlation between the density (measured in nw4 ♯2) and the potential (nw4 ♯3) fluctuations as the degree of neutralization and the B field strength are varied. (N_2^+ - e^- plasmas, $\phi_e = -200$ V).

Results

In partially neutralized plasmas, the measured oscillations of the plasma potential ($\widetilde{\phi}$) in nw4 ♯2 present a modest delay with respect to nw4 ♯3 ($-45°$ on average, see Fig. 4.14-left for a series of B field and ϕ_e sweeps). Fig. 4.14-right shows that the average phase difference between the density fluctuations ($\widetilde{n}$) in nw4 ♯2 and $\widetilde{\phi}$ in nw4 ♯3 is $-55°$. Thus, $\widetilde{n}$ and $\widetilde{\phi}$ are very close to being in phase [2] at the location of the probe nw4 ♯2 (which corresponds to $\psi \approx 0.15$).

In CNT's electron-rich plasmas the equilibrium distribution function of electrons on each magnetic surface is $n_e = N(\psi) \exp\left(e\phi/T_e(\psi)\right)$ [59]. Therefore, since the plasma is subjected to small oscillatory perturbations ($|e\widetilde{\phi}|/T_e < 1$, see Fig. 3.19), $\widetilde{\phi}$ and $\widetilde{n}$ are predicted to be in phase if the electron fluid remains in equilibrium, which agrees with the experimental observations.

[2] There is better than 95% confidence that the phase shift between $\widetilde{n}$ and $\widetilde{\phi}$ lies within the interval $-10° \pm 69°$

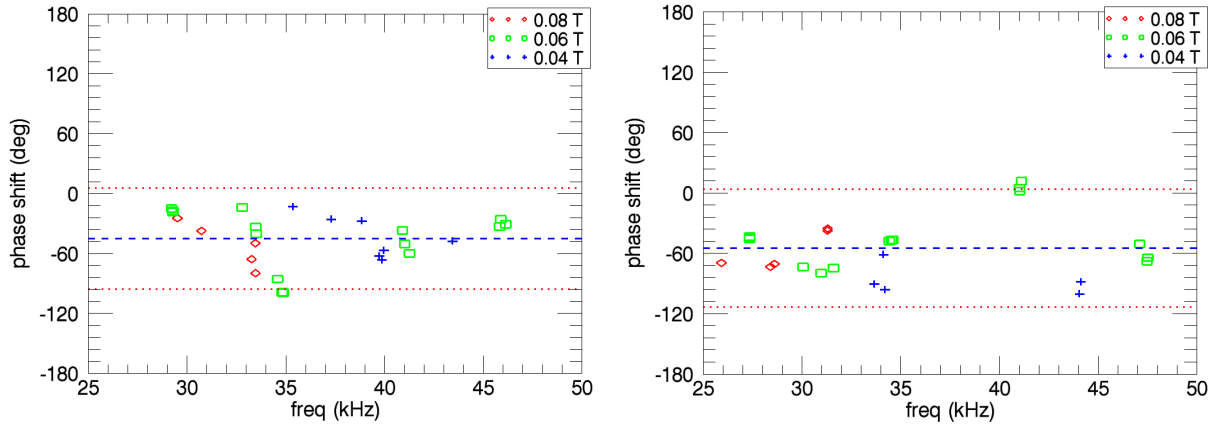

Phase $\widetilde{\phi}_2$ - $\widetilde{\phi}_3$ Phase $\widetilde{n}_2$ - $\widetilde{\phi}_3$

Figure 4.14: *Left:* Phase difference between the potential fluctuations measured in nw4 ♯2 and nw4 ♯3. *Right:* Phase difference between the density (measured in nw4 ♯2) and the potential (nw4 ♯3) fluctuations. The dashed blue line represents the average phase shift, and the $\pm 2\sigma$ confidence interval is given by the two red dotted lines. Partially neutralized N_2^+ - e^- plasmas, $-300 < \phi_e < -150$ V, $0.04 < B < 0.08$ T.

4.3 Spatial Structure

4.3.1 Theoretical considerations

Equilibrium for a pure electron plasma in a stellarator is in a minimum energy state [58], and parallel force balance pertains to a whole magnetic surface [59]. Any macroscopic motion of the plasma away from the magnetic surfaces implies the breaking of the parallel force balance [59].

In a stellarator, the rotational transform (ι) describes the poloidal twist of the field lines around the torus [7]. A *rational magnetic surface* is a surface where ι is equal to a low order rational number $\iota = n/m$, and the field lines close on themselves after n poloidal and m toroidal transits around the torus [9]. Therefore, perturbations can exist in a resonant rational surface without breaking the parallel force balance.

CNT's ion-driven instability was first characterized by Marksteiner in [50] for the 64° tilt angle configuration prior to the installation of a conducting boundary at the edge of the plasma. A set of capacitive probes around the thick poloidal cross section of the plasma

was used to determine that the azimuthal mode number of these oscillations was $m = rk_\theta = 1$. This result posed a challenge to theory, since an azimuthal mode m = 1 mode had been observed in Penning and pure-toroidal traps [17, 19, 24, 76, 79], but this oscillation was predicted to be damped by the magnetic surfaces much faster than the period of an oscillation [50, 59] (the ι profile of CNT for these experiments grows monotonically from $\iota(\psi = 0) = 0.12$ to $\iota(\psi = 1) = 0.23$). Hence, in CNT's 64° configuration the magnetic surfaces are not able to stabilize the ion-driven instability, and the parallel force balance is broken. This was, indeed, the first time that an instability non-resonant with a rational surface was observed in a stellarator.

There are still interesting questions that remain to be answered regarding the characterization of the ion-driven instability in a stellarator, most importantly: the effect of the ι profile, and the determination of the toroidal mode number (n) of the oscillations.

The 78° tilt angle presents an almost flat $\iota \approx 1/3$ profile [41]. This Section will explore whether the ion-driven mode aligns with the magnetic field lines in the 78° configuration (and presents a resonant m = 3 structure) or, on the contrary, this instability also breaks parallel force balance even in the presence of low order rational surfaces. The magnetic shear plays an important role in suppressing diocotron instabilities [40], therefore experiments in the 78° tilt angle configuration can provide valuable information for the understanding of this instability.

In the *infinite conductivity* approximation Ohm's law is simply $\vec{E} + \vec{u} \times \vec{B} = 0$. The consequences of *infinite conductivity* in Magnetohydrodynamics (MHD) are that the plasma is tied to the magnetic field lines, and the magnetic flux through any closed contour moving with the plasma is conserved [27]. The diocotron mode in a pure toroidal trap presents a m = 1, n = 0 structure [75]. However, stellarators must have a finite poloidal flux through the hole of the torus, which will remain unchanged if integrated through an area bounded by any closed tube moving with the $E \times B$ drifting plasma. Therefore, the ion-driven mode in a stellarator is predicted to have a toroidal mode number n > 0 to conserve the poloidal magnetic flux (even if the parallel force balance is broken).

The experiments explained below investigate the spatial structure of the ion-driven mode detected in electron-rich non-neutral plasmas for the 78° tilt angle configuration, and study the influence of the ι profile in the spatial structure of the instability.

4.3.2 Experimental results

The toroidal and poloidal structure of the ion resonant mode in the 78° configuration was measured with two perpendicular arrays of capacitive probes (described in Section 2.5.2). The oscillations detected in the capacitive probes are very well correlated with the signal in the floating emissive probe. Indeed, it has been observed that the measured frequency of the oscillations is exactly the same at different radial locations (Section 4.2.5) and at edge of the plasma (measured with the capacitive probes), so the ion resonant mode is a global instability.

The poloidal array of capacitive probes consists of 5 copper disks located around the thick poloidal cross-section of the plasma ($\varphi = 90°$), providing enough spatial resolution to determine the poloidal mode number of the oscillation. The layout of the poloidal capacitive probes can be seen in Fig. 4.15, along with the measured phase shift of the signal in each probe relative to TP ♯3. The phase difference between the image charge measurements corresponds to the phase of the dominant mode of the cross-correlation power spectrum [37]. Fig. 4.15 also shows the predicted phase shift of a m = 1, 2, and 3 mode assuming a circular cross-section of the plasma at $\varphi = 90°$. The mode travels in the $E \times B$ direction of rotation of the plasma, and all the measured phase differences are consistent with a m = 1 poloidal mode structure, except the recorded phase shift on probe P♯4, which always lies between the predicted m = 1 and m = 2 phase. It is not understood why the measurements at P♯4 do not fit the predicted m = 1 mode as well as the rest of the probes. Nevertheless, the experiment was performed at different emitter bias voltages ($-300 < \phi_e < -150$ V), and magnetic field strengths ($0.04 < B < 0.08$ T), providing enough evidence to conclude that the mode is m = 1.

Since the 78° tilt angle presents an almost flat $\iota \approx 1/3$ profile [41], it was originally thought that the ion-driven mode might align with the magnetic field lines in this configuration and have a resonant m = 3 poloidal structure. However, the phase shift measurements give strong evidence to suggest that ion-driven instability in the 78° configuration has a m = 1 mode number, which is the same as that of ion-driven instabilities in Penning and pure-toroidal traps [17, 24, 76, 79] and CNT's 64° conf. [50], and implies that the ion instability breaks parallel force balance in a stellarator even in the presence of low order rational

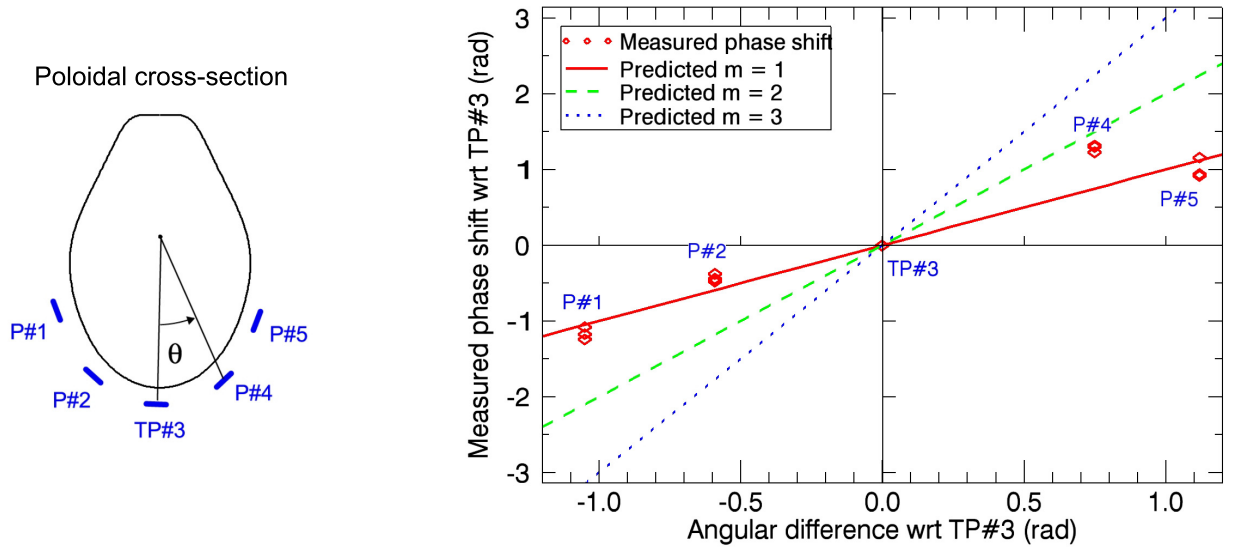

Figure 4.15: Measured phase shift of the ion-driven mode detected on the poloidal capacitive probes. The phase on probe TP ♯3 is used as the reference. $p_n = 4 \cdot 10^{-7}$ Torr of N_2, $\phi_e = -200$ V, B = 0.08 T, 78° configuration.

surfaces.

The mechanism causing the violation of the parallel force balance in the stellarator is not completely understood, but it might be due to the presence of an anisotropic ion pressure tensor ($\overleftrightarrow{p}_i$) [6]. Largely unmagnetized ions are drawn electrostatically into the electron-rich plasma without collisions, and the distribution function of ions is predicted to be non-Maxwellian and anisotropic. The force balance of the ion fluid can be written as:

$$m_i n_i \frac{\partial \vec{u}_i}{\partial t} + \vec{\nabla} \cdot \overleftrightarrow{p}_i = e n_i (\vec{E} + \vec{u}_i \times \vec{B}) \tag{4.2}$$

where the ion fluid velocity is $\vec{u}_i = \int \vec{v} f_i d^3v$, and the ion pressure tensor is $\overleftrightarrow{p}_i = \int m_i \vec{v}\vec{v} f_i d^3v$.

The expression for the electron force balance is analogous, but the electrons have negligible inertia, are magnetized, and the pressure tensor is likely to be isotropic:

$$\vec{E} + \vec{u}_e \times \vec{B} = -\frac{\vec{\nabla} p_e}{e n_e} \tag{4.3}$$

The plasma force balance is obtained summing Eqs. 4.2 and 4.3:

$$m_i n_i \frac{\partial \vec{u}_i}{\partial t} + \vec{\nabla} \cdot \overleftrightarrow{p} = e(n_i - n_e)\vec{E} + \vec{j} \times \vec{B} \tag{4.4}$$

where $\vec{j} \equiv en_i\vec{u}_i - en_e\vec{u}_e$ is the electrical current and $\overleftrightarrow{p} = \overleftrightarrow{p}_i + p_e\overleftrightarrow{1}$ is the pressure tensor. The anisotropic $\overleftrightarrow{p}$ can modify parallel force balance in a way that an isotropic pressure cannot, and might explain the existence of an ion-driven mode not aligned with the magnetic field lines.

The toroidal structure of the oscillations was investigated with a set of 6 capacitive probes which covered 105° along the toroidal angle of the torus (Fig. 4.16). The measured phase difference of the image charge oscillations in each probe with respect to TP ♯3 is also shown in Fig. 4.16, suggesting that the toroidal mode number of the oscillation is n = 0 (the predicted phase shifts in Fig. 4.16 assumed a circular magnetic axis). Experiments at different emitter bias voltages ($-300 < \phi_e < -150$ V), and magnetic field strengths ($0.04 < B < 0.08$ T) produced very similar results. In order to verify the n = 0 structure of the ion mode, an additional capacitive probe was installed 180° away toroidally from probe TP ♯3, and the phase difference between the two probes was measured. Fig. 4.17 shows that the signals in two probes separated by 180° toroidally are nearly in phase for a series of ϕ_e and B field sweeps (there is better than 95% confidence that the phase shift between the two probes is within the interval 0.5 ± 0.6 rad).

Hence, there is strong evidence indicating that the spatial structure of the ion-driven driven mode is m = 1, n = 0, which is identical to the diocotron mode detected in pure toroidal traps [75]. This implies that the global ion mode observed in CNT is not aligned with the magnetic field lines, and the poloidal magnetic flux is not conserved in a close tube of plasma moving with this mode. It is believed that the presence of an anisotropic pressure tensor in the plasma force balance (Eq. 4.4) might also explain the n = 0 structure of this mode (since it introduces a $\vec{\nabla} \cdot \overleftrightarrow{p}$ term that is usually neglected in the ideal MHD approximation of Ohm's law).

4.4 Multi-mode oscillations in partially neutralized plasmas.

This thesis focuses on the investigation of the single mode oscillations observed in partially neutralized and quasi-neutral plasmas (Sections 4.2 and 5.2 respectively). However, the

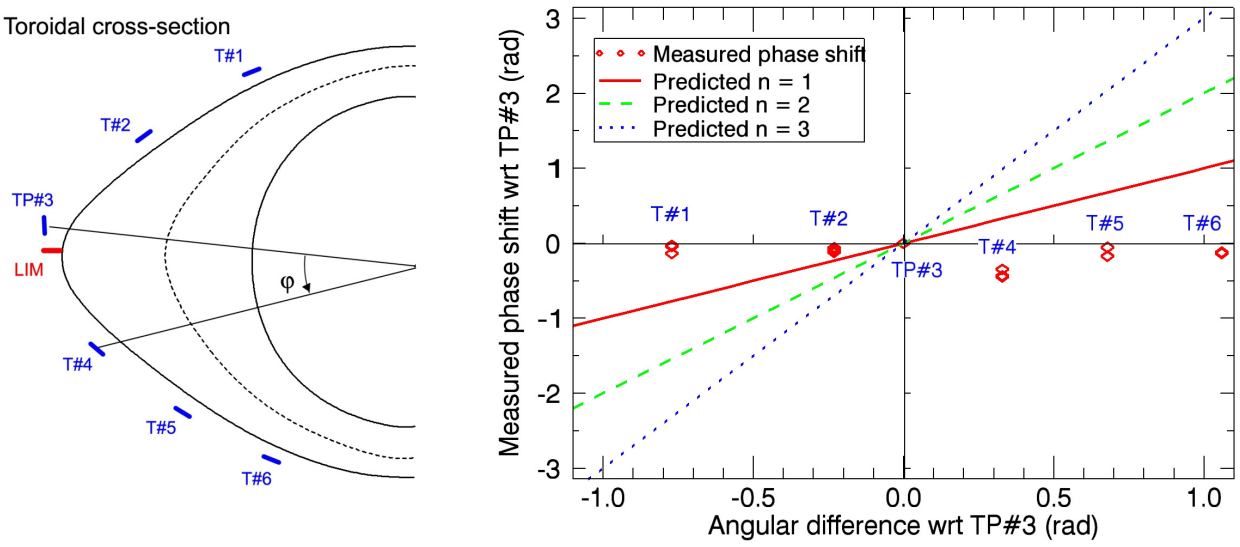

Figure 4.16: Measured phase shift of the ion-driven mode detected on the toroidal capacitive probes. The phase on probe TP ♯3 is used as the reference. $p_n = 4 \cdot 10^{-7}$ Torr of N_2, $\phi_e = -200$ V, B = 0.08 T, 78° configuration.

presence of broadband fluctuations and the jumps between equilibrium states are also very characteristic of partially neutralized plasmas. A summary of the first observations of multi-mode oscillations in partially neutralized plasmas is presented in this Section with the aim of inspiring future research on this largely unexplored regime of plasma physics. A detailed study of the physics behind this behavior is outside of the scope of this thesis, and will not be discussed in depth.

4.4.1 Multi-mode oscillations

There are two regions where partially neutralized plasmas present multi-mode oscillations: 1) for degrees of non-neutralization between $\eta = 0.1$ and 0.01, and 2) for η ranging from $\eta = 0.01$ to 10^{-4} (Fig. 3.18).

The first kind of multi-mode oscillations ($0.1 > \eta > 0.01$) are only observed when the plasma contains essentially unmagnetized ions (such as N_2^+ at 0.02 T), bouncing chaotically in the electron-rich plasma. The dominant peaks of the Fourier Spectrum (typically < 100 kHz) are in the same range as the ion bounce frequency [49] and the $E \times B$ rotation of the

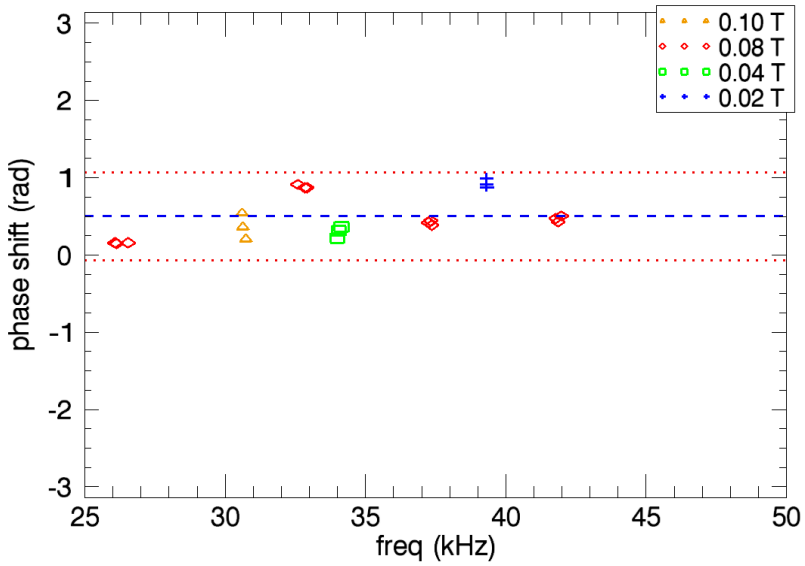

Figure 4.17: Measured phase difference between two capacitive probes separated 180° toroidally from each other. The phase on probe TP ♯3 is used as the reference. The dashed blue line represents the average phase shift, and the $\pm 2\sigma$ confidence interval is given by the two red dotted lines. Partially neutralized N_2^+ - e^- plasmas, $p_n = 4 \cdot 10^{-7}$ Torr, 78° configuration. Measurements performed for a series of ϕ_e, and B field sweeps: $-300 < \phi_e < -150$ V, $0.04 < B < 0.08$ T.

plasma, but it is unclear if the multiple harmonics detected in the spectrum are part of the ion driven instability or are a different kind of oscillation. It is not understood either how the fact that $\varepsilon_\perp < 0$ for $B < 0.04$ T (Fig. 3.15) may affect the multiple peak oscillations. The multi-mode behavior of this regime degenerates into a single mode when more magnetized ions ($r_{Li} < \langle a \rangle$) are introduced in the plasma (see Section 4.2). The amplitude of the oscillations grows as more ions are introduced into the plasma (Fig. 3.17), and the plasma is always more unstable when multiple modes are excited. For a given η, the RMS of the fluctuations is higher when the plasma exhibits multiple modes than when only the single mode ion-driven oscillation is excited.

Multiple peak oscillations are also detected when η ranges from $\eta = 0.01$ to 10^{-4}. This regime is very rich in relevant changes occurring in the plasma: the potential profiles decouple rather abruptly from the emitter bias, the onset of the saturation of the charge loss rate is reached at $\eta \approx 3 \cdot 10^{-3}$, and the maximum amplitude and broadest power spectrum of the oscillations are observed simultaneously at $\eta \approx 5 \cdot 10^{-3}$. Multiple mode oscillations are always observed between $\eta = 0.01$ and 10^{-4} independently of the degree of magnetization of the ions. In this range of η, most of the power of the oscillations is normally contained in a broad dominant peak between 100 and 200 kHz, but also narrower peaks related to the $E \times B$ rotation of the plasma are observed. The frequency of these $E \times B$ peaks decreases as the degree of non-neutralization approaches quasi-neutrality (Fig. 3.18) due to the decoupling of the plasma from the emitter bias. The power spectrum of the oscillations in this regime narrows down for stronger magnetic field strengths and degrees of non-neutralization closer to quasi-neutral.

4.4.2 Jumps between equilibrium states

Rather abrupt changes in the emission current and the plasma potential occur when the ion content exceeds $5 \cdot 10^{13}$ m^{-3} (corresponding to $\eta < 10^{-2}$) (see more details in Section 3.3.2). Fig. 4.18 shows that sometimes during the same shot the plasma switches back and forth between a stable equilibrium state (characterized by a plasma potential close to the emitter bias and low emission currents) and a metastable state (in which the plasma is detached from the emitter bias and the emission current is significantly higher). The jumps between

equilibrium states in partially neutralized plasmas typically occur in $\sim$ 100 ms, which is a timescale much slower than the parallel equilibration of the plasma. The timescale of the jumps observed in the emission current and the floating potential are in very good agreement, and these measurements were performed with completely different electronic circuits. Also, the fastest sudden change in the voltage that the current source circuit is able to detect is 20 V/ms, while the slopes measured between equilibrium states were $\sim$ 0.6 V/ms (i.e., the electronic circuits used are sufficiently fast to measure the time constant of the jumps between two equilibrium states).

Transport jumps have been previously observed in CNT's pure electron plasmas [30], but in that case the potential profiles of the two equilibrium states were only slightly different. Hence, the physics behind the two equilibrium states in partially neutralized plasmas appears to be very different from the transport jumps of pure electron plasmas. Since the separation of the plasma potential from the emitter bias is caused by the presence of a finite ion fraction, not due to an emission limit (see Section 3.3.2), the jumps between states in partially neutralized plasmas could be explained in terms of a process that enhances ionization. The plasma becomes denser and hotter as we approach quasi-neutrality (Chapter 3), increasing the ionization rate in the plasma, which might lead to a non-linear self-enhancing process. The jumps between equilibrium states here occur when the plasma density is comparable to the density limit of non-neutral plasmas confined in magnetic surfaces [8], however the physics involved in this case also seem to be different.

4.5 Summary and discussion

The single mode oscillations detected in electron-rich non-neutral plasmas have many characteristics in common with the first observations of the ion-driven fluctuations reported by Q.R. Marksteiner et al. in Ref. [50]. In all the different configurations studied so far (64° conf. with and without a conducting boundary, and 78° tilt angle), CNT's electron-rich plasmas exhibit a 20 - 100 kHz mode related to the $\mathbf{E} \times \mathbf{B}$ rotation when a certain ion threshold is exceeded. The measured frequency of the mode is not just determined by $\omega_{E\times B}$, but also the depends weakly on the ion species introduced: when the mass of the ions introduced in the plasma is increased by a factor of 10 (Ar^+ vs. He^+), 30% lower frequencies are typically

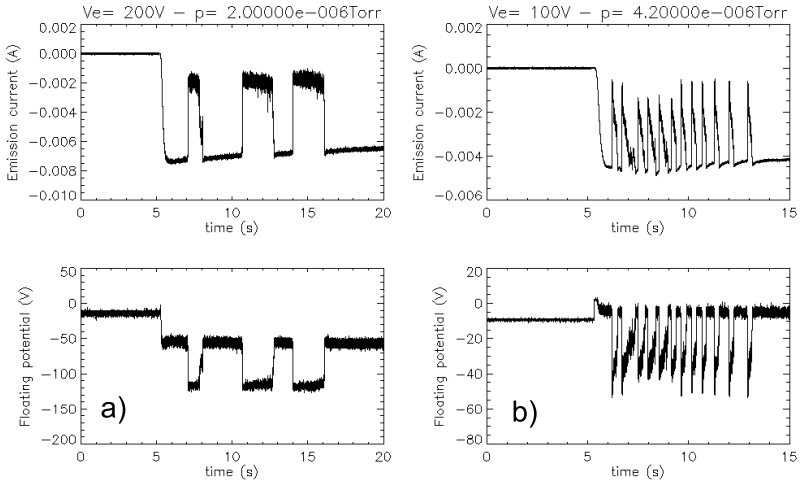

Figure 4.18: Evolution of the emission current (top) and the floating potential at $\psi \approx 0.14$ (bottom) as function of time for two different shots: *a*) $\phi_e = -200$ V, B = 0.08 T and $p_n = 2 \cdot 10^{-6}$ Torr; and *b*) $\phi_e = -100$ V, B = 0.04 T and $p_n = 4.2 \cdot 10^{-6}$ Torr. The plasma switches between two equilibrium states.

measured for a given ϕ_p/B ratio (Fig. 4.8). An offset frequency of ~ 10 kHz is also observed at $\phi_p/B = 0$ (Fig. 4.5-right), which does not agree either with a purely $\mathbf{E} \times \mathbf{B}$ rotation of plasma.

The spatial structure of the oscillations for the 78° tilt angle was measured with two perpendicular arrays of capacitive probes (Fig. 2.2). The ion-driven mode is a global mode of the plasma which travels in the direction of the $\mathbf{E} \times \mathbf{B}$ drift, and exhibits a m = 1 poloidal mode number for both the 64° [49, 50] and the 78° configurations (Fig. 4.15). This implies that CNT's ion resonant instability cannot be stabilized by the magnetic surfaces, even when low number rational magnetic surfaces are present (78° tilt angle). These oscillations are not aligned with the magnetic field lines, and the mode breaks parallel force balance.

The toroidal mode number (n) of the ion-driven oscillations in a stellarator was measured for the first time in this thesis. The mode was determined to be n = 0 for the 78° tilt angle (Fig. 4.16), which is identical to the diocotron mode detected in the absence of magnetic surfaces (m = 1, n = 0 structure in pure toroidal traps [75]), and indicates that the poloidal flux is not conserved in a close tube of plasma moving with the ion-resonant mode. It is

possible that the presence of an anisotropic pressure tensor in the plasma force balance (Eq. 4.4) might explain the apparent breaking of parallel force balance, and the violation of the conservation of poloidal magnetic flux.

One of the most significant differences between the results presented in this thesis and [49, 50] is the observation of two rather different regimes of oscillations in partially neutralized plasmas: 1) the single mode ion-resonance instability, and 2) multi-mode / broadband power spectrum oscillations. In the experiments conducted for this thesis, single mode oscillations were only detected for $0.1 > \eta > 0.01$ at high B field strengths (B > 0.04 T) or when light ion species (He^+) are present in the electron-rich plasma. Hence, the presence of ions with small ion gyro-radius ($r_{Li} < \langle a \rangle$) seems to play an essential role in the development of a single mode ion resonance instability. Multi-mode oscillations are observed for plasmas with degrees of non-neutralization between 10^{-4} and 10^{-2}, and also when largely unmagnetized ions are present in the plasma for $0.1 > \eta > 0.01$. The plasma is more unstable when multiple modes are excited. The detected fluctuations always present broadband power spectrum when the RMS of the oscillations and the charge loss rate reach the highest values (Figs. 3.17 and 3.18).

Davidson's publication [19] studies the effect of a finite ion Larmor radius in a non-neutral plasma column, showing that the fundamental $l = 1$ diocotron mode is unaffected by the value of the ion Larmor radius, but for $l \geq 2$ azimuthal mode number, finite Larmor radius effects can have a strong stabilizing influence. A detailed analysis of the ion motion in the complicated geometry of CNT is provided in Chapter 6 of [49]. Ions exhibit a bouncing motion as they are accelerated in the electron-rich plasma. As shown in Fig. 3.14, massive ions (such as N_2^+) at low magnetic field strengths (B = 0.02 T) are largely unmagnetized ($r_{Li} \gg \langle a \rangle$), the ion motion is highly chaotic in the plasma, and multiple modes are excited. However, for N_2^+ at 0.1 T, the ion gyro-radius is smaller than the torus minor radius ($r_{Li} \lesssim \langle a \rangle$) and the ions turn around before they are accelerated all the way into the plasma. Magnetized ions in CNT (such as, N_2^+ at 0.1 T, or H_2^+ for $0.02 \leq B \leq 0.1$ T) travel close to the $E \times B$ velocity and excite the ion-resonant mode, which scales very close to linear with E/B. The mechanism for instability of these oscillations seems to be identical to the ion resonant instability observed in Penning traps [19], but for the complicated geometry of CNT, the presence of magnetized ions traveling close to the $E \times B$ drift is essential for single

mode behavior. Otherwise, broadband oscillations are detected in the plasma.

Chapter 5

Oscillations in CNT's quasi-neutral plasmas

Quasi-neutral plasmas are routinely used in CNT to produce visualizations of the magnetic surfaces [12]. When the background neutral pressure in the chamber exceeds 10^{-5} Torr ($\eta < 10^{-5}$), the plasma emits sufficient light in the visible range to be seen even with the naked eye. These visualizations are systematically used as a diagnostic for probe alignment, and confirmation of the magnetic topology [12], but CNT's quasi-neutral plasmas had not been studied in depth in the past.

Section 5.1 of this Chapter summarizes the first equilibrium measurements of quasi-neutral plasmas in CNT. The rest of the Chapter is devoted to the detailed characterization of the spontaneous oscillations detected for degrees of non-neutralization $\eta < 10^{-4}$. Section 5.2 investigates the dependence of the mode on experimentally adjustable parameters, and Section 5.3 presents the studies on the spatial structure of the oscillations, providing fundamental information to understand the underlying physics behind CNT's quasi-neutral fluctuations.

5.1 Equilibrium measurements in quasi-neutral plasmas

The potential, temperature and density of quasi-neutral plasmas have been measured by the interpretation of the signal in emissive and Langmuir probes using the same techniques described in [42] for pure-electron plasmas in CNT. The presence of ions in quasi-neutral plasmas simplifies some of these measurements (the density of quasi-neutral plasmas can be determined through the ion saturation current [34], while the lack of ions in a pure electron plasma makes the measurement of n_e much harder [42]).

In the quasi-neutral regime the plasma potential profiles are completely decoupled from the emitter bias voltage ($0 < \phi_p/\phi_e < 0.1$), and the magnetic field strength determines the equilibrium. $|\phi_p|$ increases with the magnetic field strength (Fig. 3.13), and typically higher $|\phi_e|$ are associated to slightly lower measured values of $|\phi_p|$. The reader is referred to Section 3.3 for a complete description of the potential measurements. Fig. 5.1 shows that the electron temperature at $\psi \approx 0.15$ ranges between 30 and 45 eV in the quasi-neutral regime, but does not have a clear relationship with the B field strength.

The power supplies used to bias our probes cannot handle the ion saturation currents collected by a $7.4\,\mathrm{cm}^2$ ion probe in the quasi-neutral regime (this ion probe was originally installed for the determination of n_i in electron-rich plasmas, see Section 3.1). Instead, for quasi-neutral plasmas a small cold filament ($\phi = 0.7\,\mathrm{mm}$, $\mathrm{L} = 3\,\mathrm{mm}$) is used as an ion probe (enough signal is collected by the filament, and $\mathrm{I_{sat}}$ does not exceed the technical limits of the power supplies). $\mathrm{I_{sat}}$ is determined as the current at which the probe filament is 100 V more negative than the local plasma potential. The Bohm sheath criterion was used to calculate the density profiles shown in Fig. 5.2. The plasma density is slightly higher at stronger B fields, and a centrally peaked density profile is always measured in CNT's quasi-neutral plasmas (Fig. 5.2). The Debye length in this regime is $\lambda_D \lesssim 1\,\mathrm{mm}$, which is more than one order of magnitude smaller than λ_D for CNT's pure-electron plasmas [43].

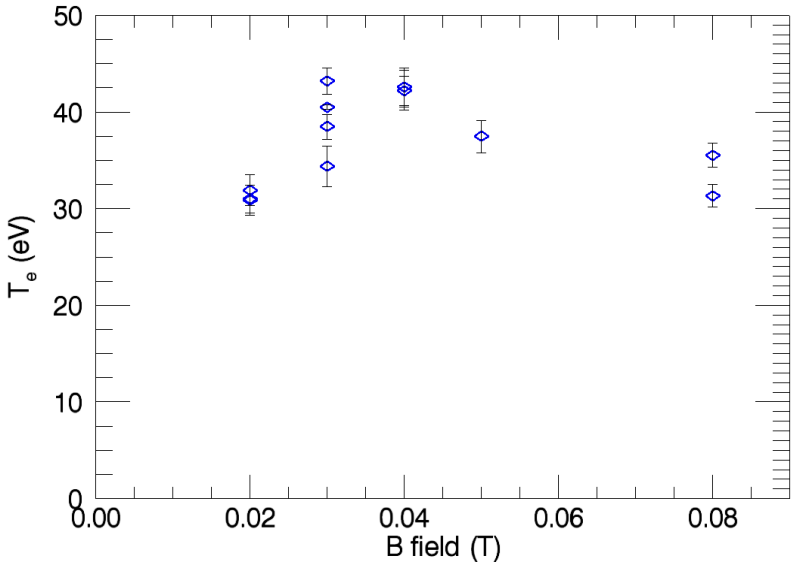

Figure 5.1: Measured T_e at $\psi \approx 0.15$ vs. B field strength in quasi-neutral plasmas. $\phi_e = -200$ V, $p_n = 2 \cdot 10^{-5}$ Torr of N_2. 78° configuration.

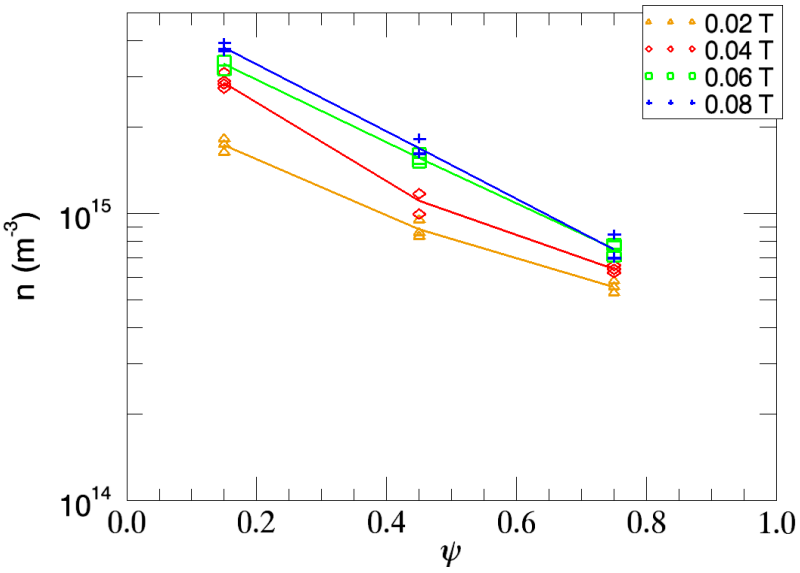

Figure 5.2: Measured density profiles in the nw♯4 probe array for B = 0.02 T, B = 0.04 T, B = 0.06 T, and B = 0.08 T. Quasi-neutral plasmas. $\phi_e = -200$ V, $p_n = 2 \cdot 10^{-5}$ Torr of N_2. 78° configuration.

5.2 Parameter dependence of the oscillations

In contrast to pure electron plasmas, quasi-neutral plasmas in CNT are characterized by weak electric fields (the plasma comes closer to the E field set by ambipolarity). As plasmas evolve to quasi-neutrality ($\eta < 10^{-5}$), the power spectrum of the fluctuations narrows down and its amplitude decreases until the oscillations settle into a steady state with approximately constant amplitude and a single dominant frequency between 1 and 20 kHz.

This Section gives an overview on the possible mechanisms that might be driving these oscillations, studies the dependence of the frequency and amplitude of the mode on experimentally adjustable parameters, investigates the local phase shift between density and potential fluctuations, and presents the frequency profile of the oscillations at different radial locations across the plasma.

5.2.1 Theoretical considerations

It is unlikely that the driving mechanism of CNT's quasineutral mode is the same ion resonance that we see in electron-rich non-neutral plasmas (the ion resonant instability is stable in quasi-neutral plasmas [18, 19]).

The ratio of plasma pressure to magnetic pressure (β) is very low in CNT's quasi-neutral plasmas. Other quasi-neutral stellarators estimate the average β of the plasma ($\langle\beta\rangle$) from measurements of the magnetic flux generated by the diamagnetic or the Pfirsch-Schlüter currents [53, 66]. $\langle\beta\rangle \leq 2\%$ is typical in other quasi-neutral stellarators [35, 78]. However, in CNT the plasma currents produce a negligible perturbation to the vacuum magnetic field created by the coils, and based on the equilibrium measurements, $\langle\beta\rangle$ is at least three orders of magnitude lower than in other stellarators. Therefore, it is very unlikely that the spontaneous mode detected in CNT's quasi-neutral plasmas is driven by some MHD instability, that usually limit the maximum achievable β in a stellarator. Also, the detected oscillations travel at a velocity much slower than the Alfven speed, $v_A = B/\sqrt{m_i n_i \mu_0}$ [27] (in CNT $v_A \approx 0.01c$, where c is the speed of light in vacuum).

Low-β plasmas confined in toroidal magnetic configurations can develop different low frequency instabilities that propagate at velocities in the order of the $E \times B$ rotation of the plasma (in agreement with the observations in CNT). These low frequency instabilities have

been classified according to their drive mechanism into: Drift waves, Kelvin-Helmholtz, and Rayleigh-Taylor instabilities [38].

Drift waves are low frequency oscillations of the plasma driven by the pressure gradient across the magnetic field. The wave frequency of these oscillations is normally Doppler shifted by the $E \times B$ frequency, and the measured frequency in the laboratory frame is $\omega = \omega_{E\times B} \pm \omega_*$. ω_* is the drift wave frequency $\omega_* = k_\perp \rho_s c_s / L_n$, where $\rho_s = c_s/\omega_i$, c_s is the ion acoustic speed $c_s = \sqrt{T_e/m_i}$, and L_n is the density scale length [64]. The growth rate of drift waves is comparable to ω_*, $\gamma \sim \omega_*$. In non-resistive drift waves, the electron density and potential fluctuations are in phase [27]. The introduction of non-zero resistivity causes a small phase shift ($< 45°$, [38]) between $\widetilde{n}$ and $\widetilde{\phi}$, which drives transport of plasma across the confining magnetic field [33].

The Kelvin-Helmholtz instability is a hydrodynamic instability driven by the velocity shear ($\partial/\partial r \left(-\partial\phi/\partial r/B\right)$) [16]. This instability propagates perpendicularly to the magnetic field lines ($k_{||} = 0$), its phase velocity is 0.2 to 0.6 times the $E \times B$ rotation of the plasma, and it is characterized by a large local phase shift between $\widetilde{n}$ and $\widetilde{\phi}$ (90° to 180°, [38]).

Rayleigh-Taylor instabilities in magnetized plasmas are driven by anti-parallel magnetic field curvature and pressure gradient (such as in the outboard side of a torus). They have characteristics of flute instabilities ($k_{||} = 0$), propagate at the $E \times B$ velocity of the plasma, and the local $\widetilde{n} - \widetilde{\phi}$ phase shift is typically between 45° and 90° [38].

The local phase shift between $\widetilde{n}$ and $\widetilde{\phi}$ has been traditionally used as a discriminating quantity to determine the nature of these low frequency instabilities [14, 26, 38, 65]. Results on the local phase difference between $\widetilde{n}$ and $\widetilde{\phi}$ in CNT's quasi-neutral mode are presented in Section 5.2.5.

5.2.2 Dependence on η, ϕ_{plasma}, B field strength, and different ion species

The frequency of the mode has a negligible dependence on neutral pressure. Fig. 5.3 presents the Fourier Spectrum of these oscillations as a function of the neutral pressure, showing that the frequency of the dominant mode at higher pressures is somewhat lower (since higher pressures are associated to slightly more modest electric fields).

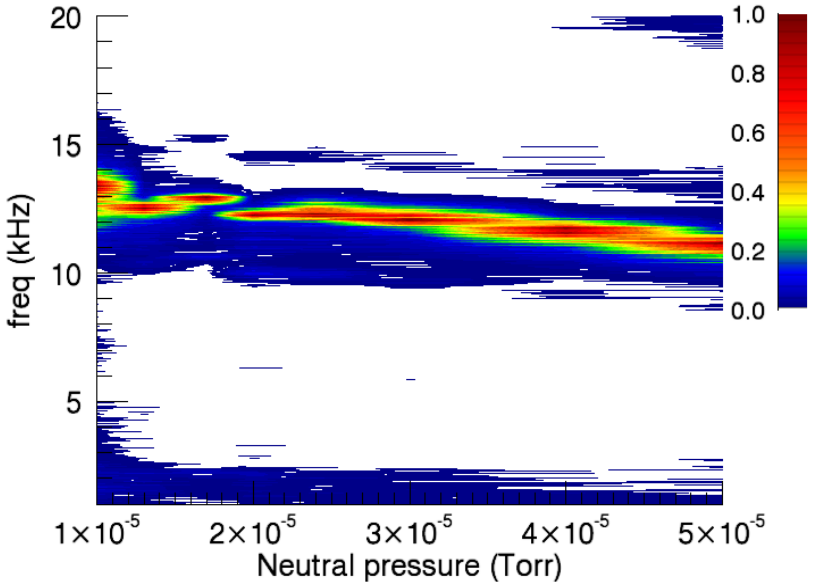

Figure 5.3: Power spectrum of the signal on a floating emissive probe vs. neutral pressure of N_2. Quasi-neutral plasmas, $\phi_e = -200$ V, B = 0.08 T, 64° configuration.

The amplitude and frequency of the mode grow with the B field strength (Fig. 5.4). This increase of the frequency with the B field was unexpected, but it is due to the scaling of the plasma potential with the magnetic field in this regime. Quasi-neutral plasmas are fully decoupled from the emitter bias voltage (see Section 3.3), and ϕ_{plasma} is largely determined by the magnetic field strength (stronger B fields present more negative ϕ_{plasma}). A linear scaling can be inferred plotting the frequency of the mode against ϕ_{plasma} (Fig. 5.5).

However, the *emissive probe floating potential* method used to the determine the potential of our quasi-neutral plasmas introduces large uncertainties in this regime (see Section 3.3.1). And the scaling of the measured frequency on ϕ_{plasma}/B (Fig. 5.6 for different ion species) does not give enough evidence to conclude if these oscillations are convected by the $\mathbf{E} \times \mathbf{B}$ drift or are related to other instabilities seen in quasi-neutral stellarators.

5.2.3 Effect of the magnetic configuration

The behavior of the low frequency oscillations observed in quasi-neutral plasmas was also investigated in the 78° configuration, showing almost identical characteristics to what was

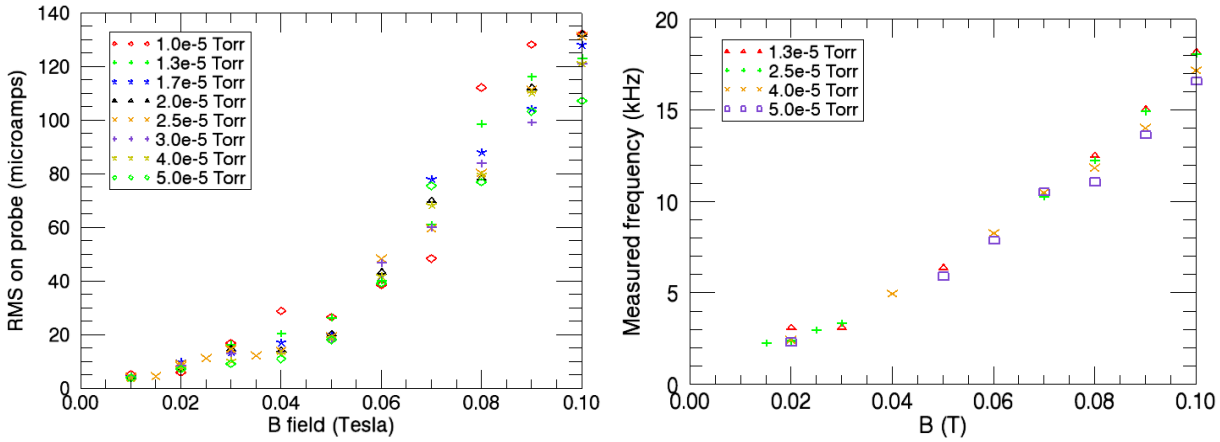

Amplitude vs. B field

Frequency vs. B field

Figure 5.4: Measured amplitude and dominant frequency of the oscillations in quasi-neutral plasmas vs. magnetic field strength. $\phi_e = -200$ V, 64° configuration.

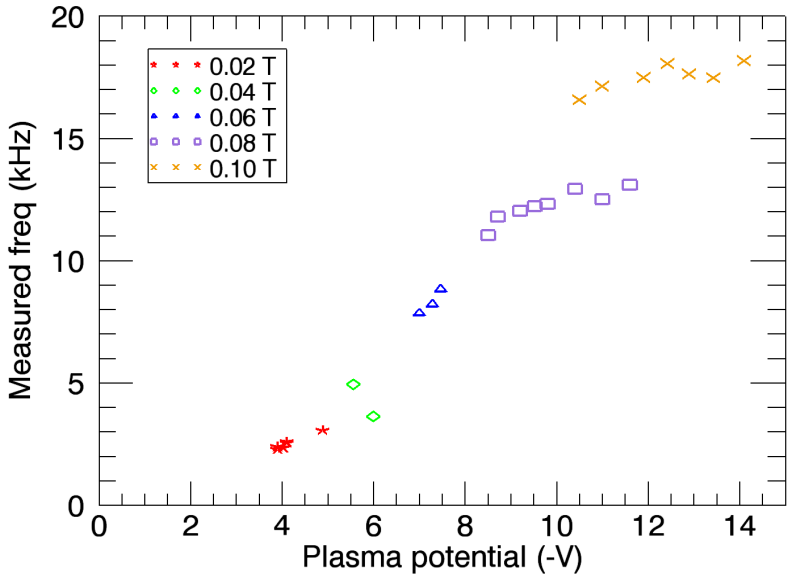

Figure 5.5: Measured frequency of the mode in quasi-neutral plasmas vs. ϕ_{plasma}. $\phi_e = -200$ V, 64° configuration.

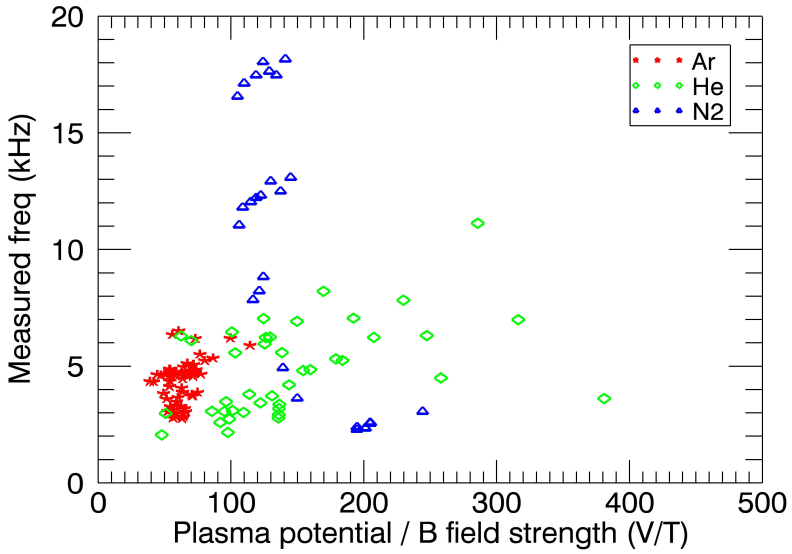

Figure 5.6: Measured frequency vs. ϕ_{plasma}/B for quasi-neutral plasmas with background pressures of Ar, He, and N_2. 64° configuration.

seen in the 64° tilt angle (described in section 5.2.2). The amplitude of the fluctuations increases with the magnetic field strength, and its frequency also scales close to linear with the measured plasma potential in the 78° conf (Fig. 5.7-left). Fig. 5.7-right shows how the frequency of the mode depends on ϕ_p/B for a range of pressures, emitter bias voltages, and magnetic field strengths. High ϕ_p/B ratios cause higher frequency oscillations, but a linear E/B scaling of the measured frequency is not evident either in the 78° configuration.

5.2.4 Frequency profiles across the plasma

The frequency of the oscillations was measured with floating emissive probes at different locations along the se8 probe array to investigate the velocity profile of the fluctuations across the plasma. Since the frequency of the mode can vary slightly from shot to shot even when we try to reproduce the same experimental conditions, the fluctuations were also recorded in an emissive probe held at $\psi \approx 0.15$ for these experiments, and this probe was used as a reference. Thus, the frequency difference between the oscillations in the core of the plasma and at each location of the se8 array can always be compared to investigate the

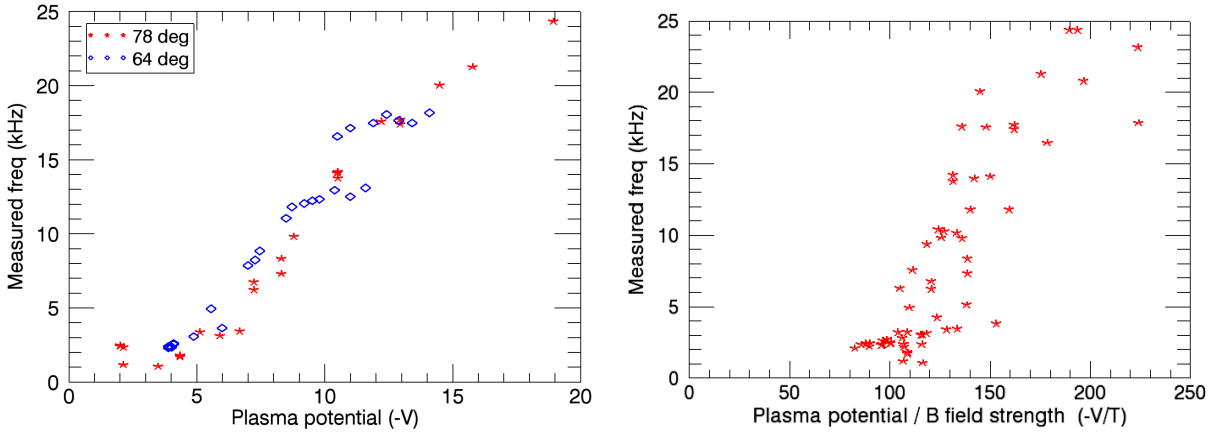

Freq vs. ϕ_{plasma} Freq vs. ϕ_{plasma}/B

Figure 5.7: Measured frequency of the dominant mode in quasi-neutral plasmas vs. ϕ_{plasma} and ϕ_{plasma}/B. *Left:* Freq vs. ϕ_{plasma} ($\phi_e = -200$ V, 64° vs. 78° configuration). *Right:* Freq vs. ϕ_{plasma}/B ($0.02 \leq B \leq 0.10$ T, $-400 \leq \phi_e \leq -100$ V, 78° conf).

presence of velocity shear.

The frequency of the oscillations have a flat radial profile for magnetic field strengths B $\leq$ 0.04 T (Fig. 5.8), showing that the detected instability is a global mode (the plasma moves as a whole), and no velocity shear is observed. This was verified in the observations of the mode with a high speed camera (Section 5.3).

For magnetic fields above 0.05 T (Fig. 5.9), the interpretation of the frequency profiles is not as clear as the data shown in Fig. 5.8. The Fourier transforms at the different locations of the se8 array have three peaks (Fig. 5.9-left). The lowest frequency mode has a flat frequency profile, but the frequency of the other two modes grows as we move away from the magnetic axis, and at some locations one of these two higher frequency modes nearly disappears. However, Fig. 5.9-right shows that the power spectrum of the oscillations in the core of the plasma ($\psi \approx 0.15$) behaves quite similarly compared to Fig. 5.9-left as we vary the location of the secondary emissive probe in the se8 array. It is not clear why the location of a secondary emissive probe affects the frequency of the oscillations in the plasma, but no frequency difference was observed between the modes in the core of the plasma and the different locations of the se8 array, implying that no velocity shear was detected either for

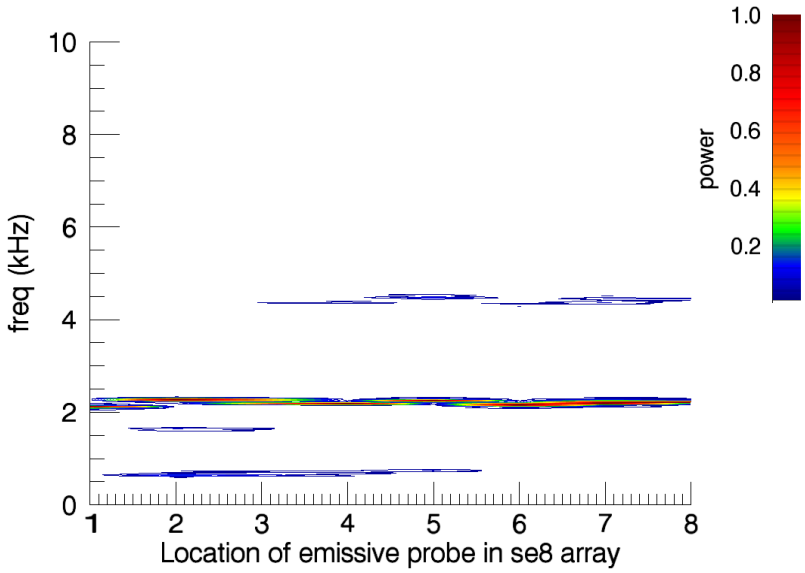

Figure 5.8: Frequency profile of the quasi-neutral mode. The figure shows the Fourier power spectrum of the signal in floating emissive probes at different locations of the se8 array. se8♯1 is the innermost filament (located on the magnetic axis), while se8♯8 is close to the plasma edge. $p_n = 2 \cdot 10^{-5}$ Torr of N_2, $\phi_e = -200$ V, B = 0.03 T, 78° configuration.

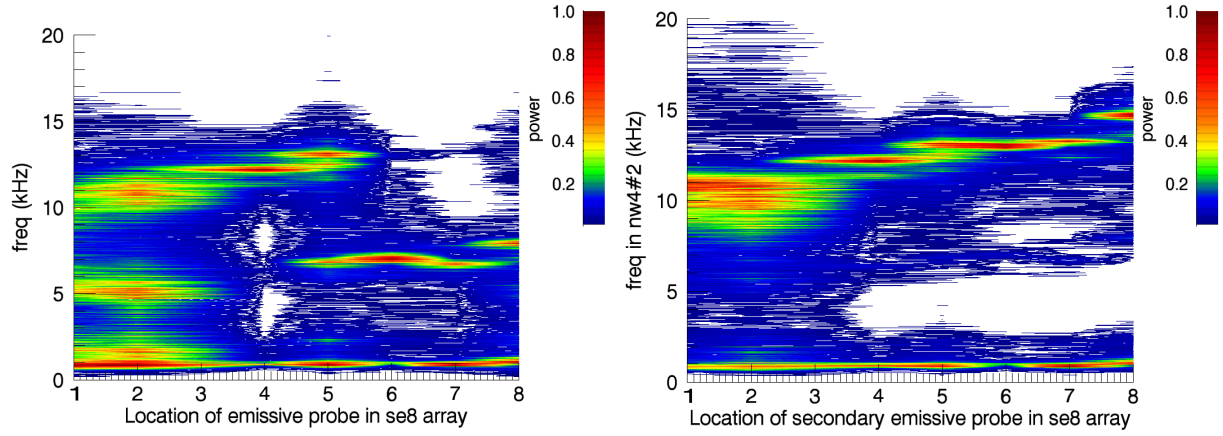

Fourier spectrum at different se8 locations

Fourier spectrum at nw4♯2

Figure 5.9: *Left:* Fourier power spectrum of the signal in floating emissive probes at different locations of the se8 array. *Right:* Fourier power spectrum of the signal in nw4♯2 ($\psi \approx 0.15$) as the position of a secondary floating emissive probe is varied along the se8 probe array. se8♯1 is the innermost filament (located on the magnetic axis), while se8♯8 is close to the plasma edge. Quasi-neutral plasmas at $p_n = 2.5 \cdot 10^{-5}$ Torr of N_2, $\phi_e = -200$ V, B = 0.06 T, 78° configuration.

magnetic field strengths B > 0.05 T.

5.2.5 Local phase shift between density and potential fluctuations

The procedure explained in section 4.2.5 was also used to measure the local phase shift between density and potential fluctuations in quasi-neutral plasmas. In this case, the plasma potential oscillations in nw4 ♯2 ($\psi \approx 0.15$) and ♯3 ($\psi \approx 0.45$) seem to be in phase (Fig. 5.10-left) for all magnetic field strengths above 0.03 T (the $\pm 2\sigma$ confidence interval shown in Fig. 5.10 only takes into account measurements at B $\geq$ 0.03 T). At low magnetic field strengths (B = 0.02 T) the plasma potential oscillations in nw4 ♯3 seem to lead the potential oscillations measured at nw4 ♯2 by $60° \pm 25°$.

The oscillations in the ion saturation current (I_{sat}) were also measured in a cold filament located at nw4 ♯3 and biased 100 V more negatively than the local plasma potential. The collected current in an ion probe scales like $I_{sat} \propto -n\sqrt{T_e}$ [34], and the amplitude of the T_e

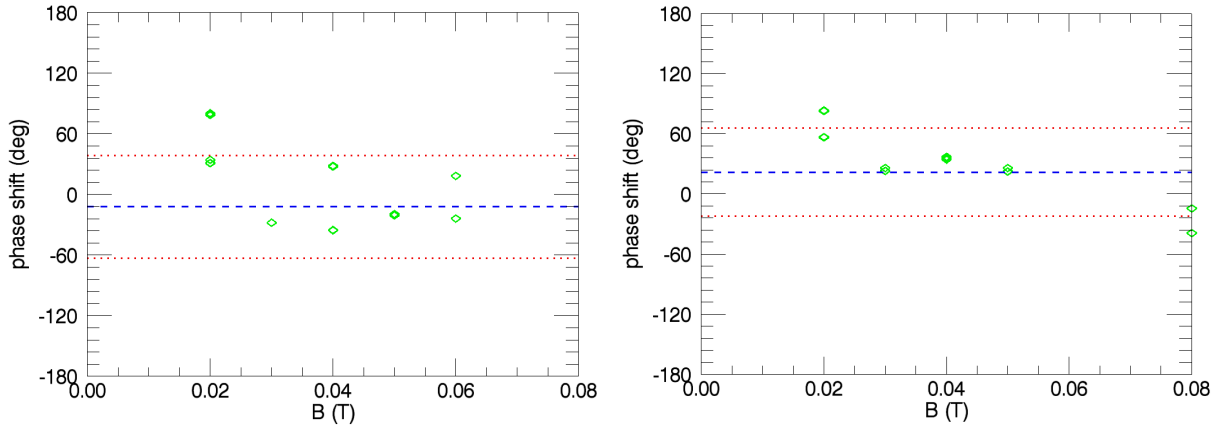

Figure 5.10: *Left:* Phase difference between the potential fluctuations measured in nw4 ♯3 and nw4 ♯2. *Right:* Phase difference between the density (measured in nw4 ♯3) and the potential (nw4 ♯2) fluctuations. The dashed blue line represents the average phase shift, and the $\pm 2\sigma$ confidence interval is given by the two red dotted lines (only taking into account measurements at B $\geq$ 0.03 T). Quasi-neutral plasmas with a background neutral pressure of N_2, $\phi_e = -200$ V.

oscillations is small ($\widetilde{T}_e \,/\, \overline{T_e} \leq 0.1$ in a cycle of Langmuir I-V characteristics. More details are provided in the paragraphs below). The oscillations in I_{sat} are therefore mainly caused by fluctuations of the plasma density. Fig. 5.10-right shows that $\widetilde{n}$ in nw4 ♯3 and $\widetilde{\phi}$ in nw4 ♯2 are close to being in phase for B $\geq$ 0.03 T. At B = 0.02 T, the signal in probe nw4 ♯3 leads nw4 ♯2 by a small phase shift. But comparing Figs. 5.10-left and right, we can see that there is evidence suggesting that $\widetilde{n}$ and $\widetilde{\phi}$ are close to being in phase at nw4 ♯3 for all the B fields explored, which eliminates the possibility of having a Kelvin-Helmholtz instability (characterized by a $\widetilde{n}$ - $\widetilde{\phi}$ local phase shift between 90° and 180° [38]). However, the large uncertainties in the determination of the local phase shift ($\widetilde{n}$ leads $\widetilde{\phi}$ at nw4 ♯3 by $34° \pm 57°$) do not allow us to discern if the instability is a drift wave (predicted local phase shift between 0° and 45°), or a Rayleigh-Taylor instability (phase shift between 45° and 90°).

A typical Langmuir I-V characteristic in CNT's quasi-neutral plasmas is presented in Fig. 5.11-left, showing that the amplitude of the current oscillations is quite large compared to its average value, and that I_{probe} scales linearly with V_{probe} at the most negative probe

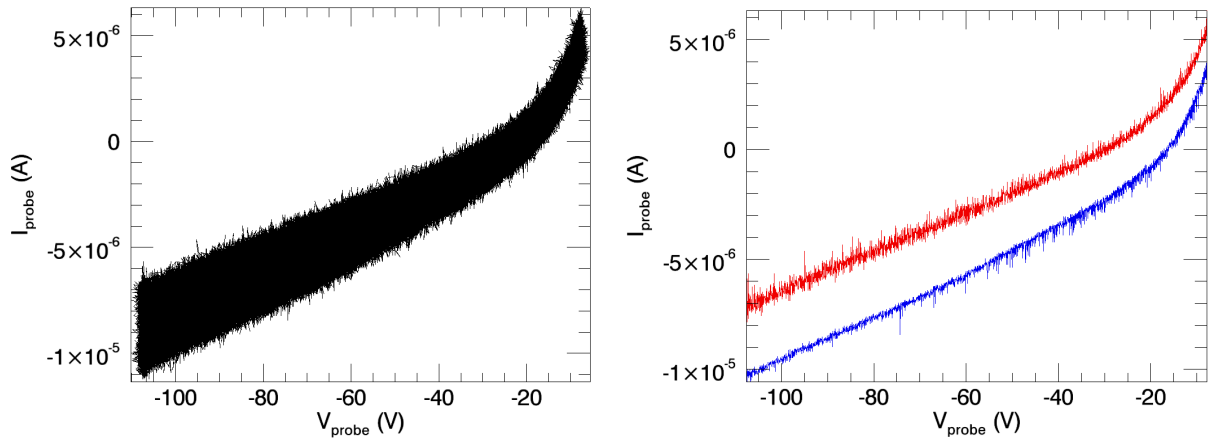

Figure 5.11: *Left:* Langmuir I-V characteristic. *Right:* Langmuir $I_{max} - V$ (red) and $I_{min} - V$ (blue) characteristics. Only the maximum and minimum value of I_{probe} at each cycle of the dominant mode of the oscillations are plotted. Quasi-neutral plasma at $p_n = 2.5 \cdot 10^{-5}$ Torr of N_2, $\phi_e = -200$ V, B = 0.02 T, 78° configuration.

potentials (due to the growth of the sheath thickness at increasingly negative potentials). The I_{probe} oscillations were Fourier analyzed, and the maximum and minimum values of I_{probe} were extracted for each cycle of the dominant mode (shown in the two I-V traces of Fig. 5.11-right). Then, I_{probe} was resampled using 10 arbitrary phase bins between two consecutive maxima, and consequently, 10 different I-V characteristics were obtained from a single V_{probe} sweep.

This method provides a valuable tool to examine the fluctuations in the Langmuir probe, since n, T_e and ϕ_{float} can be determined self-consistently interpreting each IV trace at a particular phase of the dominant mode of the I_{probe} oscillations. It seems even possible to use this method to study the local phase shift between $\widetilde{n}$ and $\widetilde{\phi}_{plasma}$. However, in CNT quasi-neutral plasmas ϕ_{plasma} cannot be determined from ϕ_{float} and T_e using the simple textbook equation, $\phi_{float} = \phi_{plasma} - \frac{T_e}{2e}(1 + \ln[m_i/(2\pi m_e)])$ [34], because in CNT the electrons are magnetized, but the ions are very unmagnetized compared to the sheath size. This results in a reduction of the electron current since the electron flow is affected by the magnetic field [34].

The estimate of n used for Fig. 5.10-right assumes a small sheath compared to the size of

the probe and small T_e oscillations. However, the sheath is larger than the size of the probe filament, and grows for increasingly negative probe potentials (Fig. 5.11). Therefore, n has been also calculated for each IV trace, taking into account the growth of the sheath, and using the corresponding measured T_e for each IV characteristic. This involves an iterative process that first estimates the sheath thickness (x_s) using Eq. 5.1 [34], then assumes a cylindrical sheath ($A_{sheath} \approx A_{probe}[1 + x_s/r_{probe}]$) to determine n from $\mathrm{I_{sat}}$ (measured value of $\mathrm{I_{probe}}$ at $\mathrm{V_{probe}} = \phi_{float} - 70$ V), and finally recalculates x_s for the estimated value of n until the error in n is less than 1%.

$$\frac{x_s}{\lambda_D} = \frac{2}{3}\left[\frac{2}{\exp(-1)}\right]^{1/4}\left[\left(\frac{-eV_{probe}}{T_e}\right)^{1/2} - \frac{1}{\sqrt{2}}\right]^{1/2}\left[\left(\frac{-eV_{probe}}{T_e}\right)^{1/2} + \sqrt{2}\right] \tag{5.1}$$

This procedure results in one order of magnitude lower values of n than the ones reported in Fig. 5.2 (since now the growth of the sheath thickness is taken into account). However, the oscillations of n assuming a small sheath, and small T_e oscillations are perfectly in phase with the estimate of n that considers self-consistently the growth of x_s and the variation of T_e (Fig. 5.12). This confirms that the oscillations in $\mathrm{I_{probe}}$ are mainly caused by fluctuations of n (and not T_e), and suggests that $\widetilde{n}$ leads $\widetilde{\phi}$ by $34^\circ \pm 57^\circ$ (Fig. 5.10).

5.3 Spatial Structure

The spatial structure of the quasi-neutral mode can be investigated by using any of the diagnostics available in CNT for this purpose (capacitive probes, conducting boundary, or high speed camera). The results reported in this section will focus on the measurements obtained with the fast camera since this method provides the highest spatial resolution. Section 5.3.3 summarizes the results obtained with the capacitive probes, showing good agreement between the high speed camera and the capacitive probes.

5.3.1 Fast camera. Experimental considerations

CNT's plasmas are usually created emitting electrons from a 10 W halogen filament. When the background neutral pressure in the chamber is above 10^{-5} Torr ($\eta < 10^{-5}$), a glowing

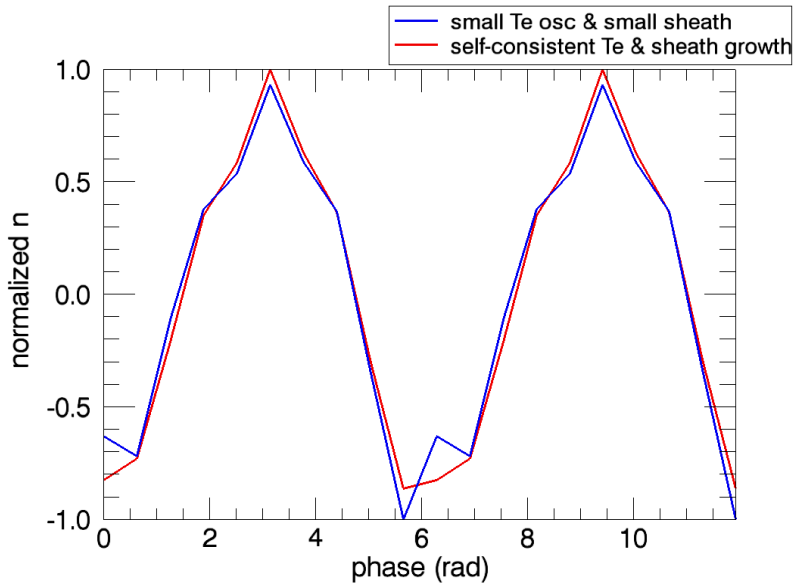

Figure 5.12: *Blue:* Oscillations in n assuming a small sheath, and small T_e oscillations. *Red:* Estimate of n considering self-consistently the growth of the sheath thickness, and the variation of T_e. Same shot as in Fig. 5.11.

plasma can be seen even with the naked eye. However, when using the fast camera at high frame rates, the shutter only remains open for a few micro-seconds, and the amount of light produced is not enough to excite the camera sensor. This is a very common issue in fast camera imaging experiments in plasma physics. In other experiments, either image intensifiers are used to improve the signal level (TJ-II stellarator, [15]) or gas puffing is employed to increase the brightness of the plasma (Helitron-J and GAMMA 10 tandem mirror, [54]).

In CNT the luminescence of the plasma can be increased by different means. Raising the neutral pressure in the chamber is proven to be an effective method, however the length of the visible trace of electrons decreases at high pressures (for $p_n > 2 \cdot 10^{-4}$ Torr only a few transitions of the electron trace can be observed around the torus). High wattage filaments are able to emit higher emission currents, increasing the plasma density and, in turn, enhancing significantly the brightness of our plasmas. Therefore, the plasmas diagnosed with the fast camera are created emitting electrons from a 50 W halogen filament. The

filament was installed in the innermost spot of the se8 probe array, and experiments were conducted with the filament emitting on axis, and a few centimeters (4 to 12 cm) away from axis in order to increase the volume of the glowing plasma.

The best visualizations of the oscillations in the plasma were recorded for neutral pressures between $2 \cdot 10^{-5}$ and $2 \cdot 10^{-4}$ Torr and for emitter bias voltages $\phi_e \leq -150$ V. Plasmas biased at -50 V and -100 V were too faint, and the amplitude of the light fluctuations of the pixels decreased dramatically when sampling above 1,000 fps or even no oscillations were observed in most of the pixels. Once the $\phi_e = -150$ V threshold is exceeded, emitting at more negative bias voltages does not improve significantly the brightness of the plasma. Experiments were also performed at different magnetic field strengths (0.02 to 0.08 T), but the luminescence of the plasma is not a strong function of the B field strength.

Parameter dependence of the oscillations in plasmas created by 50 W filaments

Low frequency oscillations were captured with the fast camera using a 50 W filament to increase the brightness of the plasma. Basic observations of these movies show glowing structures along the field lines moving poloidally in the plasma surfaces. The question remains on how these oscillations relate to previously observed fluctuations in the same range of operational parameters but emitting from a 10 W filament. For this purpose, the influence of the pressure, magnetic field, and emitter bias voltage on the frequency of the oscillations was explored in plasmas created with a 50 W filament, and the results were compared to previous experiments.

For both 10 and 50 W filaments, the measured frequency decreases slightly with the neutral pressure in the chamber, because degrees of non-neutralization closer to $\eta = 0$ present weaker electric fields. The plasma potential in CNT's quasineutral plasmas is independent of the emitter bias voltage, and is largely determined by the magnetic field strength (higher magnetic fields confine charge better). Experimentally, we can see that more negative emitter bias voltages are associated to somewhat lower frequencies, this is a result of the increased ion content at higher emitter biases. Also, the frequency of the oscillation raises with the B field (Fig. 5.13), as observed earlier in experiments with 10 W filaments. Therefore, the scaling of the oscillations in plasmas created with a 50 W filament is in very good agreement

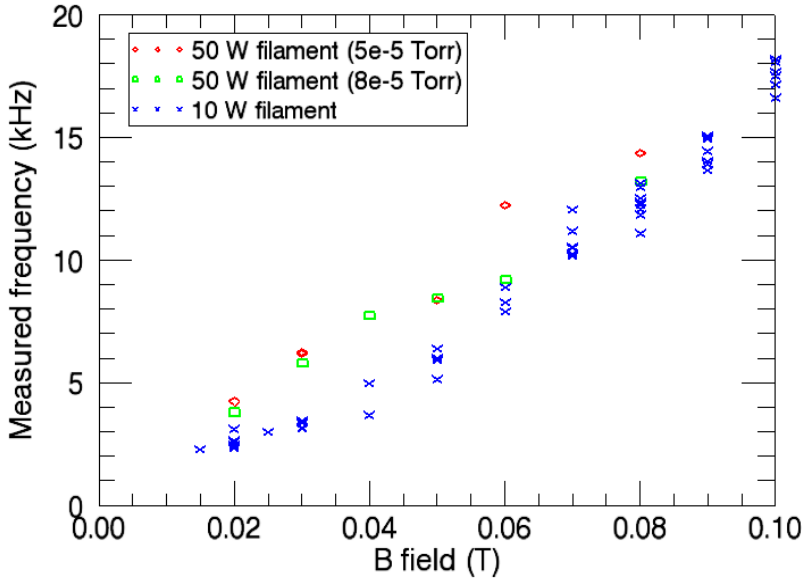

Figure 5.13: Measured frequency vs. magnetic field strength emitting from a 50 W and a 10 W filament ($\phi_e = -200$ V. 64° configuration).

with the experiments using a 10 W filament.

Visualization of the magnetic field line traces

Additionally, the luminescent traces of the field lines were recorded with the fast camera in order to study the alignment of the observed mode with the magnetic field lines. Once a series of movies of the plasma oscillations was recorded from a specific location, the traces of the field lines were visualized emitting an electron beam from the same emitter filament. For the visualizations of the field line traces, the volume of the close magnetic surfaces was intersected with a grounded aluminum rod (preventing the formation of the plasma), and the neutral pressure in the chamber was raised to $p_n \approx 5 \cdot 10^{-4}$ Torr, so that only 3 to 5 transitions of the electron beam could be observed around the torus. The average light intensity of each pixel was computed for the movies visualizing the field line traces, and the resulting "average frame" was used to identify the luminescent traces. A spline was drawn along the brightest pixels of each field line trace, and their coordinates were stored to be used in comparisons with movies and phase plots of the plasma fluctuations. Error bars were

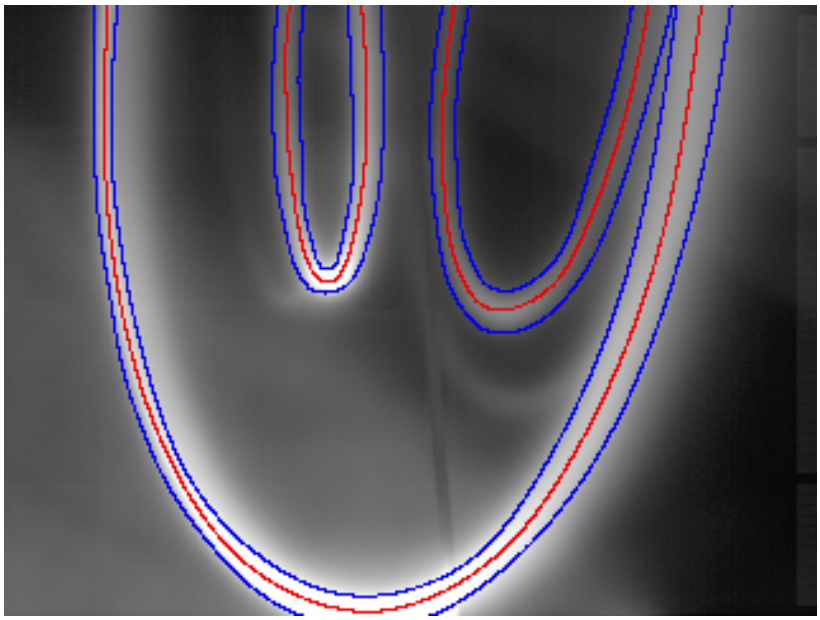

Figure 5.14: Luminescent trace of a magnetic field line. 3 transitions of the field line around the torus as seen from the top window of the chamber. A red line is drawn following the brightest pixels of each field line trace. Error bars are also identified in blue.

also identified in the luminescent traces (see Fig. 5.14).

The method to compare the alignment of the oscillations with the field lines relies on the fact that the visualizations of the field lines were taken right after a series of movies of the plasma oscillations was recorded, so the position and orientation of the camera were identical in both sets of movies. This could also be confirmed comparing the position of easily identifiable characteristics in both the visualizations of the field lines and the movies of the plasma fluctuations (such as the edge of a coil or a weld seam). In Fig. 5.15 a) and b) two edges of a coil are marked in both sets of movies and the traces are overlaid in Fig. 5.15 c) showing that the orientation of the camera has not changed. This method confirmed that the comparison of the structure of the oscillations with its corresponding visible field line traces was adequate in almost all of the cases. The procedure also allowed us to rule out one set of movies in which the orientation of the camera changed slightly when the luminescent field lines were recorded (Fig. 5.16).

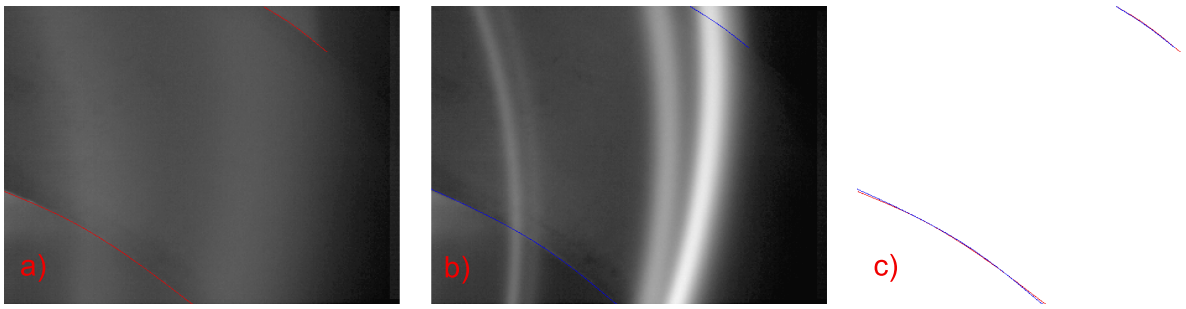

Figure 5.15: A set of movies properly aligned. a) Two edges of an IL coil are identified in the movie of the plasma oscillations. b) The same characteristics are marked in the visualization of the field lines. c) The traces from both movies are overlaid.

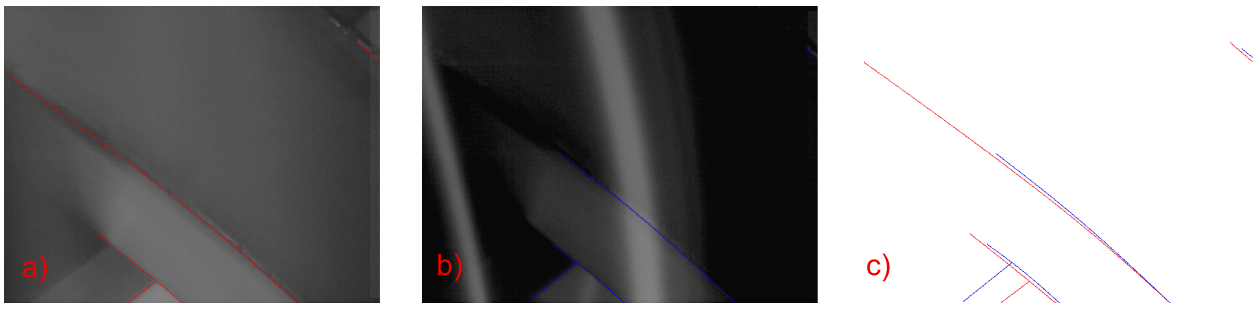

Figure 5.16: This procedure allowed to rule out a few movies in which the orientation of the camera changed slightly when the luminescent field lines were recorded. a) Four edges of the IL coils are identified in the movie of the plasma oscillations. b) The same characteristics are marked in the visualization of the field lines. c) The traces from both movies are overlaid showing a mismatch between the characteristics of both movies.

5.3.2 Fast camera. Experimental results

The spatial structure of the low frequency oscillations in the quasi-neutral regime has many characteristics in common for the two tilt angles at which CNT has operated so far (64° and 78° tilt angles). In both configurations, a global mode is observed moving poloidally in the plasma surfaces. Qualitatively, the mode propagates perpendicularly to the magnetic field lines, and the direction of propagation is in agreement with the $\mathbf{E} \times \mathbf{B}$ rotation of the plasma.

Statistics of the light fluctuations have been calculated, and correlations with the signal in a floating emissive probe located at $\psi \approx 0.15$ have been performed. In movies of 256×64 pixels the statistic analyses have been performed using the first 6,000 frames after the trigger (1,250 frames were analyzed in the 320×240 pixel movies).

Fourier Analysis

The Fourier Transform of each oscillating pixel has been computed, showing that most of the pixels in the movies oscillate at the same frequency as the current in the floating emissive probe. The results are summarized in plots like Figs. 5.17 and 5.18, where the dominant frequency of each pixel is shown in a contour plot (Fig. 5.17), and the number of pixels oscillating at a particular frequency is displayed in an histogram and compared to the power spectrum of the signal in the floating probe (Fig. 5.18). The histogram presents two clear peaks: one at 0 kHz (white (not-oscillating) pixels in Fig. 5.17), and other at 3.5 kHz (green pixels in Fig. 5.17) coinciding with the dominant frequency of the electrostatic probe.

Coherence and Phase Analysis

The coherence between the signal in the electrostatic probe and each oscillating pixel was analyzed using the cross-correlation function ($C_{1,2}$) [37] (Eq. 5.2). As expected from their almost identical Fourier spectrum, the coherence analysis indicates that the density fluctuations (proportional to the light intensity in each pixel) are well correlated with the oscillations of the plasma potential.

The phase information was also obtained from the cross-correlation analysis. The phase (α) is a function of the frequency, thus the value of α plotted in Figs. 5.19 to 5.23 corresponds

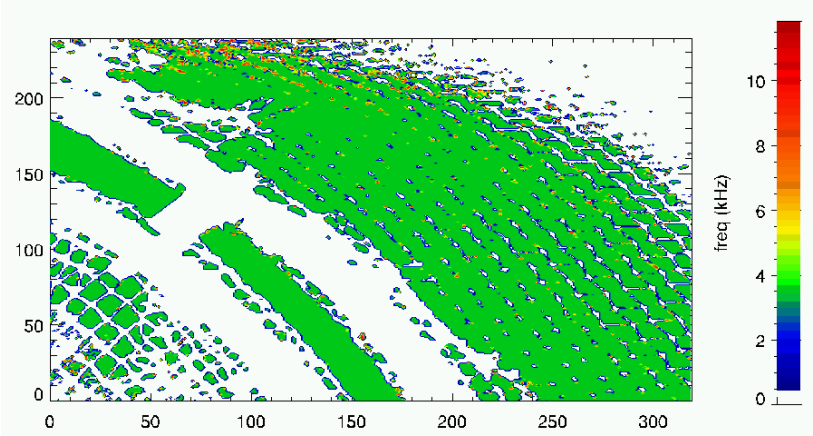

Figure 5.17: Contour plot of the dominant frequency at each pixel. Most of the pixels exhibit the same color, indicating a uniform dominant frequency in the movie (white color indicates the pixel does not oscillate). View from the "nw" side port. $p_n = 8 \cdot 10^{-5}$ Torr of N_2, B = 0.02 T, $\phi_e = -200$ V, 64° configuration.

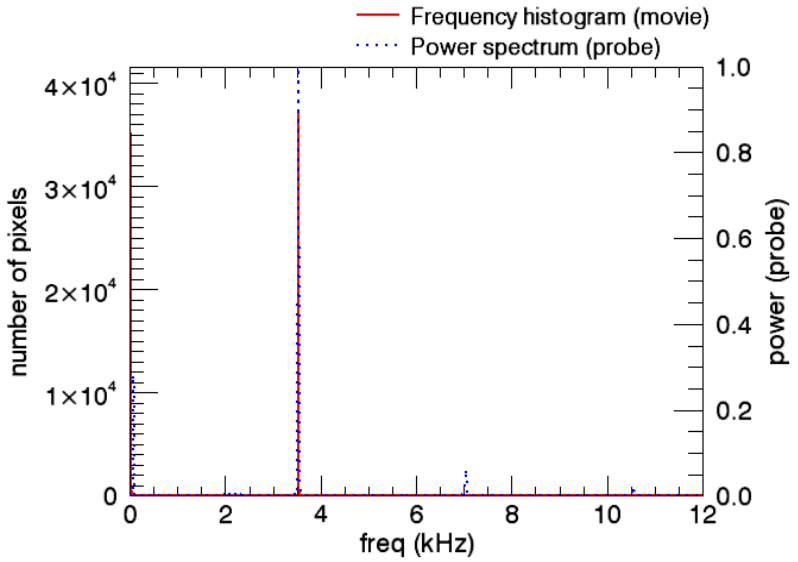

Figure 5.18: Histogram of the number of pixels oscillating at a particular frequency (red). Power spectrum of the floating probe overlaid (blue dots). Same shot as in Fig. 5.17.

to the phase at the dominant frequency of the cross-correlation power spectrum. The phase plots in this Section only contain the phase information of the pixels whose RMS was greater than 10% of the average RMS of the oscillating pixels in a movie, thus avoiding the potentially random phase of low amplitude oscillations.

$$\begin{aligned} &\text{Fourier Transform} && g(t) \rightarrow^{FT} \rightarrow G(\omega) \\ &\text{Cross correlation} && C_{1,2}(\omega) \equiv G_1 G_2^* \\ &\text{Phase} && \alpha_{1,2}(\omega) \equiv \arctan\left(\frac{\mathbf{Im}\left[C_{1,2}(\omega)\right]}{\mathbf{Real}\left[C_{1,2}(\omega)\right]}\right) \end{aligned} \tag{5.2}$$

Field alignment and mode number

64° *configuration*

Experiments in the 64° tilt angle configuration showed that the mode number of the oscillations jumps when the B field strength is raised above 0.05 T. Low frequency oscillations (experiments at B = 0.02 T) seem to have a low poloidal mode number (m = 1 or 2), as can be seen in the phase plot of Fig. 5.19 or the ensemble movies of Fig. 5.25. If this observation is confirmed, this would imply that the quasi-neutral mode also breaks parallel force balance, even though the mechanism driving the instability in this regime is different from the ion driven mode described in Chapter 4.

However, high frequency oscillations (experiments at B $\geq$ 0.05 T) exhibit higher poloidal mode numbers (two regions with the same phase are identified in a small strip of the plasma in Fig. 5.21). In order to capture these higher frequency oscillations, the sampling frequency of the camera was raised up to 75,000 fps, which reduced significantly the size of the frames and only a narrow strip in the thick cross-section of the torus could be recorded. For comparison, a black rectangle is drawn in Fig. 5.20 showing the area recorded by the camera in Fig. 5.21. The copper mesh [1] can be used to obtain a rough estimate of $k_\perp$ ($k_\perp \approx 63$ m^{-1} at the edge of the plasma). This estimate is consistent with a m = 5 to 9 mode (resonant with the rational magnetic surfaces in this configuration [2]), suggesting that at high B field

[1] The size of the openings of the mesh is 8 mm.

[2] The rotational transform varies from $\iota = 0.12$ (on axis) to $\iota = 0.23$ (at the plasma edge) in the 64° configuration

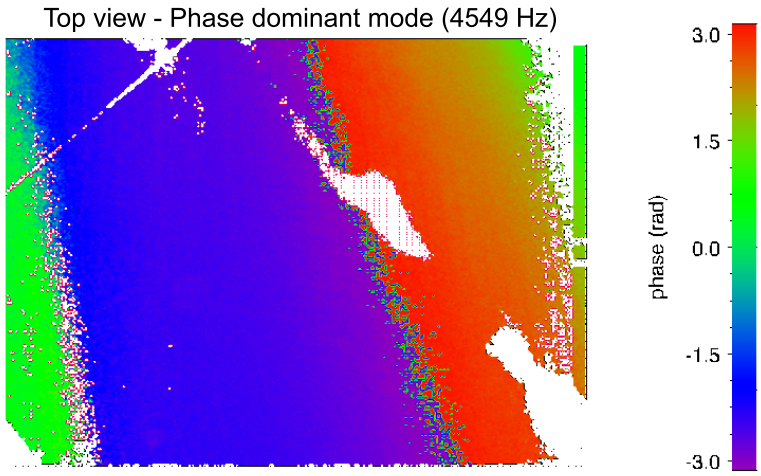

Figure 5.19: Contour plot of the phase at the dominant frequency of the cross-power spectrum (4549 Hz). View from the top view port. White color indicates that the amplitude of the light oscillations in that pixel is small (the RMS of the oscillations in a pixel is lower than 10% of the average RMS of the oscillating pixels in the movie). $p_n = 5 \cdot 10^{-5}$ Torr of N_2, B = 0.02 T, $\phi_e = -200$ V, 64° tilt angle.

strengths the mode can exist without breaking parallel force balance.

78° *configuration*

In the fast imaging experiments conducted for the 78° tilt angle configuration the visible traces of the field lines were recorded and overlaid with the phase plots. These plots can be used to obtain valuable information on the alignment of the oscillations with the field lines and the mode number. Since the stabilization along the field lines occurs at least 20 times faster than these oscillations, the phase of the oscillations is almost perfectly aligned with the magnetic field lines (Fig. 5.22). The top view shown in Fig. 5.23 looks perpendicularly at the thick poloidal cross section of the plasma. Two regions with the same phase can be clearly identified in this phase plot, indicating that the poloidal mode number of the oscillations seems to be m = 2. However, when these phase plots are analyzed, we have to take into account that the camera is recording the light intensity integrated across the torus.

The simulation of the integral light intensity generated by modes rotating in the torus is essential for a correct interpretation of the mode number. Therefore, the propagation of

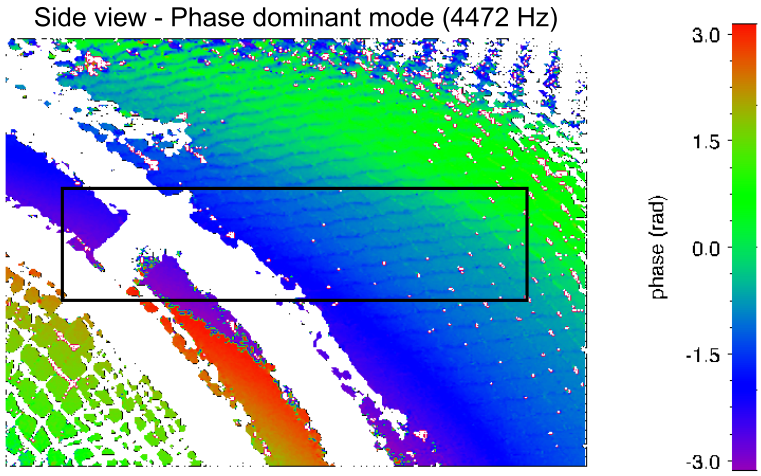

Figure 5.20: Contour plot of the phase at the dominant frequency of the cross-power spectrum (4472 Hz). View from the "nw" side port. White color indicates that the amplitude of the light oscillations in that pixel is small. A black rectangle is drawn showing the area recorded by the camera in Fig. 5.21. $p_n = 5 \cdot 10^{-5}$ Torr of N_2, B = 0.02 T, $\phi_e = -200$ V, 64° tilt angle.

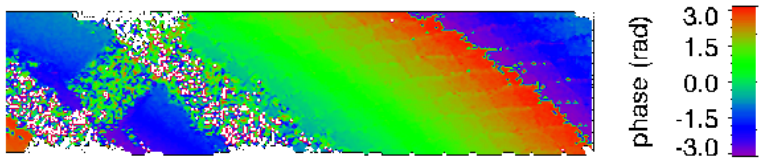

Figure 5.21: Contour plot of the phase at the dominant frequency of the cross-power spectrum (8452 Hz). $p_n = 8 \cdot 10^{-5}$ Torr of N_2, B = 0.05 T, $\phi_e = -200$ V, 64° tilt angle.

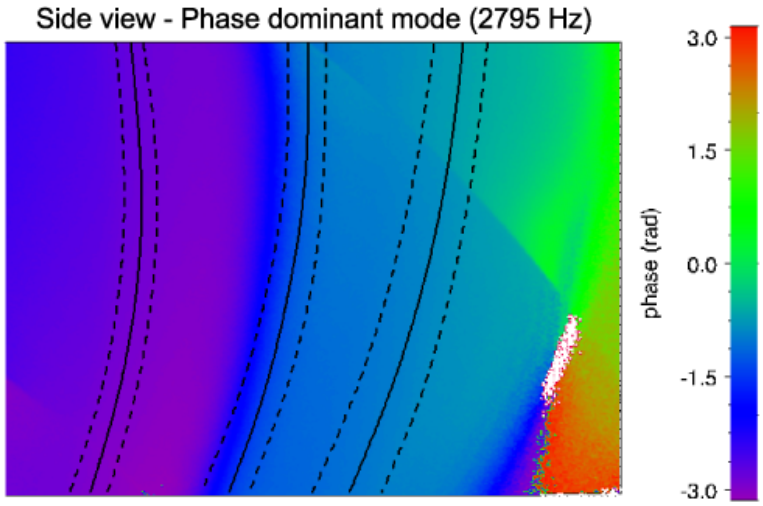

Figure 5.22: Contour plot of the phase at the dominant frequency of the cross-power spectrum (2795 Hz). View from the "nw" side port. The solid black lines correspond to the trace of a field line in the magnetic surface where the electrons are emitted (the dashed lines are the error bars). White color indicates that the amplitude of the light oscillations in that pixel is small. $p_n = 5 \cdot 10^{-5}$ Torr of N_2, B = 0.04 T, $\phi_e = -200$ V, 78° tilt angle.

field aligned m = 1, 2, 3 and 4 modes was simulated in a half CNT torus (details on these simulations are provided on Appendix A). Comparing the experimentally obtained phase plot (Fig. 5.23) with the phase plots of the simulated modes (Fig. 5.24), the structure of the observed oscillations is closer to the simulated m = 3 mode. The 78° coil configuration presents an almost flat iota profile close to $\iota = 1/3$ [41], thus a poloidal m = 3 mode resonates with the rational magnetic surfaces in this configuration.

Although the plasma potential is almost identical for both tilt angles in the quasi-neutral regime (Fig. 3.13), the measured frequencies in the 78° configuration are lower compared to the 64° tilt angle and cannot be increased too much by raising the magnetic field strength (2-5 kHz in the 78° tilt angle, while the frequency could be varied between 2 and 18 kHz in the 64° configuration). This provides additional evidence to the fact that quasi-neutral oscillations jump to a higher mode number at stronger B fields in the 64° conf. The quasi-neutral oscillations in the 78° configuration present a resonant m = 3 mode number independently

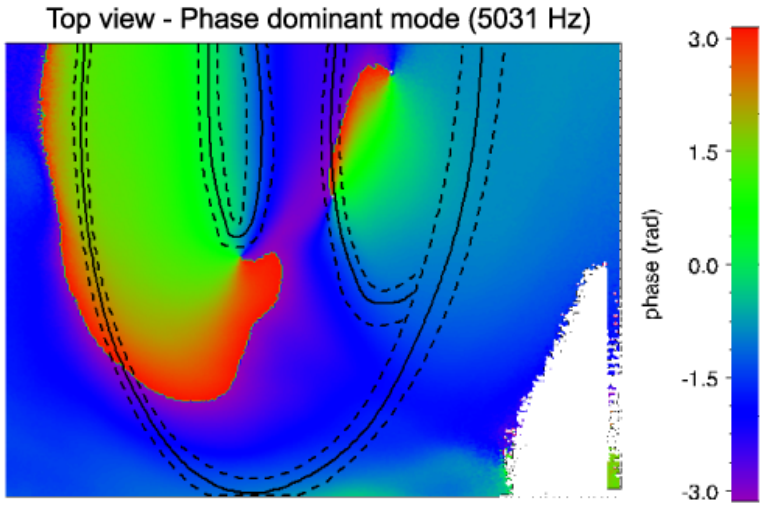

Figure 5.23: Contour plot of the phase at the dominant frequency of the cross-power spectrum (5031 Hz). View from the top window of the chamber. The solid black lines correspond to the trace of a field line in the magnetic surface where the electrons are emitted (the dashed lines are the error bars). White color indicates that the amplitude of the light oscillations in that pixel is small. $p_n = 5 \cdot 10^{-5}$ Torr of N_2, B = 0.08 T, $\phi_e = -200$ V, 78° tilt angle.

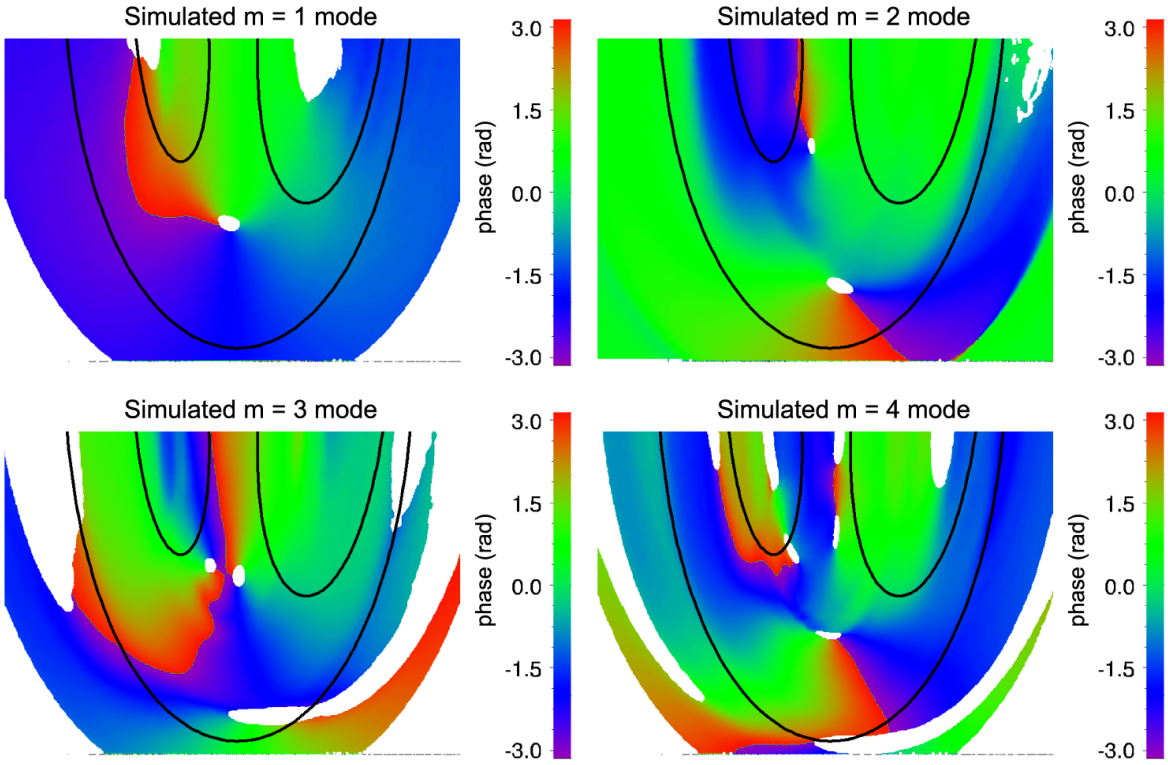

Figure 5.24: Phase plot of the simulated m = 1, 2, 3 and 4 modes. These graphs simulate the visualization from the top window of the chamber. The solid black lines correspond to the trace of a field line in the magnetic surface where the electrons are emitted. 78° tilt angle. White color indicates that the amplitude of the light oscillations in that pixel is small.

of the B field strength, whereas in the 64° tilt angle the mode only seems to resonate with the rational magnetic surfaces at strong B fields. Since the lowest poloidal mode numbers of the resonant surfaces in the 64° configuration are m = 5 to m = 9, the measured frequency is higher than in the 78° conf.

Ensemble movies

Efforts have also been devoted to relate movies from the top and the "nw" side ports using a floating probe located at $\psi \approx 0.15$ as the time reference. Particularly, the time reference is chosen to be the phase of the mode that dominates the vast majority of the cross correlations between the pixels of a movie and the signal in the electrostatic probe. In order to improve the synchronization between the fast camera and the DAQ, a single acquisition card recorded the oscillations in the floating probe and controlled the trigger sent to the fast camera. Since the sampling frequency of the probe and the fast camera was different, the datasets had to be resampled and interpolated at a common frequency arbitrary 10 times higher than the dominant mode of the cross-power spectrums (10 phase bins per cycle of the dominant mode). Then, the ensemble average of the signal at each phase bin (F_i) was computed for the probe and for every pixel as:

$$F_i = \frac{1}{M/10} \sum_{j=1}^{M/10} f_{i,j} \tag{5.3}$$

where, M is the total number of samples and $f_{i,j}$ are the samples of the dataset already sorted in 10 different i bins.

The results are presented in movies like Fig. 5.25. In the top left corner we can see the ensemble movie of the oscillations in the plasma from the top view port. Below we have the corresponding ensemble signal of the floating probe in the same shot. An ensemble movie taken from the "nw" side view port at the same experimental conditions can be seen in the top right corner, with its corresponding ensemble signal of the electrostatic probe below. To improve the visualization of the movies, the DC level of the light intensity has been subtracted, and the 8-bit greyscale of the camera has been replaced by a blue (minimum light intensity) to red (maximum light intensity) scale. The view of the plasma is partially obstructed by the copper mesh and other objects in these movies, so some pixels do not

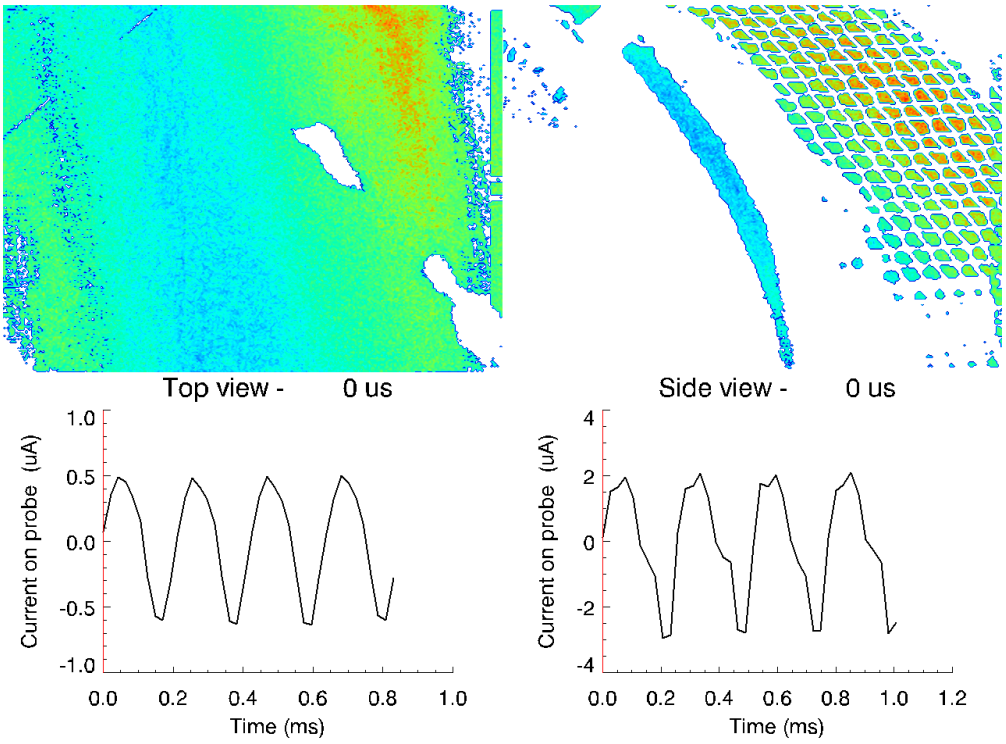

Figure 5.25: Two views of the plasma taken with one camera. Top and side view are synchronized with the signal of the electrostatic probe. URL: `http://hdl.handle.net/10022/AC:P:10261`.

oscillate and are colored in white. Although both movies were taken at the same experimental conditions, the frequency of the dominant mode in the two shots is not identical (4.7 kHz in the left shot, and 3.9 kHz in the right shot), and thus the time scale in the left and the right hand movies is not exactly the same. Nevertheless, the aim of these visualizations is successfully fulfilled, since they are intended to synchronize the oscillations in the plasma from different view ports taking the phase of the floating probe as the reference.

Experiments at reversed polarity

The frequency of the oscillations in the quasi-neutral regime scales linearly with the plasma potential, and grows with the ϕ_p/B ratio. The analysis of the fast camera movies shows that the mode is almost perfectly aligned with the magnetic field lines, propagates perpendicularly to the field lines, and the direction of propagation is in agreement with the $\mathbf{E} \times \mathbf{B}$ rotation of the plasma. Everything seems to indicate that the $\mathbf{E} \times \mathbf{B}$ drift is convecting these oscillations, but it remained to be studied how the direction of the magnetic field affected the rotation of the mode. Therefore, the polarity of the coils was switched, consequently reversing the direction of the magnetic field and the $\mathbf{E} \times \mathbf{B}$ drift while the magnetic surfaces remained unchanged.

The top window of the chamber looks perpendicularly at the thick poloidal cross section of the plasma. Movies recorded from this view port provide an excellent evidence of how changing the direction of the magnetic field involves reversing the rotation of the mode, thus confirming the role of the $\mathbf{E} \times \mathbf{B}$ drift. The movies in Fig. 5.26 are ensemble movies of the oscillations, but the reversal of the direction of rotation when the polarity of the coils is flipped can also be observed in the raw data movies.

5.3.3 Capacitive probes

The fast camera provides much better spatial resolution for the characterization of the quasi-neutral mode, but the set of capacitive probes shown in Fig. 2.2 was also used to investigate the spatial structure of the mode in the 78° configuration. Fig. 5.27 plots the measured phase differences of the mode in each poloidal capacitive probe relative to TP ♯3 using the same procedure described for the ion-resonant mode in electron-rich plasmas (section 4.3).

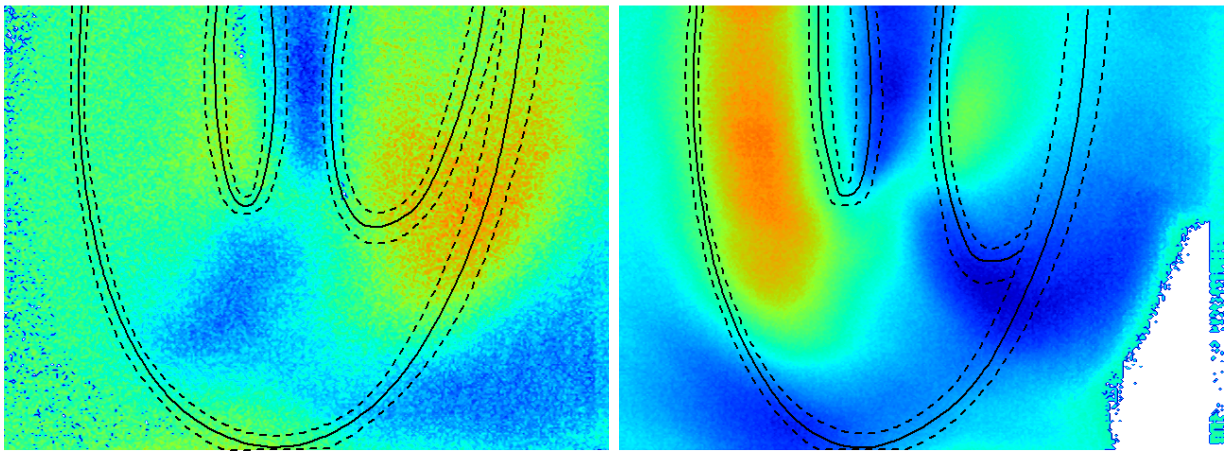

Usual polarity Reversed polarity

Figure 5.26: Ensemble movies from the top window.
Left: At the usual polarity the mode propagates counterclockwise. URL:
`http://hdl.handle.net/10022/AC:P:10262`.
Right: Whereas at reversed polarity the mode propagates clockwise. URL:
`http://hdl.handle.net/10022/AC:P:10263`.

The quasi-neutral oscillations propagate in the direction of the $E \times B$ rotation of the plasma, and the measured phase shifts indicate that the poloidal structure of the mode is m = 3. Similar results were obtained for all the experiments conducted at B $\leq$ 0.04 T. For B $\geq$ 0.05 T the Fourier spectrum of the oscillations present broader peaks at the edge of the plasma (Fig. 5.9) and it was harder to study the phase shift of the mode.

Hence, agreement between the results obtained with the fast camera and the capacitive probes is generally very good.

5.3.4 Discussion

The set of fast imaging experiments exploring the spatial structure of the quasi-neutral oscillations show that this mode presents many characteristics in common for the two tilt angles studied so far in CNT. In both configurations, a global mode is detected moving poloidally in the plasma surfaces, the mode propagates perpendicularly to the magnetic field lines ($\mathbf{k} \cdot \mathbf{B} \approx 0$), and the direction of propagation is in agreement with the $\mathbf{E} \times \mathbf{B}$ drift. But

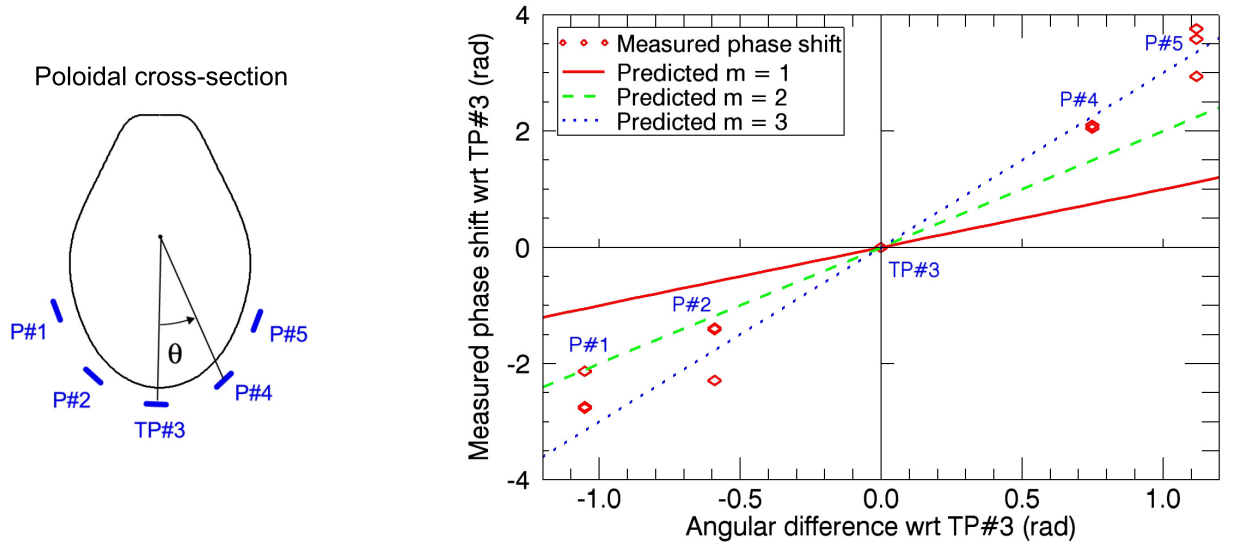

Figure 5.27: Measured phase shift of the quasi-neutral oscillations detected on the poloidal capacitive probes. The phase on probe TP ♯3 is used as the reference. $p_n = 2 \cdot 10^{-5}$ Torr of N_2, $\phi_e = -200$ V, B = 0.02 T, 78° configuration.

also significant differences have been identified between the two configurations.

The experiments in the 78° configuration provide enough evidence to conclude that the low frequency mode of our quasi-neutral plasmas is a *flute* instability, almost perfectly aligned with the magnetic field lines and has a m = 3 mode number (resonant with rational magnetic surfaces). This poloidal m = 3 structure was determined comparing the phase plots of the oscillations recorded from the top view port (Fig. 5.23) with simulations of field aligned m = 1 to m = 4 modes in the torus (Fig. 5.24), and also from the results obtained with a set of capacitive probes at the edge of the plasma (Fig. 5.27).

The rotational transform in the 64° tilt angle configuration varies from $\iota = 0.12$ to $\iota = 0.23$, i.e, the lowest poloidal mode numbers of the resonant surfaces in this configuration are m = 5 to m = 9. For this tilt angle, the quasi-neutral oscillations seem to exhibit a low poloidal mode number (clearly, m < 5) at low B field strengths (B = 0.02 T), suggesting that the parallel force balance might be broken (as observed in the ion driven instability of CNT's electron-rich plasmas, although the physics causing the unstable fluctuations here are different). When the magnetic field is raised above 0.05 T the poloidal structure of the

oscillations jumps to a higher mode number. This is clearly observed in the movies and the phase plots (Fig. 5.21), but also in the measured frequency of the mode (for almost identically potentials in the 64° and 78° tilt angle, the measured frequency is always higher for the 64° conf). The estimate of $k_\perp \approx 63$ m^{-1} and the measured frequency of the mode suggests that at strong B fields the mode might be resonant with rational magnetic surfaces in the 64° configuration, allowing this perturbation to exist without breaking parallel force balance.

5.4 Summary and Discussion

Quasi-neutral plasmas ($\eta < 10^{-5}$) have been systematically studied for the first time in CNT. In this regime the plasma is completely decoupled from the emitter bias voltage, and develops spontaneous single-mode low frequency oscillations (1 - 20 kHz). The plasma presents slightly negative plasma potentials ($0 < \phi_p/\phi_e < 0.1$), which are mainly determined by the magnetic field strength (the measured ϕ_p is more negative at higher magnetic field strengths). The electron temperature in the core of the plasma ($\psi \approx 0.15$) ranges between 30 and 45 eV, but does not have a clear relationship with the B field strength. CNT quasi-neutral plasmas are also characterized by centrally peaked density profiles, with average densities of $n_e \approx 10^{15}\,\mathrm{m}^{-3}$. The Debye length in this regime is typically $\lambda_D \lesssim 1\,\mathrm{mm}$, which is more than one order of magnitude smaller than λ_D in pure-electron plasmas [43].

The measured frequency of the quasi-neutral fluctuations has a negligible dependence on η, and grows with the $|\phi_p/B|$ ratio. However, it does not present a clear linear scaling with E/B (Fig. 5.6). The investigation on the spatial structure of the mode shows that detected instability is a global mode almost perfectly aligned with the magnetic field lines, and propagates in the direction of the $E \times B$ rotation of the plasma. The spatial structure of the oscillations was studied in detail in the 78° configuration with two independent diagnostics (a high speed camera and a set of capacitive probes) providing strong evidence to conclude that the mode has a m = 3 poloidal structure (resonant with rational magnetic surfaces).

Low frequency instabilities in low-β plasmas have being traditionally classified according to their drive mechanism into: Drift waves, Kelvin-Helmholtz, and Rayleigh-Taylor instabilities [38]. The frequency of the oscillations is identical in the core of the plasma and

at different radial locations across the plasma (Fig. 5.8). Therefore, no velocity shear is observed, which confirms that the detected instability is a global mode, and eliminates the possibility of having a Kelvin-Helmholtz instability.

The plasma oscillations were measured simultaneously in a floating emissive probe and an ion saturation probe to study the local phase shift between $\widetilde{n}$ and $\widetilde{\phi}$ and discern the nature of CNT quasi-neutral fluctuations. The analysis presented in Section 5.2.5 studies the influence of the variation of T_e and the growth of the sheath in the oscillations of the current collected by the ion probe. The fluctuations in $\mathrm{I_{probe}}$ are mainly caused by oscillations of n (and not T_e), and it is observed that the local phase shift between $\widetilde{n}$ and $\widetilde{\phi}$ is $34° \pm 57°$. This confirms that the instability is not driven by the velocity shear (characterized by large phase differences between $\widetilde{n}$ and $\widetilde{\phi}$). Although the measurements slightly favor drift waves, the experimental uncertainties in the determination of the local phase shift are too large to enable us to discriminate between drift waves and a Rayleigh-Taylor instability.

The drift wave frequency is $\omega_* = k_\perp \rho_s c_s / L_n$, where $\rho_s = c_s/\omega_i$, c_s is the ion acoustic speed $c_s = \sqrt{T_e/m_i}$, and L_n is the density scale length. The measured frequency (ω) of a drift wave is normally Doppler shifted by the $E \times B$ rotation of the plasma, $\omega = \omega_{E\times B} \pm \omega_*$ [64]. Rayleigh-Taylor instabilities, however, propagate at the $E \times B$ velocity of the plasma [38].

For a $\phi_e = -200$ V quasi-neutral plasma at B = 0.04 T in the 78° configuration, the measured plasma potential is typically $\phi_p \approx -7$ V (Fig. 3.13), so $f = m f_{E\times B} \approx 3.7\,\mathrm{kHz}$, which is consistent with the measured frequency of CNT quasi-neutral mode. For a plasma of the same characteristics, T_e ranges between 30 and 45 eV (Fig. 5.1), thus $f = m f_* \approx 15 - 24\,\mathrm{kHz}$, which is significantly higher than the measured frequency of the instability at B = 0.04 T. Since $\phi_p < 0$ in CNT, electron drift wave fluctuations will add to the $E \times B$ rotation of the plasma.

Table 5.1 compares features of CNT's quasi-neutral wave with the predicted values for drift waves and Rayleigh-Taylor instabilities [38]. It is difficult to discern between both types of instabilities based on the available measurements, however the mode seems to propagate closer to $\omega_{E\times B}$, and a rough estimate of the growth rates (γ) of the instabilities shows that $\gamma_{RT} \sim c_s/\sqrt{L_p R_c}$ is faster than $\gamma_{DW} \sim \omega_*$ (assuming the pressure scale length, L_p, as the minor radius of the torus, and the radius of curvature, R_c, as the major radius). Hence, CNT's instability might be described as density blobs expanding where the pressure gradient

Table 5.1: Comparison of experimental results and theoretical predictions. The predicted features for drift waves and Rayleigh-Taylor instabilities are based on the criteria derived by Jassby [38], unless otherwise stated.
c_s is the ion acoustic speed, $c_s = \sqrt{T_e/m_i}$. L_p is the pressure scale length, $L_p^{-1} = |\nabla p|/p$. R_c is the radius of curvature.

	CNT quasi-neutral oscillations	Drift waves	Rayleigh-Taylor
frequency	$\sim \omega_{E\times B}$	$\omega_{E\times B} \pm \omega_*$	$\omega_{E\times B}$
local $\widetilde{n}$ - $\widetilde{\phi}$ phase shift	$34^\circ \pm 57^\circ$	0° to 45°	45° to 90°
$k_{\|\|}$	~ 0	> 0	0
mode number, m	3	no restriction	1 or 2 [a]
$\left\|e\widetilde{\phi}/T_e\right\| / \|\widetilde{n}/n\|$	usually < 1	$\lesssim 1$	$\gtrsim 1$
growth rate, γ	-	$\sim \omega_*$ [33, 64]	$\sim c_s/\sqrt{L_p R_c}$ [27]

[a] In the absence of magnetic surfaces

is anti-parallel to the magnetic field curvature, like the flute instability observed in magnetic mirrors [27, 69]. CNT, indeed, can be seen as two linked magnetic mirrors. Rayleigh-Taylor and drift instabilities might also coexist and couple in CNT. The study of the transition from a regime dominated by drift waves to a regime dominated by interchange modes has been an active area of research in other experiments [14, 32, 64, 77], and can be of interest for future investigations in CNT.

The oscillations detected in the quasi-neutral regime are a global *flute* instability ($\mathbf{k}\cdot\mathbf{B} \approx 0$) convected by the $E \times B$ flow, and probably driven by the bad curvature in the outboard side of a torus (i.e., Rayleigh-Taylor / interchange instability), or the coupling of both drift and interchange modes.

The presence of magnetic shear has a stabilizing effect on these instabilities [27, 33] and should have been manifested comparing the behavior of the quasi-neutral oscillations in the 78° (essentially shear-less) and the 64° (reversed shear) configurations. However, the oscillations behave very similarly under completely different shear configurations (Fig. 5.7). These results therefore challenge our theoretical understanding of magnetic shear stabilization.

Chapter 6

Conclusions

The study of partially neutralized plasmas lies between two traditionally separated fields in plasma physics: non-neutral plasma physics (focused on the study of single component plasmas), and quasi-neutral plasmas. The physics of partially neutralized plasmas remains largely unexplored, partly because of the difficulty of confining such plasmas. Penning-Malmberg and pure toroidal traps have been successfully used to study single component plasmas, but cannot confine partly neutralized or quasi-neutral plasmas. Tokamaks, on the other hand, require large internal currents for confinement, which cannot be driven in the low densities typical of non-neutral plasmas [8, 13]. However, stellarators can confine plasmas of any degree of neutralization (from pure electron to quasi-neutral) without the need for a plasma current. The studies conducted for this thesis in the CNT stellarator represent the first experimental characterization of plasmas of arbitrary neutrality. This Chapter summarizes and discusses the results reported in this thesis.

The degree of neutralization of the plasma can be parameterized through the quantity $\eta \equiv |n_e - Zn_i|/|n_e + Zn_i|$. CNT can vary continuously η from pure electron ($\eta = 1$) to quasi-neutral ($\eta \ll 1$) by adjusting the neutral pressure in the chamber, which controls the steady state balance between the volumetric ionization of neutrals and the recombination of ions in the ceramic rods. CNT can operate steadily at any given value of η between 10^{-5} and 1.

Pure electron plasmas in CNT are in macroscopically stable equilibria [43], and are characterized by a close match between the local plasma potential and the emitter filament

bias voltage. The emitter bias dictates the plasma potential on the magnetic axis, which determines the total electron content through Poisson's equation. However, the accumulation of ions alters very significantly the equilibrium of electron-rich plasmas. As η evolves from pure electron to quasi-neutral, the plasma potential decouples from the emitter bias, and spontaneous fluctuations appear.

The presence of a second ceramic rod halves the ion content in the plasma for a given neutral pressure [49]. The neutral pressure threshold for the decoupling of the plasma potential, and the appearance of fluctuations, is doubled when an additional ceramic rod is inserted in the plasma (which corresponds approximately to the same ion content). This confirms that the accumulation of ions (and not the presence of neutrals or an emission limit) is responsible for the separation of the plasma potential and the development of unstable oscillations. CNT plasmas develop unstable fluctuations for $\eta < 0.8$, and the abrupt separation of the plasma potential profiles from the emitter voltage occurs when a threshold of $\eta \approx 10^{-3}$ is exceeded.

As a result of the decoupling of the plasma potential from the emitter bias, the emitted electrons are accelerated, and become hotter. T_e in a typical CNT pure electron plasma ranges between 2 and 7 eV in the core of the plasma, while quasi-neutral plasmas ($\eta < 10^{-5}$) exhibit T_e between 30 and 45 eV.

Ions, on the other hand, cool down as the plasma detaches from the emitter bias. As the ions are drawn into the electron-rich plasma, part of the potential drop across the plasma is transferred to the ions' kinetic energy. Massive ions (such as N_2^+) are largely unmagnetized at $\eta \approx 1$, but when the plasma potential decouples (becomes less negative), the ion gyro-radius (r_{Li}) gets smaller than the minor radius of the torus, $\langle a \rangle$. For $\eta < 10^{-5}$, $r_{Li}/\langle a \rangle < 1$.

The fluctuations detected in plasmas of arbitrary neutrality confined in CNT can be classified into three categories according to their behavior (single mode or multi-mode) and their degree of neutrality: 1) single mode oscillations in electron-rich plasmas ($0.01 < \eta < 0.8$), 2) multiple mode fluctuations in electron-rich plasmas ($10^{-4} < \eta < 0.1$), and 3) single mode oscillations in quasi-neutral plasmas ($\eta < 10^{-5}$). The presence of magnetized ions traveling close to the $E \times B$ drift is essential for the excitation of a single mode instability in electron-rich plasmas. Otherwise, largely unmagnetized ions bounce chaotically in the electron-rich plasma and multiple modes are excited. This thesis describes the single mode

oscillations observed in partially neutralized and quasi-neutral plasmas.

Ion-driven fluctuations were predicted to be damped by the magnetic surfaces much faster than the period of an oscillation [50, 59]. However, electron-rich plasmas ($0.01 < \eta < 0.8$) confined on magnetic surfaces exhibit a single mode ion-driven oscillation at high B field strengths (B > 0.04 T) or when light ion species (He^+) are present. The instability observed in CNT has characteristics in common with the ion resonant mode previously studied in Penning-Malmberg [5,63], and pure toroidal traps [75,76]. The frequency of CNT's ion-driven mode ranges between 20 and 100 kHz, and scales close to linearly with ϕ_p/B, suggesting a relation to the $E \times B$ flow of the plasma. However, the measured frequency of the mode also presents a small dependence on the ion species introduced, which implies that the mode is not a purely $E \times B$ rotation of the plasma. The density and potential fluctuations driven by the ion-resonant instability seem to be in phase, which is in agreement with the predictions for small oscillatory perturbations ($|e\widetilde{\phi}|/T_e < 1$) in an electron-rich plasma confined on magnetic surfaces.

The spatial structure and the direction of propagation of CNT's ion-driven mode were investigated with a set of capacitive probes. The instability is a global mode propagating in the $E \times B$ direction. The ion-driven mode presents a m = 1 poloidal mode number for both magnetic configurations studied so far in CNT (64° [50] and 78° tilt angle, reported in this thesis). This implies that even low order rational magnetic surfaces cannot stabilize the ion resonant mode, and the instability breaks the parallel force balance. The mechanism leading to the violation of parallel force balance in the magnetic surfaces is not totally understood at this point, but might be related to the presence of an anisotropic pressure tensor which modifies the plasma force balance equation in a way that an isotropic pressure cannot.

The ion-driven mode in a stellarator is predicted to have a toroidal mode number n > 0 in order to conserve the poloidal magnetic flux (even if the parallel force balance is broken). However, the toroidal structure of the ion-driven mode has now been determined to be n = 0. This implies that the poloidal flux is not conserved in a close tube of plasma moving with the ion-driven mode. The explanation for this behavior probably lies in the presence of a non-scalar pressure (due to the large fraction of trapped particles in CNT), which invalidates the ideal MHD approximation of Ohm's law in CNT (fundamental assumption for the conservation of magnetic flux in an ideal plasma).

Quasi-neutral plasmas ($\eta < 10^{-5}$) in CNT are characterized by much weaker electric fields ($|e\phi_p| < T_e$), and the presence of spontaneous single mode low frequency oscillations (1 - 20 kHz). The measured frequency of the mode grows with the $|\phi_p/B|$ ratio, but does not present a clear linear scaling with E/B.

A high speed camera and a set of capacitive probes were used to study the spatial structure of the quasi-neutral oscillations, showing very good agreement between both diagnostics. The detected instability is a global mode propagating in the $E \times B$ direction of the plasma and almost perfectly aligned with the magnetic field lines. The oscillations were determined to have a m = 3 poloidal mode number, which is resonant with the almost flat $\iota \approx 1/3$ profile of the 78° configuration.

The ion-driven instability detected in CNT's electron-rich plasmas is stable in the quasi-neutral regime [18, 19]. It is also clear that the driving mechanism behind CNT's quasi-neutral oscillations cannot be a Kelvin-Helmholtz instability since no velocity shear was observed, and the local phase difference between density and potential fluctuations is small. Although the measured $\widetilde{n}$ - $\widetilde{\phi}$ phase shift slightly favors drift waves, the large uncertainty in the determination of the phase difference does not allow to discriminate between drift waves and a Rayleigh-Taylor instability by simply measuring this quantity.

Both drift waves and Rayleigh-Taylor instabilities are potential candidates for driving CNT's quasi-neutral mode. Nevertheless, the mode seems to propagate close to $\omega_{E\times B}$ (characteristic of R-T instabilities), and the growth rate γ_{RT} appears to be faster than γ_{DW}. Therefore, CNT's global flute instabilities are likely to be density blobs expanding due to the bad curvature in the outboard side of a torus, or perhaps, a combination of bad curvature and drift instabilities.

Chapter 7

Possible Future Studies

This thesis describes the first experimental observations of plasmas of arbitrary neutrality, varying η continuously from pure electron to quasi-neutral. Many questions remain to be answered to understand the physics of partially neutralized plasmas. Some ideas for future research in this largely uncharted territory for plasma physics are summarized below:

- **Understanding how CNT's ion-driven instability breaks parallel force balance and the conservation of the poloidal magnetic flux**. The measured m = 1, n = 0 spatial structure of CNT's ion resonant mode suggests that the instability violates parallel force balance and the conservation of the poloidal magnetic flux in the stellarator. Preliminary interpretations explain the violation of parallel force balance as a consequence of the large fraction of trapped particles which remain in a locally perturbed region, and do not stream along the field lines, allowing the instability to exist breaking parallel force balance [50]. This thesis also discusses how the presence of an anisotropic pressure tensor modifies the plasma force balance equation, which invalidates the ideal MHD Ohm's law, and might explain the apparent breaking of parallel force balance, and the violation of the conservation of poloidal magnetic flux. However, further studies are needed to confirm these hypotheses.

- **Multi-mode / broad band oscillations in partially neutralized plasmas**. This thesis mainly investigates the single mode oscillations detected in partially neutralized and quasi-neutral plasmas. However, the presence of broadband fluctuations are also

very characteristic of partially neutralized plasmas.

Multiple peak oscillations occur for degrees of non-neutrality between $\eta = 0.01$ and 0.1 when the ions are largely unmagnetized and bounce chaotically in the electron rich plasma. The multiple modes excited present frequencies below 100 kHz, which is in the range of the $E \times B$ rotation and the ion bounce frequency in the plasma, but it is unclear what is the driving mechanism of these modes.

For $10^{-4} < \eta < 0.01$ the maximum amplitude and broadest power spectra of the oscillations are always observed. The Fourier spectrum in this regime is typically dominated by a broad peak between 100 and 200 kHz, but lower frequency modes are also detected whose frequency decreases as η approaches quasi-neutrality. Plasmas with more magnetized ions present narrower power spectra.

Further experimental and theoretical studies have to be conducted for a comprehensive understanding of multi-mode oscillations in partially neutralized plasmas.

- **Jumps between equilibrium states in partially neutralized plasmas**. For degrees of neutralization close to $\eta \approx 10^{-3}$ the plasma decouples rather abruptly from the emitter bias voltage and the emission current grows significantly. Sometimes during the same shot the plasma switches back and forth between a stable equilibrium state (plasma potential close to the emitter bias and low emission currents) and a metastable state (in which the plasma is decoupled from the emitter bias and the emission current is much higher). Since the separation of the plasma potential from the emitter bias is caused by the accumulation of ions (Section 3.3.2), the jumps between states in partially neutralized plasmas could be explained in terms of a process that enhances ionization.

  Preliminary observations are described in Section 4.4.2, but future research is needed to understand these jumps between equilibrium states. The characterization of the equilibrium states before and after the decoupling from emitter bias voltage will be of particular interest.

- **Measurements of the ion temperature in CNT.** An interesting study to be conducted in order to understand the behavior of partially neutralized plasmas would

be the measurement of the ion distribution function. Ions are generated in our plasmas by electron-neutral collisions and are drawn electrostatically into the plasma without collisions, therefore the distribution function of ions is predicted to be non-Maxwellian. A gridded energy analyzer [34] can be used to measure the ion distribution function, which has not been studied experimentally yet in CNT.

- **A more detailed investigation on the drift / interchange nature of CNT's quasi-neutral mode.** It has been difficult to discriminate the driving mechanism of CNT's quasi-neutral oscillations between drift and Rayleigh-Taylor instabilities. Both types of instabilities might also couple in CNT. Further investigations are essential for a deeper understanding of CNT's flute instability, and can connect research in CNT with the study of the controlled transition from regimes dominated by drift waves to regimes showing interchange character [14, 32, 64, 77].

Bibliography

[1] K. Avinash. On toroidal equilibrium of non-neutral plasma. *Phys. Fluids B*, 3(12), 1991.

[2] J.W. Berkery, Q.R. Marksteiner, T. Sunn Pedersen, J.P. Kremer, and R.G. Lefrancois. Ion accumulation in a pure electron plasma confined on magnetic surfaces. *Phys. Plasmas*, 14:084505, 2007.

[3] J.W. Berkery, T. Sunn Pedersen, J.P. Kremer, Q.R. Marksteiner, R.G. Lefrancois, M.S. Hahn, and P.W. Brenner. Confinement of pure electron plasmas in the Columbia Non-neutral Torus. *Phys. Plasmas*, 14(6), 2007.

[4] J.W. Berkery, T. Sunn Pedersen, and L. Sampedro. A retractable electron emitter for the creation of unperturbed pure electron plasmas. *Rev. Sci. Instrum.*, 78(1):013504, 2007.

[5] G Bettega, F Cavaliere, M Cavenago, A Illiberi, R Pozzoli, and M Rom. Experimental investigation of the ion resonance instability in a trapped electron plasma. *Plasma Physics and Controlled Fusion*, 47(10):1697, 2005.

[6] A. H. Boozer. Private communication.

[7] Allen H. Boozer. What is a stellarator? volume 5, pages 1647–1655. AIP, 1998.

[8] Allen H. Boozer. Density limit for electron plasmas confined by magnetic surfaces. *Phys. Plasmas*, 12(10):104502, 2005.

[9] Allen H. Boozer. Physics of magnetically confined plasmas. *Rev. Mod. Phys.*, 76(4):1071–1141, Jan 2005.

[10] P. Brenner, T. S. Pedersen, X. Sarasola, and M. Hahn. Confinement studies in the Columbia Non-neutral Torus. volume 50, pages 678–682. WILEY-VCH Verlag, 2010.

[11] P.W. Brenner. *Confinement of Non-Neutral Plasmas in Stellarator Magnetic Surfaces*. PhD thesis, Columbia University, 2011.

[12] P.W. Brenner, T.S. Pedersen, J.W. Berkery, Q.R. Marksteiner, and M.S. Hahn. Magnetic surface visualizations in the Columbia Non-neutral Torus. *Plasma Science, IEEE Transactions on*, 36(4):1108–1109, Aug. 2008.

[13] Leon Brillouin. A theorem of Larmor and its importance for electrons in magnetic fields. *Phys. Rev.*, 67(7-8):260–266, Apr 1945.

[14] F. Brochard, E. Gravier, and G. Bonhomme. Transition from flute modes to drift waves in a magnetized plasma column. *Physics of Plasmas*, 12(6):062104, 2005.

[15] D. Carralero et al. Turbulence studies by fast camera imaging experiments in the TJ-II stellarator. *Journal of Nuclear Materials*, 390-391:457 – 460, 2009.

[16] N. D'Angelo and S. v. Goeler. Investigation of the Kelvin-Helmholtz instability in a Cesium plasma. *Physics of Fluids*, 9(2):309–313, 1966.

[17] J. D. Daugherty, J. E. Eninger, and G. S. Janes. Experiments on the injection and containment of electron clouds in a toroidal apparatus. *Phys. Fluids*, 12(12):2677, 1969.

[18] R. C. Davidson. *Physics of Nonneutral Plasmas*. Imperial College Press and World Scientific Publishing, London, UK, Second edition, 2001.

[19] R. C. Davidson and Hwan sup Uhm. Influence of finite ion Larmor radius effects on the ion resonance instability in a nonneutral plasma column. *Physics of Fluids*, 21(1):60–71, 1978.

[20] Benoit Durand de Gevigney. *Theoretical and Numerical Investigation of Transport in the Columbia Non-neutral Torus*. PhD thesis, Columbia University, 2010.

[21] Benoit Durand de Gevigney, Thomas Sunn Pedersen, and Allen H. Boozer. Numerical investigation of electron trajectories in the Columbia Non-neutral Torus. *Physics of Plasmas*, 16(12):122502, 2009.

[22] T. Estrada et al. Electron internal transport barrier formation and dynamics in the plasma core of the TJ-II stellarator. *Plasma Phys. Control. Fusion*, 46:277, 2004.

[23] J. Fajans. Non-neutral plasma equilibria, trapping, separatrices, and separatrix crossing in magnetic mirrors. *Physics of Plasmas*, 10(5):1209–1214, 2003.

[24] K. S. Fine, C. F. Driscoll, and J. H. Malmberg. Measurements of a nonlinear diocotron mode in pure electron plasmas. *Phys. Rev. Lett.*, 63(20):2232–2235, Nov 1989.

[25] D.T. Garnier, A.K. Hansen, J. Kesner, M.E. Mauel, P.C. Michael, J.V. Minervini, A. Radovinsky, A. Zhukovsky, A. Boxer, J.L. Ellsworth, I. Karim, and E.E. Ortiz. Design and initial operation of the LDX facility. *Fusion Engineering and Design*, 81(20-22):2371 – 2380, 2006. Proceedings of the Fifteenth International Toki Conference on Fusion and Advanced Technology - ITC-15 SI.

[26] J. C. Glowienka, W. C. Jennings, and R. L. Hickok. Experimental investigation of a coherent flute instability using a heavy ion beam probe. *Physics of Fluids*, 31(9):2704–2709, 1988.

[27] R.J. Goldston and P.H. Rutherford. *Introduction to Plasma Physics*. Taylor & Francis, 1995.

[28] M. Hahn, T. Sunn Pedersen, Q. Marksteiner, and J. W. Berkery. Confirmation of a large density variation along the magnetic axis of the Columbia Non-neutral Torus. *Phys. Plasmas*, 15:020701, 2008.

[29] Michael Hahn. *Pure Electron Plasma Equilibrium and Transport Jumps in The Columbia Non-neutral Torus*. PhD thesis, Columbia University, 2009.

[30] Michael Hahn, Thomas Sunn Pedersen, Paul W. Brenner, and Quinn Marksteiner. Confinement jumps in a non-neutral plasma. *Phys. Plasmas*, 16(2):022105, 2009.

[31] T.C. Hender et al. Chapter 3: MHD stability, operational limits and disruptions. *Nuclear Fusion*, 47(6):S128, 2007.

[32] B.-G. Hong, W. Horton, S. Hamaguchi, M. Wakatani, M. Yagi, and H. Sugama. Transition from resistive-g to η_i- driven turbulence in stellarator systems. *Physics of Fluids B: Plasma Physics*, 3(7):1638–1643, 1991.

[33] W. Horton. Drift waves and transport. *Rev. Mod. Phys.*, 71(3):735–778, Apr 1999.

[34] I. H. Hutchinson. *Principles of Plasma Diagnostics*. Cambridge University Press, second edition, 2002.

[35] K. Ichiguchi, M. Wakatani, T. Unemura, T. Tatsuno, and B.A. Carreras. Improved stability due to local pressure flattening in stellarators. *Nuclear Fusion*, 41(2):181, 2001.

[36] S. Ide and the JT-60 Team. Overview of JT-60U progress towards steady-state advanced tokamak. *Nuclear Fusion*, 45(10):S48, 2005.

[37] Emmanuel C. Ifeachor and Barrie W. Jervis. *Digital Signal Processing: A Practical Approach*. Prentice Hall, 2001.

[38] D. L. Jassby. Transverse velocity shear instabilities within a magnetically confined plasma. *Phys. Fluids*, 15(9):1590–1604, 1972.

[39] W. Knauer. Diocotron instability in plasmas and gas discharges. *Journal of Applied Physics*, 37(2):602–611, 1966.

[40] Shigeo Kondoh, Tomoya Tatsuno, and Zensho Yoshida. Stabilization effect of magnetic shear on the diocotron instability. *Phys. Plasmas*, 8(6):2635–2640, 2001.

[41] J.P. Kremer. *The Creation and First Studies of Electron Plasmas in the Columbia Non-neutral Torus*. PhD thesis, Columbia University, 2006.

[42] J.P. Kremer, T. Sunn Pedersen, Q. Marksteiner, and R.G. Lefrancois. Diagnosing pure-electron plasmas with internal particle flux probes. *Rev. Sci. Instrum.*, 78(1):013503, 2006.

[43] J.P. Kremer, T. Sunn Pedersen, Q. Marksteiner, and R.G. Lefrancois. Experimental confirmation of stable, small Debye length pure electron plasma equilibria in a stellarator. *Phys. Rev. Lett.*, 97, 2006.

[44] R.G. Lefrancois and T. Sunn Pedersen. Large density variation predicted along the magnetic axis for cold electron plasmas in the Columbia Nonneutral Torus (CNT). *Phys. Plasmas*, 13:120702, 2006.

[45] R.G. Lefrancois, T. Sunn Pedersen, A.H. Boozer, and J.P. Kremer. Numerical investigation of three-dimensional single-species plasma equilibria on magnetic surfaces. *Phys. Plasmas*, 12:072105, 2005.

[46] Jr. Lyman Spitzer. The stellarator concept. *Phys. Fluids*, 1(4):253–264, 1958.

[47] J. H. Malmberg and J. S. deGrassie. Properties of nonneutral plasmas. *Phys. Rev. Lett.*, 35:577–580, 1975.

[48] J. H. Malmberg and C. F. Driscoll. Long-time containment of a pure electron plasma. *Phys. Rev. Lett.*, 44(10):654–657, Mar 1980.

[49] Q.R. Marksteiner. *Studies of Non-neutral Ion Electron Plasmas Confined on Magnetic Surfaces*. PhD thesis, Columbia University, 2008.

[50] Q.R. Marksteiner, T. Sunn Pedersen, J.W. Berkery, M.S. Hahn, J.M. Mendez, B. Durand de Gevigney, and H. Himura. Observations of an ion driven instability in nonneutral plasmas confined on magnetic surfaces. *Phys. Rev. Lett.*, 100(6):065002, 2008.

[51] M.E. Mauel, H.H. Warren, and A. Hasegawa. An experiment to measure collisionless radial transport of energetic electrons confined by a dipole magnetic field. *Plasma Science, IEEE Transactions on*, 20(6):626 –630, December 1992.

[52] D.A. Maurer. *Magnetic Island Dynamics Induced by Rotating Magnetic Perturbations in Tokamak plasma*. PhD thesis, Columbia University, 2000.

[53] S. Morimoto, N. Yanagi, M. Nakasuga, T. Obiki, A. Iiyoshi, and K. Uo. Measurements of Pfirsch-Schlüter current and pressure profile for the high density ECH plasmas in Heliotron DR. *Nuclear Fusion*, 28(9):1491, 1988.

[54] N. Nishino, T. Mizuuchi, et al. 2-D image diagnostic technique for edge turbulence using fast cameras. *Plasma and Fusion Research*, 2:S1055–S1055, 2007.

[55] N. Ohno, A. Komori, M. Tanaka, and Y. Kawai. Instabilities associated with a negative rf resistance in current-carrying ion sheaths. *Physics of Fluids B: Plasma Physics*, 3(1):228–235, 1991.

[56] T. M. O'Neil. A confinement theorem for nonneutral plasmas. *Phys. Fluids*, 23:2217, 1980.

[57] T. M. O'Neil and R. A. Smith. Stability theorem for a single species plasma in a toroidal magnetic configuration. *Phys. Plasmas*, 8(2430), 1994.

[58] T. Sunn Pedersen. Numerical investigation of two-dimensional pure electron plasma equilibria on magnetic surfaces. *Phys. Plasmas*, 10(2):334–338, 2003.

[59] T. Sunn Pedersen and A.H. Boozer. Confinement of noneutral plasmas on magnetic surfaces. *Phys. Rev. Lett.*, 88(20):205002, 2002.

[60] T. Sunn Pedersen, A.H. Boozer, J.P. Kremer, and R.G. Lefrancois. Confinement of plasmas of arbitrary neutrality in a stellarator. *Phys. Plasmas*, 11(5):2377–2381, 2004.

[61] T. Sunn Pedersen, A.H. Boozer, J.P. Kremer, R.G. Lefrancois, W.T. Reiersen, F. Dahlgreen, and N. Pomphrey. The Columbia Nonneutral Torus: A new experiment to confine nonneutral and positron-electron plasmas in a stellarator. *Fusion Science and Technology*, 46:200–208, 2004.

[62] T. Sunn Pedersen, J.P. Kremer, R.G. Lefrancois, Q. Marksteiner, N. Pomphrey, W.T. Reiersen, F. Dahlgreen, and X. Sarasola. Construction and initial operation of the Columbia Nonneutral Torus. *Fusion Science and Technology*, 50:372–381, 2006.

[63] A. J. Peurrung, J. Notte, and J. Fajans. Observation of the ion resonance instability. *Phys. Rev. Lett.*, 70(3):295–298, Jan 1993.

[64] F. M. Poli, P. Ricci, A. Fasoli, and M. Podesta. Transition from drift to interchange instabilities in an open magnetic field line configuration. *Physics of Plasmas*, 15(3):032104, 2008.

[65] G Prasad, D Bora, Y C Saxena, and G C Sethia. Study of low-frequency flute-type coherent fluctuations in a toroidal plasma. *Plasma Physics and Controlled Fusion*, 37(4):387, 1995.

[66] J. Qin et al. Measurements of plasma beta in stellarators. *Nuclear Fusion*, 36(3):381, 1996.

[67] Robert J. Renka. Multivariate interpolation of large sets of scattered data. *ACM Trans. Math. Softw.*, 14:139–148, June 1988.

[68] B.W. Rice, K.H. Burrell, J.R. Ferron, C.M. Greenfield, G.L. Jackson, L.L. Lao, R.J. La Haye, T.C. Luce, B.W. Stallard, E.J. Strait, E.J. Synakowski, T.S. Taylor, A.D. Turnbull, and M.R. Wade. Progress towards sustainment of advanced tokamak modes in DIII-D. *Nuclear Fusion*, 39(11Y):1855, 1999.

[69] M. N. Rosenbluth and C. L. Longmire. Stability of plasmas confined by magnetic fields. *Annals of Physics*, 1(2):120 – 140, 1957.

[70] H. Saitoh, Z. Yoshida, C. Nakashima, H. Himura, J. Morikawa, and M. Fukao. Confinement of pure-electron plasmas in a toroidal magnetic-surface configuration. *Phys. Rev. Lett.*, 92(25):255005, 2004.

[71] H. Saitoh, Z. Yoshida, and S. Watanabe. Stable confinement of toroidal electron plasmas in an internal conductor device prototype-ring trap. *Phys. Plasmas*, 12:092102, 2005.

[72] M. K. Vijaya Sankar, E. Eisner, A. Garofalo, D. Gates, T. H. Ivers, R. Kombargi, M. E. Mauel, D. Maurer, D. Nadle, G. A. Navratil, and Q. Xiao. Initial high beta operation of the HBT-EP tokamak. *Journal of Fusion Energy*, 12:303–310, 1993. 10.1007/BF01079674.

[73] M. Shimada et al. Chapter 1: Overview and summary. *Nuclear Fusion*, 47(6):S1, 2007.

[74] M. R. Stoneking, P. W. Fontana, R. L. Sampson, and D. J. Thuecks. Electron plasmas in a "partial" torus. *Phys. Plasmas*, 9(3):766, 2002.

[75] M. R. Stoneking, M. A. Growdon, M. L. Milne, and R. T. Peterson. Millisecond confinement and observation of the m = 1 diocotron mode in a toroidal electron plasma. *AIP Conference Proceedings*, 692(1):310–319, 2003.

[76] M.R. Stoneking, M.A. Growdon, M.L. Milne, and R.T. Peterson. Poloidal $E \times B$ drift used as an effective rotational transform to achieve long confinement times in a toroidal electron plasma. *Phys. Rev. Lett.*, 92(9), 2004.

[77] Hideo Sugama, Masahiro Wakatani, and Akira Hasegawa. Study of resistive drift and resistive interchange modes in a cylindrical plasma with magnetic shear. *Physics of Fluids*, 31(6):1601–1608, 1988.

[78] A. Weller et al. Survey of magnetohydrodynamic instabilities in the advanced stellarator wendelstein 7-as. *Physics of Plasmas*, 8(3):931–956, 2001.

[79] W. D. White, J. H. Malmberg, and C. F. Driscoll. Resistive-wall destabilization of diocotron waves. *Phys. Rev. Lett.*, 49(25):1822–1826, Dec 1982.

[80] M. Y. Ye and S. Takamura. Effect of space-charge limited emission on measurements of plasma potential using emissive probes. *Phys. Plasmas*, 7(8):3457–3463, 2000.

[81] Puravi Zaveri, P. I. John, K. Avinash, and P. K. Kaw. Low-aspect-ratio toroidal equilibria of electron clouds. *Phys. Rev. Lett.*, 68(22):3295, 1992.

Appendix A

Simulation of the mode number in quasi-neutral plasmas

Movies simulating the propagation of field aligned m = 1, 2, 3 and 4 modes have been produced to determine the mode number of the quasi-neutral oscillations. The only input required for these simulations was the coordinates of the field lines in the magnetic surfaces, which were obtained from the Field Line Follower code [41].

The Follower code takes small steps along magnetic field lines many times around the torus, and returns the cylindrical coordinates of every step taken. For the simulations of the mode number described in this Appendix, 5 irrational field lines producing good nested magnetic surfaces between $\psi \approx 0.05$ and $\psi \approx 0.5$ were chosen (this ψ range presumably corresponds to the surfaces that glow most in the experiments with the fast camera). Coordinates from only one period of CNT's torus (between $\varphi = 0°$ and 180°) were used for simplicity, and also for flexibility (if the whole torus had been used, the resonant m = 3 mode would have been the only possible low mode aligned with the field lines). Each of the 5 field lines was split in as many segments as transitions the field line performed around the torus. The poloidal angle of each field line segment was computed at the $\varphi = 90°$ poloidal cross section of the torus, and a "simulated light intensity" was assigned to each field line segment taking into account its poloidal angle, and the simulated mode number.

The last main step in the simulation involves the interpolation of the light intensity of the field lines in a regular grid. 3D interpolation methods like the Modified Shepard's

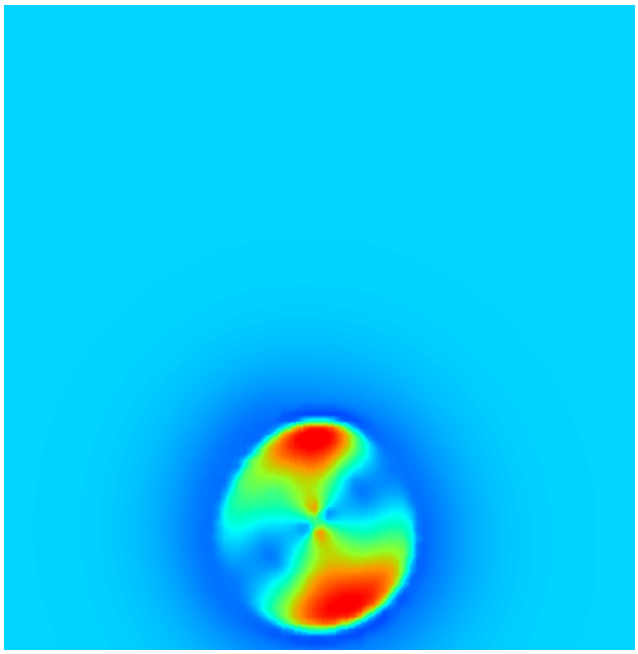

Figure A.1: Interpolated light intensity of a m = 2 mode in the mid horizontal plane. Normalized x and y coordinates.

Method [67] failed to produce satisfactory results for the high number of field line coordinates supplied. Since the aim of the simulation is the computation of the integrated light intensity along the z axis, the torus was divided in 100 horizontal (z = constant) slices, and the light intensity was interpolated in a 100×100 grid in each horizontal plane using the 2D kriging interpolation method implemented in IDL . An example of the interpolated light intensity of a m = 2 mode in a horizontal plane is provided in Fig. A.1. The only trivial step that remains for the creation of a simulated movie frame is the summation along z of the light intensity coming from all the 100 horizontal slices in a resulting 100×100 grid. A frame containing the integrated light intensity across the torus of all the simulated mode numbers is shown in Fig. A.2. Finally, a function was defined to rotate the light intensity pattern perpendicularly to the field lines around the torus, and the routines described in this paragraph were repeated for 72 different frames to produce a movie of one period of the oscillation.

This method produces realistic simulations which have been essential to determine the

mode number of the quasi-neutral oscillations by comparison with the experimental movies recorded with the fast camera (see Section 5.3.2). In order to improve the interpretation of the results, solid black lines representing the trace of a field line in a glowing magnetic surface were overlaid in the movies (Fig. A.2), and phase plots were computed using the same routines explained in Section 5.3.2 (Fig. 5.24).

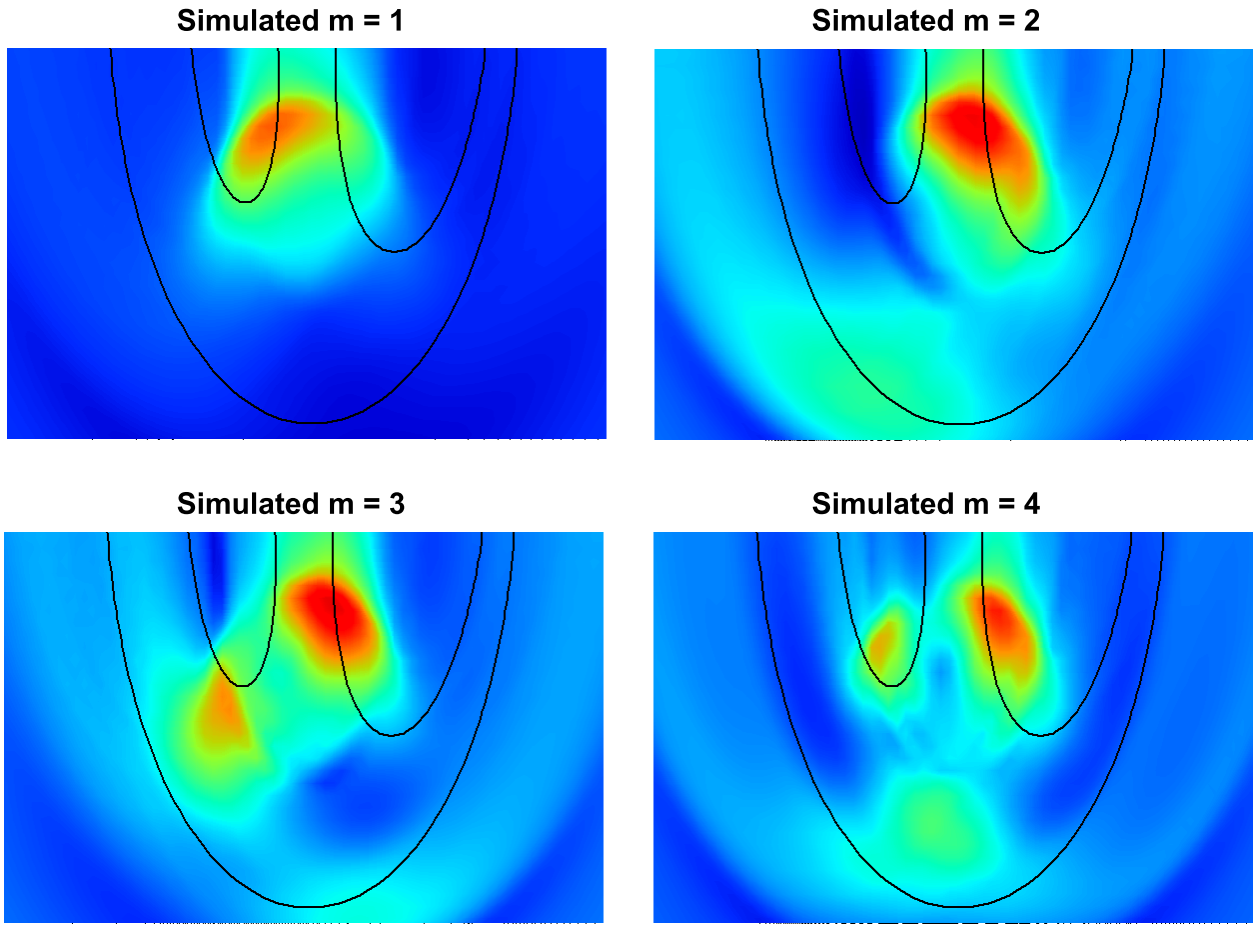

Figure A.2: Frames of the simulated integral light intensity from the top window of the chamber. The corresponding movies can be found on the links below. The solid black lines represent the trace of a field line in a glowing magnetic surface.

Top left: Simulated m = 1. URL: `http://hdl.handle.net/10022/AC:P:10264`.

Top right: Simulated m = 2. URL: `http://hdl.handle.net/10022/AC:P:10265`.

Bottom left: Simulated m = 3. URL: `http://hdl.handle.net/10022/AC:P:10266`.

Bottom right: Simulated m = 4. URL: `http://hdl.handle.net/10022/AC:P:10267`.

Appendix B

Symbols and variables

This Appendix presents a listing of symbols and variables commonly used throughout this thesis.

Table B.1: Table of symbols and variables

Symbol	Definition
e	Elementary charge
q_i	Ion charge
B	Magnetic field strength
ϕ	Electric potential
ϕ_{plasma}, ϕ_p	Plasma potential
ϕ_e	Emitter bias voltage
$\mathrm{p_n}$	Neutral pressure
m_e, m_i	Electron and ion mass
n_e, n_i	Electron and ion number density
T_e, T_i	Electron and ion temperature (always in "energy units", so the Boltzmann constant k never appears)
ω_{ce}, ω_{ci}	Electron and ion cyclotron frequency

Continued on Next Page...

Table B.1 – Continued

Symbol	**Definition**
η	Degree of non-neutrality (defined in Section 3.2)
N_e	Total number of electrons in the plasma
τ_e	Confinement time
ε_0	Permittivity of free space
μ_0	Permeability of free space
λ_D	Debye length, $\lambda_D = \sqrt{\varepsilon_0 T_e/(e^2 n_e)}$
$\langle a \rangle$	Average minor radius of the CNT torus, $\langle a \rangle = 0.15$ m
R	Average major radius of the torus, $R = 0.3$ m
r_{Li}	Ion gyro-radius, $r_{Li} = m_i v_\perp / q_i B$
ψ	Radial coordinate of the torus proportional to the toroidal magnetic flux
θ	Poloidal angle (around the minor circumference of the torus)
φ	Toroidal angle (around the major circumference of the torus)
ι	Rotational transform (poloidal twist of the magnetic field lines around the torus [7])
$k_\parallel$, $k_\perp$	Parallel and perpendicular wave number (with respect to the magnetic field lines)